SAND80-7023
Unlimited Release
UC-62 Distribution

RECORD COPY
DO NOT TAKE FROM THIS ROOM

Mean Wind Forces on Parabolic - Trough Solar Collectors

J. A. Peterka, J. M. Sinou, and J. E. Cermak
Colorado State University

Prepared for Sandia National Laboratories under Contract No. 13-2412

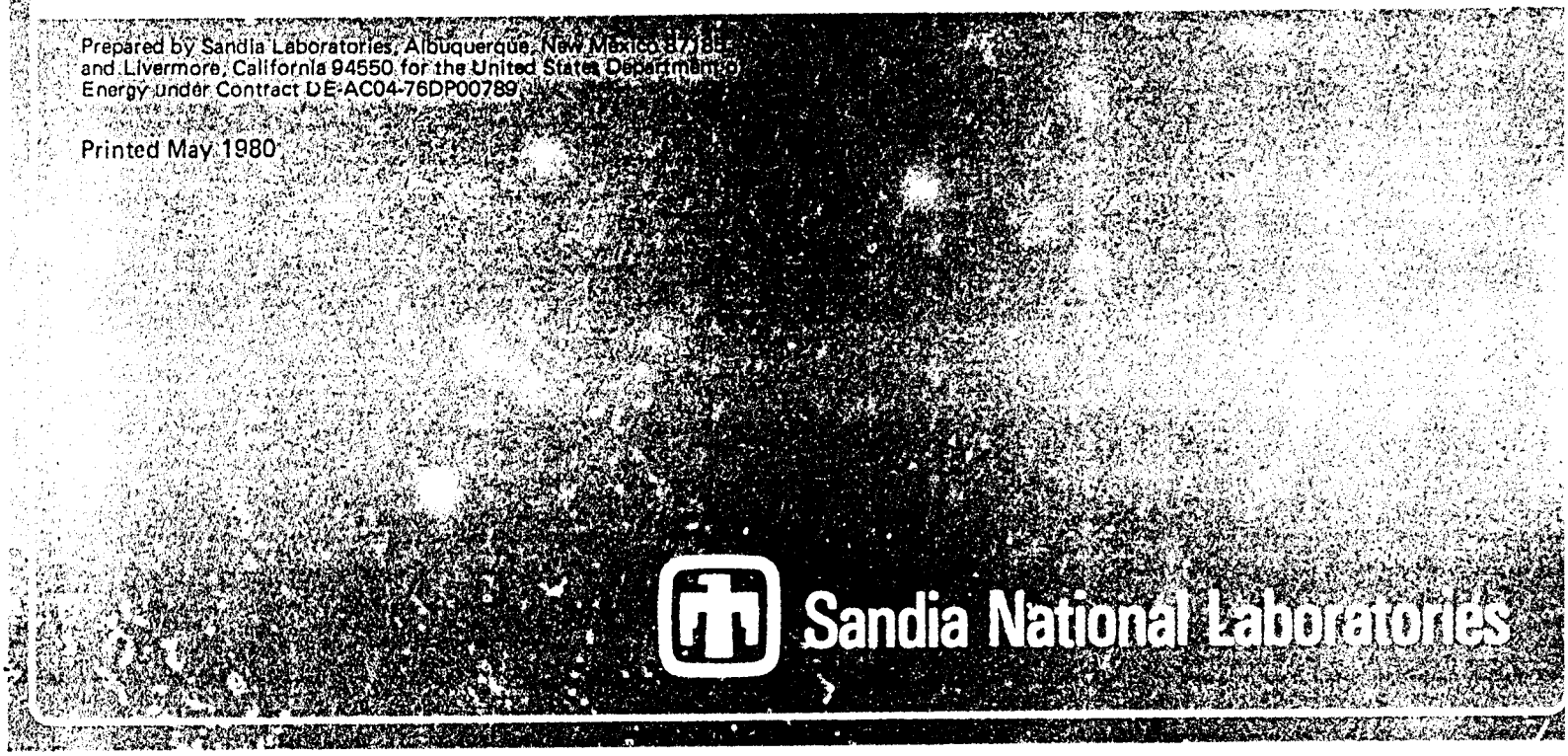

Prepared by Sandia Laboratories, Albuquerque, New Mexico 87185 and Livermore, California 94550 for the United States Department of Energy under Contract DE-AC04-76DP00789

Printed May 1980

Sandia National Laboratories

Issued by Sandia Laboratories, operated for the United States Department of Energy by Sandia Corporation.

NOTICE

This report was prepared as an account of work sponsored by the United States Government. Neither the United States nor the Department of Energy, nor any of their employees, nor any of their contractors, subcontractors, or their employees, makes any warranty, express or implied, or assumes any legal liability or responsibility for the accuracy, completeness or usefulness of any information, apparatus, product or process disclosed, or represents that its use would not infringe privately owned rights.

Printed in the United States of America

Available from
National Technical Information Service
U. S. Department of Commerce
5285 Port Royal Road
Springfield, VA 22161

Price: Printed Copy $6.50 ; **Microfiche $3.00**

SAND80-7023
Unlimited Release
Printed May 1980

Distribution
Category UC-62

MEAN WIND FORCES ON PARABOLIC-TROUGH SOLAR COLLECTORS

J. A. Peterka
J. M. Sinau
J. E. Cermak

Fluid Mechanics and Wind Engineering Program
Fluid Dynamics and Diffusion Laboratory
Department of Civil Engineering
Colorado State University
Fort Collins, CO 80523

Prepared for Sandia National Laboratories under Contract No. 13-2412

TABLE OF CONTENTS

LIST OF TABLES

LIST OF TABLES

LIST OF FIGURES

LIST OF SYMBOLS

A	constant
B	subscript, referenced to the base of foundation or a constant
C	aperture width of the collector (see Figure 5)
d_F	parabolic focal distance
d_G	distance between the center of gravity G and the pivot point
E	voltage
F	subscript referenced to the focal point F
F	total force applied to the collector in the x-z plane
F_x	lateral force, positive along the x axis (see Figure 5)
FH	fence height
F_L	lift force, positive along the z axis (see Figure 5)
FS	fence distance upwind of lead collector
F_{xP}	lateral force coefficient
F_{zP}	lift force coefficient
G	gap width (see Figure 6)
G	subscript referenced to the center of gravity of the trough G
H	distance between the collector pivot point and the force balance axis (see Figure 4)
HCL	distance between the collector pivot point and the floor (see Figure 4)
K_I	selected ratio HCL/C to run configurations 1-4
L	collector length
M'_{xP}	rolling moment about x_P axis
M_{xP}	rolling moment coefficient
M'_{yB}	pitching moment about y_B axis
M_{yB}	pitching moment coefficient about y_B axis
M'_{yF}	pitching moment about y_F axis

LIST OF SYMBOLS

M_{yF}	pitching moment coefficient about y_F axis
M'_{yG}	pitching moment about y_G axis
M_{yG}	pitching moment coefficient about y_G axis
M'_{yP}	pitching moment about y_P axis
M_{yP}	pitching moment coefficient about y_P axis
M'_{zP}	yawing moment about z axis
M_{zP}	yawing moment coefficient about z axis
n	constant
P	pivot point reference location
q_c	tunnel dynamic pressure at collector pivot point height HCL
q_∞	tunnel dynamic pressure at the top of the boundary layer (45 inches high)
R	row spacing
S	projected area of the collector, S=LC
U	velocity
U_{H_o}	wind speed at H_o height
X_P, Y_P, Z_P	coordinate system at pivot point (see Figure 5)
X_B, Y_B, Z_B	coordinate system at base of foundation (see Figure 5)
θ	pitch angle or elevation angle (see Figure 5)
θ_{max}	pitch angle where the maximum lift occurs
ν	kinematic viscosity
ρ	air density
ϕ	parabolic rim angle (see Figure 2)
ψ	yaw angle or azimuth angle (see Figure 5)
η, ξ	coordinate system for definition of collector shape

1. INTRODUCTION

Structures such as parabolic trough solar collectors are being considered for power plant thermal sources. A significant factor influencing the economic viability of these collectors is the magnitude of the wind load and the resulting structural requirements. The shape of the collector, its height above the ground, the collector pitch angle, the number and arrangement of collectors in an array and the direction of the wind are several parameters which can modify the loads applied to the collector. Since an analytical or a numerical approach cannot be considered for such a complicated geometry, a simulation in a wind tunnel in which the atmospheric boundary layer is modeled was conducted at the request of Sandia Laboratories (1).

The purpose of this study was to investigate characteristics of mean wind loads produced by airflow in and around several configurations of parabolic trough solar collectors with and without a wind fence. Four basic parabolic shapes were investigated as single units and one shape was studied as part of several array fields. One 1:25 scale model of each parabolic shape was constructed for mounting on a force balance to measure two forces and three moments. The effects of several dominant variables were investigated in this study: wind-azimuth (or yaw), trough elevation (or pitch) angle, array field configuration, and protective wind fence characteristics. All measurements were made in a boundary-layer flow developed by the meteorological wind tunnel at the Fluid Dynamics and Diffusion Laboratory of Colorado State University.

The primary consideration in modeling wind forces on structures in a wind tunnel is that the wind characteristics in the tunnel simulate

natural boundary-layer winds at the actual site. In general, this requires that the vertical distribution of mean velocity and turbulence in the wind-tunnel boundary layer match those at the site and that the Reynolds numbers of the model and the prototype be equal. In addition, the small-scale model must be geometrically similar to its prototype. A detailed discussion of these requirements and their implementation in the wind-tunnel environment can be found in references 2, 3, and 4.

The construction of a 1:25 scale model of the prototype structure and its immediate surroundings (in this case, a flat, open area), submerged in a turbulent boundary layer of the meteorological wind tunnel shown in Figure 1, satisfies all the above criteria except those of equal Reynolds numbers and similarity of turbulence intensity and scale.

In the Reynolds number $\frac{UD}{\nu}$, ν is the same for both the tunnel and the full-scale structure. Because of this, the wind-tunnel air speed, U, would have to be 25 times the full-scale value if the model and prototype Reynolds numbers are to be equal. Testing at such high wind speeds is not feasible. However, for Reynolds numbers larger than 2×10^4 for sharp-edged structures where the flow separation point is fixed, there is no significant change in the values of aerodynamic coefficients as the Reynolds number increases. For flows over curved surfaces, the velocity required for Reynolds number independence ranges from below 10^5 to nearly 10^6 depending on surface roughness of the curved surface and turbulence structure in the approach flow. Since typical Reynolds number values are 10^6-10^7 for high-wind, full-scale flow and about 7×10^4 for wind-tunnel flows, acceptable flow similarity is achieved without equality of Reynolds numbers for cases where flow

separation is fixed at the edge of the parabolic collector. For cases where flow separation could be on the smooth curvature of the back of the collector, a small Reynolds number dependence may be included in the simulation. Because of the large turbulence intensity in the approach flow, Reynolds number dependence is expected to be quite small.

At a model scale of 1:25, the larger scales of turbulence in the atmospheric boundary layer are not simulated in the wind-tunnel flow. However, because the flow about the parabolic trough approximates the flow about a flat plate at elevation angles near to zero degrees and because the integral scale of the turbulence in the wind tunnel was 2 to 3 times the largest dimension of the model collector, the influence of the scale of turbulence was not expected to be significant (5). Evidence exists which demonstrates some influence of turbulence intensity on drag of flat plates (5,6,7). Because the turbulence intensity difference between the current simulation and a simulation with complete similarity of turbulent structure is not large, the effects due to turbulence intensity should be small (a few percent at most). For cases where an upstream collector disturbs the approach flow, turbulence characteristics are dominated by the wake characteristics of the upstream object and possible differences due to turbulence intensity should further decrease.

2. EXPERIMENTAL CONFIGURATION

2.1 Wind Tunnel

The study was conducted in the meteorological wind tunnel of the Fluid Dynamics and Diffusion Laboratory at Colorado State University. This low-speed, closed-circuit wind tunnel (Figure 1) is characterized by a long (96 ft) slightly diverging test section, 6 ft-8 in. wide (at the turntable) and 6 ft high to develop an appropriate atmospheric boundary layer simulation. The ceiling is adjustable to avoid a pressure gradient along the test section. This facility is driven by a 400 HP variable pitch propeller with velocity varying continuously from 0.5 fps up to 100 fps. The turntable where the tests were conducted (6½ ft diameter) was located near the downstream end of the test section. The ambient temperature was controlled at 24°C.

2.2 Flow Simulation

The purpose of the study was to evaluate loads on collectors in an atmospheric boundary layer developed over an open flat area, characterized by a $\frac{1}{7}$th power law. Since it was impossible to model the complete boundary layer, the simulation was conducted in a 45 in. deep boundary layer, whose mean velocity power law exponent was 0.15. Tests were run with a velocity at 45 in. of about 80 fps. The velocity and turbulence profiles are shown in Figure 8 and tabulated in Table 2.

The shape of the boundary layer was obtained by means of selected roughness on the wind-tunnel floor upstream of the model. Forty feet of test section length were covered with 1 in. cubes followed by a 40 ft length of pegboard with 0.25 in. diameter pegs projecting 0.5 in. above a pegboard base. In addition to the floor roughness, four triangular spires extending from the floor to the ceiling were installed at the

test section entrance in order to get a thicker boundary layer than would otherwise be obtained.

2.3 The Model

The prototype of the solar collector was a 6 ft wide and 22.5 ft long parabolic shaped unit mounted end-to-end in rows. In order to fit the dimensions of the turntable, the 1:25 scale was chosen. The models were built of brass.

Four different shapes of parabolic collectors were constructed varying the rim angle ϕ (Figure 2). The parabolic shape was defined by the equation:

$$\eta^2 = 4 F\xi$$

where the rim angle ϕ is related to the aperture C:

$$F = \frac{C}{4}\left(\frac{1}{\tan \phi} + \frac{1}{\sin \phi}\right)$$

The set of four collectors, called the metric units, were each able to be mounted on the force balance as shown in Figures 3 and 4. Their height and elevation angle could be varied manually. The force balance was fixed to the wind-tunnel turntable so that measured forces and moments were referred to a coordinate system fixed with respect to the turntable. The coordinate system used is shown in Figure 5. A further explanation of the chosen coordinate system and nonmenclature would be beneficial. It is common practice to refer to the three components of force resolved in the wind axis system as drag, cross-wind, and lift forces and to the components resolved in the body axis system as axial, side, and normal forces. This is logical due to the fact that at zero yaw angle and zero pitch angle, most aerodynamic shapes (airplanes, rockets, etc.) have their "axis" aligned with the wind. However, since the "axis" of a solar collector trough is normal to the wind at zero

azimuth angle, it was felt that referring to an "axial" force could be misleading. Therefore, "lateral" force will be used to designate that component of force acting lateral to the axis of the collector trough and "longitudinal" force that component acting along (parallel to) the axis of the trough (see Figure 5). Lift force will still be that component perpendicular to the ground (i.e., that force tending to "lift" the collector off its foundation).

Elevation angles of the collector could be set to 1 degree while azimuth positioning using the turntable was accurate to about 0.2 degrees. The four metric collectors, each mounted alone in the wind tunnel were called configurations 1-4 (Figure 2).

Five configurations of collector arrays were used in the study. Each was composed of different combinations of rows with each row being formed by three aligned collectors similar to the collector configuration 1 ($\phi = 90°$) (Figure 6). The largest array, configuration 9, could be set on the turntable, such that a rotation of the turntable moved the entire array, and the relative position of the metric collector referred to the others remained unchanged. A view of the array field in the wind tunnel is shown in Figure 7.

A study of the effects of wind barriers on collector loads was conducted by using 4 fences made of perforated sheet metal, punched with 0.375 in. diameter holes, which provided a 23 percent porosity. The heights of these fences were 1, 2, 3 and 4 inches. Two 2 in. fences were used, one with a 23 percent porosity and a modified one with 18 percent porosity. The fences were tried at several distances in front of the collector arrays.

Three solid berms of heights 1, 2, and 3 in. were used to determine the influence on loads of earth berms upwind. The 1 in. berm had a linear slope with a base width of 2 in. (Figure 6b). The 2 in. berm was composed of the 1 in. berm with a trapezoidal shape of 1 in. height and base width of 4 in. placed below it. The 3 in. berm was formed by inserting a 1 in. high section between the two portions of the 2 in. berm (Figure 6b).

Since the possibility of controlling the pitch angle of the full-scale prototype with a 1 ft diameter torque tube was under consideration, the effects produced by a 0.5 in. diameter "torque tube" attached to the back of the collector were measured.

3. INSTRUMENTATION

3.1 Velocity Profiles

To determine the approach boundary-layer characteristics, velocity and turbulence intensity profiles were measured over the turntable with no collector in place. These tests were performed with U_∞ = 80 fps at the top of the boundary layer 45 in. above the floor.

Data were obtained with a single horizontal 0.001 in. platinum hot-film probe. A vertical traverse controlled directly by an on-line computer supported the probe. The output from a Thermo-System, Inc. constant temperature anemometer was directed to a data acquisition system consisting of a Hewlett Packard 21 MX minicomputer, disk, card reader, and printer and including a Preston Scientific analog-to-digital converter, Digi-Data digital tape drive and Tektronix plotter. Data were acquired and processed under software control.

Calibration of the hot-wire anemometer was performed using a Thermo-Systems calibrator (Model 1125). The calibration data were fit to a variable exponent King's Law relationship of the form:

$$E^2 = A + BU^n$$

where E is the hot-wire output voltage, U the velocity and A, B, and n are coefficients selected to fit the data. The above relationship was used to determine the mean velocity at measurement points using the measured mean voltage. The fluctuating velocity in the form U_{rms} (root-mean-square velocity) was obtained from:

$$U_{rms} = \frac{2\ E\ E_{rms}}{B\ n\ U^{n-1}}$$

where E_{rms} is the root-mean-square voltage output from the anemometer. For interpretation turbulence measurements were divided by the mean

velocity at the height of the measurement. This result is the turbulence intensity U_{rms}/U.

3.2 Flow Visualization

It is useful to observe flow patterns about the collectors to determine how loads are applied to the collectors or how an upstream fence deflects flow over the collectors to decrease loads. Titanium oxide smoke was released from sources within and upstream of the array field and a motion picture record was obtained of the flow patterns. This movie shows the separation around a collector, the turbulent and low velocity flow within the array field, and the effect of an upwind fence. An outline of the content of the movie is given in Table 1.

3.3 Force and Moment Measurement

Forces and moments applied to each metric unit were measured with a six component INCA strain gage balance. Only five of the six components (two forces and three moments) were measured. Each collector was fixed to the balance as shown in Figures 2 and 3. The balance was, in turn, attached to the turntable. In this way, forces and moments were measured with respect to a coordinate system referred to the collector and not to the flow direction.

The strain-gage bridges of the force balance were monitored by Honeywell Acudata 118 Gage Control/Amplifier Units, which provided excitation to the bridge and amplified the bridge output. The signals were filtered by a 100 Hz low pass filter and amplified by a d.c. amplifier before being processed by the on-line data acquisition system described previously. Zeros and data were recorded for 3 minutes with a 100 Hz sample rate.

Calibration of the force balance was performed before and after the study. Forces and moments were applied to the balance by dead weights hung from a knife edge ring. The balance had a linear response on each channel. Interactions between channels were small and were accounted for in the calibration. A check of the calibration was performed by applying known loads to a collector on the force balance in place in the wind tunnel. By using the calibration matrix, the loads were recovered within 3 percent.

3.4 Force and Moment Coefficients

Forces and moments measured on the collectors were converted into nondimensional coefficients to permit ease of scaling to full-scale forces and moments. The definitions for force and moment coefficients follow. Moments were transferred from the balance center of action to either the X_P, Y_P, Z_P axes at the collector pivot point or to the X_B, Y_B, Z_B axes at ground level. The lateral force coefficient is:

$$F_{xP} = \frac{F_x}{q_c S}$$

where F_x is the lateral force, q_c is the dynamic pressure $0.5\rho U^2$ in the approach flow at the height HCL (height of the collector pivot) above the floor, and S = LC is a characteristic area of the collector. The lift force coefficient is

$$F_{zP} = \frac{F_L}{q_c S}$$

where F_L is the lift force.

The rolling moment coefficient is the moment coefficient about the X_P axis

$$M_{xP} = \frac{M'_{xP}}{q_c S C}$$

where M'_{xP} is the dimensional moment about the X_P axis.

The yawing moment coefficient is the moment coefficient about the Z axis

$$M_{zP} = \frac{M'_z}{q_c S C}$$

where M'_z is the dimensional moment about the Z axis.

The pitching moment coefficient was calculated for the moment M'_{yP} about the Y_P axis through the pivot point

$$M_{yP} = \frac{M'_{yP}}{q_c S C}$$

or for the moment M'_{yB} about the Y_B axis at ground level

$$M_{yB} = \frac{M'_{yB}}{q_c S C}$$

Values of L, C, S and standard height HCL for each collector are outlined below:

COLLECTOR NUMBER =	1	2	3	4
Rim Angle	90°	40°	65°	120°
Aperture C (inches)	2.80	2.92	2.94	3.00
Length L (inches)	10.8	10.8	10.8	10.8
Surface S (inches^2)	30.24	31.54	31.75	32.4
Standard Height of Collector Centerline ref. to the floor, HCL (inches)	2.10	1.99	2.06	2.55
HCL/C = K_I	0.75	0.68	0.70	0.85
Focal length d_F	0.70	2.01	1.15	0.43
Center of gravity position d_G	0.26	0.09	0.16	0.52

For tests in which the height HCL of the collector above the ground was varied, q_c for force and moment coefficient calculations was based on the velocity at the actual HCL used for the test.

Pitching moment coefficients with respect to the center of gravity G and to the focal point F of the collector trough were calculated. The notations are referred to Figure 5b. The force acting on the collector with the X_P - Z_P plane is

$$\|\vec{F}\| = \sqrt{F_x^2 + F_L^2}$$

$$\frac{F_x}{\|\vec{F}\|} = \cos \alpha$$

$$\frac{F_L}{\|\vec{F}\|} = \sin \alpha$$

The pitching moment around the focal point F will be

$$\begin{aligned} M'_{yF} &= M'_{yP} - \|\vec{F}\| \, d_{oF} \\ &= M'_{yP} - \|\vec{F}\| \, d_F \sin (\alpha + \theta) \\ &= M'_{yP} - \|\vec{F}\| \, d_F \, (\sin \alpha \cos \theta + \sin \theta \cos \alpha) \\ &= M'_{yP} - \, (F_L \, d_F \cos \theta + F_x \, d_F \sin \theta) \end{aligned}$$

Using the same development, the pitching moment around G is:

$$M'_{yG} = M'_{yP} - (F_L \, d_G \cos \theta + F_x \, d_G \sin \theta)$$

in terms of coefficients:

$$M_{yF} = \frac{M'_{yF}}{q_c SC} \qquad M_{yG} = \frac{M'_{yG}}{q_c SC}$$

4. TEST RESULTS

4.1 Single Collector Loads

The four different shapes of collectors, model configurations 1-4 with varying rim angle, were tested alone to determine the effect of collector shape and to establish a baseline for comparison with array field tests. The first step was to determine at a height HCL/C $\sim$ 1 and for approach azimuth $\psi = 0$, the pitch angle θ_{max} for which the lift was maximum. These data are shown in Figure 9 for the four collectors and are tabulated in Table 3. At this value of θ_{max} and at $\theta = 0$, the height of the centerline of each collector HCL was varied. These data are tabulated in Tables 4 and 5. Selected portions of these data where loads were larger are presented in Figures 10 and 11. The effect of collector height above ground is not dramatic in coefficient form with the most rapid changes in coefficients occurring for small spacing from the ground. Pitching moment about the ground level was most influenced by height effects as would be expected.

In order to determine the effects of pitch angle θ and yaw angle ψ on the loads, a standard height of collector was selected (HCL/C = 0.75, 0.68, 0.70 and 0.80 for collector configurations 1-4) and load measurements were obtained for a matrix of pitch and yaw angles. Yaw angle ψ (approach wind direction) ranged from -15° to +60° while pitch angle θ ranged from -135° to +180°. The results of these tests are listed in Table 6. Selected portions of the data are plotted in Figures 12 and 13. Several comments regarding these data can be made. The force coefficients are relatively insensitive to collector shape for $\psi = 0$ (Figure 12a, b). Pitching moment depends somewhat on collector shape (Figure 12c, d), but trends to increasing or decreasing load with

curvature of collector are mixed. Yawing moments for varying pitch at $\psi = 0$ (Figure 12e) were near zero as expected. Rolling moments for the same conditions (Figure 12f) should be zero, but showed moment coefficients from zero to 0.5 depending on pitch angle. Test loading during balance calibration did not show this behavior in rolling moment--the cause of these moments remains unexplained. It is doubtful that they arise from small imperfections in model shape. Lateral and lift forces became more dependent on collector shape at different yaw angles (Figures 13a, b, e, f). An explicit display of the effect of rim angle is shown in Figure 14.

The coefficients obtained in the case of one collector only could be compared with the drag coefficient of a flat plate or a cylinder.

In Table 6a (configuration 1)

$F_{xP} = 1.42$ at $0 = 0°$

$F_{xP} = 1.06$ at $0 = 180°$

The drag coefficient for a flat plate with the length greater than the width is

$C_D = 1.2$ if the plate is of finite length to width ratio.

In our case, we have an intermediate case where the boundary can have some effects.

At our range of Reynolds number, the drag on an infinite length cylinder is about 1.2 far from the ground and decreases somewhat for finite length cylinders to about 0.8 for length to diameter ratios similar to the L/C ratio of the collector used for this study.

4.2 Array Field Loads

Configuration 5 was formed by adding two collectors identical in shape to collector 1 as shown in Figure 6. The gap spacing G between

the center metric collector and the two outer collectors was varied in configuration 5 to find the optimum spacing to be used for load measurements on configurations 5-9. With the standard legs shown in Figure 4, it was not possible to obtain a gap spacing less than G/C = 0.54. Alternate legs were constructed which allowed a smaller G/C. Cardboard taped to this modified collector permitted gaps as small as G/C = 0.06 to be obtained. These data are shown in Table 7. The data for both sets of legs are shown in Figure 15. The discontinuity between the two collector types was probably due to the influence of the modified leg geometry. Very little influence of gap spacing on loads can be observed. A gap width of 0.54 was selected for the standard gap width for the subsequent collection of load data on configurations 5-9.

In order to establish row spacing R for the collector array field studies (see Figure 6), row spacing values of R/C = 2.0, 2.5, and 3.0 in configuration 9 were used for selected data acquisition. These data are presented in Table 8. On the basis of these data in conjunction with evaluation by the sponsor of space required for collector access, a row spacing of R/C = 2.25 was selected for all further data collection on the array field. Figure 16 shows selected data from Table 8 and data from further tests on configuration 9 (Table 9) at a row spacing of R/C = 2.25.

To determine the origin of the peak in the lift coefficient at R/C = 2.25, $\theta = \theta_{max}$ shown in Figure 16b, a smoke visualization study was conducted. The flow patterns were highly variable with time; however the essential characteristics of the flow could be observed and are shown in Figure 16c. High velocity flow was observed just above the collectors for all three row spacings, R/C = 2.0, 2.25, 2.5. In

addition, a tendency was observed for the high velocity flow to remain attached to the curved rear surface and to be pulled downward intermittently under the trailing collector. This tendency was observed to be stronger at R/C = 2.25 than for either R/C = 2.0 or R/C = 2.5. For R/C = 2.0, less quantity of high velocity flow was observed to pass under the edge of the trailing collector while for R/C = 2.5, the percentage of time when high velocity flow passed under the edge of the trailing collector was reduced as compared to the case at R/C = 2.25. This may indicate that short-duration lift loads at R/C = 2.5 could be much higher than the mean and comparable to short-duration lift loads at R/C = 2.25. With torque tubes attached to the collectors, no high velocity flow was permitted underneath the collectors--a distinct improvement over the case without torque tubes.

A matrix of conditions varying wind azimuth ψ and pitch angle θ were used to obtain loads on configurations 5-9 using a gap G/C = 0.54 and row spacing R/C = 2.25. These data are tabulated in Table 9. While obtaining data on the various configurations, fences and berms of various heights were placed in front of the first row of the array at varying distances. Table 10 shows the fence heights FH/C and placements FS/C, collector pitch angle, collector configuration and force and moment data. For some cases, a 0.5 in. torque tube was attached to the back of the collector to determine its influence on the loads. Table 11 shows conditions for the study of effects of an upwind berm. Except for Runs 300 and 302, all data on the influence of fences or berms were obtained with $\psi = 0$. The influence of array field configuration and fences on selected loads is shown in Figure 17. These data indicate that loads

drop dramatically with either a single collector upstream or with a fence upstream. The influence of fence height is shown in Figure 17d.

The loads with a torque tube attached to a single collector (configuration 1) were determined for a range of pitch angles at $\psi = 0$. These data are shown in Table 12. A comparison of single collector loads with and without the torque tube is shown in Figure 18. The torque tube had some effect on the loads. The torque tube on a single collector decreased the lift at $\pm \theta_{max}$ and at $\theta = \pm 90°$ but increased slightly the lateral force and the overturning moment M_{yB}. Increases in lateral force and overturning moment occurred at smaller values of the coefficients. Furthermore, it has been seen that in an array field, the torque tube creates a blockage on the first row, protecting the following row. Then the flow between two collector rows becomes stagnant. The presence of the torque tube showed moderate effects on array field loads (Table 10).

Moments about the focal point, F, and center of gravity, G, are compared with moments about points P and B in Tables 13 to 21. Because variation of these moments with various independent variables (θ, for example) includes other variables as well (height of point F or G), these data were not plotted. In many cases, differences in moments between P, F and G are small.

Because of flow leakage into the force balance compartment during the initial stages of testing, small errors were introduced into the data. This problem was discovered and corrected after data on the first four configurations were obtained. A correction to the data was devised by rerunning some data on configurations 1 and 4 and calculating correction factors. Figure 19 gives an example of the correction

showing the original data uncorrected, the original data with the correction factor applied, and the rerun data with the leakage problem fixed. This factor is based on force and moments evaluated upon the force balance action point which is different from the pivot P. The correction appeared to work well. All data reported herein are corrected where corrections were required.

4.3 Smoke Visualization of Fence Effect

The previous section showed the dramatic decrease in loads which occurs when an upwind collector or wind fence is included. Figure 20 shows flow visualization photographs which help to explain why this occurs. Figure 20a shows flow sweeping onto the lead collector without benefit of a wind fence. The collector sees the full effect of the wind. Figure 20b shows the low velocity, separated flow regime behind the lead collector which provides protection to downstream rows from the full force of the wind. In Figure 20c, a low fence of height FH/C = 0.36 is shown. This fence does not provide significant protection; the wind flow is deflected upward somewhat, but still impinges on the lead collector. Figure 20d shows a porous fence of FH/C = 0.71. Here the low velocity region behind the fence is just higher than the collector, even though the fence height is smaller than the collector height. As shown in Figure 17d, this height fence provides almost maximum decrease in lift or lateral force for zero or negative pitch angles. For positive pitch angles, a slightly higher fence may be required to provide maximum load decreases, since the top of the collector would be at a higher elevation.

4.4 Calculation of Full-Scale Loads

The force and moment coefficients presented in this report can be used to determine corresponding forces and moments on full-scale collectors of the same geometry and field array configuration in an open-country environment. This is possible because the force and moment coefficients are constants as long as the Reynolds number is sufficiently high (see Chapter 1). Full-scale forces and moments can be determined by multiplying the coefficients by values of q_c, S and C appropriate to the full-scale environment as demonstrated below by an example.

Consider a single exposed collector 6 ft wide and 22.5 ft long (C = 6 ft, L = 22.5 ft) at sea level exposed to a quasi steady wind U_{30} of 30 mph at 30 ft elevation in an open country environment (0.14 exponent power law profile for mean velocity). The shape of this collector is assumed to be similar to configuration 1 ($\phi = 90°$), with a height of the centerline such that: HCL/C = 0.75. It is desired to calculate the lateral force F in the X direction and the pitching moment M'_{yP} about the rotation point of the collector from the force coefficient F_{xP} and moment coefficient M_{yP} for zero pitch angle ($\theta = 0$) and zero wind angle ($\psi = 0$).

From the equations for force and moment coefficients (section 3.4)

$$F_x = q_c S F_{xP}$$

$$F_L = q_c S F_{zP}$$

$$M'_{yP} = q_c S C M_{yP}$$

From Table 6, for configuration 1, wind azimuth = 0, pitch angle = 0:

$$F_{xP} = 1.42$$

$$F_{zP} = 0.39$$

$$M_{yP} = -0.14$$

From the collector size:

$L = 22.5$ ft, $C = 6$ ft

$S = LC = (22.5 \text{ ft})(6 \text{ ft}) = 135 \text{ ft}^2$

$HCL = 0.75\ C = 0.75\ (6 \text{ ft}) = 4.5 \text{ ft}$

To determine q_c :

$$q_c = 0.5\rho U_{HCL}^2$$

($q_c = 0.00256\ U_{HCL}^2$ if U_{HCL} is in mph and q_c is in pounds per square foot, see ref. 8)

Using a mean velocity profile with a 0.14 power law,

$$U_{HCL} = U_{30} \left(\frac{HCL}{30 \text{ ft}} \right)^{.14}$$

$$= 30 \text{ mph} \left(\frac{4.5 \text{ ft}}{30 \text{ ft}} \right)^{.14} = 23.0 \text{ mph}$$

Thus $q_c = 0.00256\ (23.0)^2 = 1.35$ psf.

The forces then become

$F_x = q_c\ S\ F_{xP} = (1.35)(135)(1.42)$ $\qquad$ $F_L = (1.35)(135)\ 0.39$

$F_x = 260$ lb $\qquad$ $F_L = 70$ lb

$$M'_{yP} = q_c\ S\ CM_{yP} = (1.35)(135)(6.0)(-0.14)$$

$$M'_{yP} = -150 \text{ lb ft}$$

The moment arm of the force from the pivot point is:

$$\Delta z_T = \frac{|M'_{yP}|}{\|\vec{F}\|}$$

where $\|\vec{F}\| = \sqrt{F_D^2 + F_L^2}$

$$= \sqrt{260^2 + 70^2}$$

$$= 270 \text{ lb}$$

$$\Delta z_T = \frac{150 \text{ lb ft}}{270 \text{ lb}} = 0.56 \text{ ft}$$

5. CONCLUSIONS

Wind forces acting on parabolic trough solar collectors were modeled in a boundary-layer wind tunnel in which atmospheric winds were simulated. Wind loads were measured on four collectors with different rim angles. Loads were also obtained on several array field configurations including wind fences.

The following conclusions can be drawn:

1. Maximum lift on a single collector occurs for negative pitch angles (collector pointed downward) and occurs at different pitch angles for different rim angles.
2. Maximum lateral force on a single collector occurs for wind directly into a collector at zero pitch angle.
3. Maxima in pitching moments on a single collector tended to occur at more than one pitch angle.
4. Collectors downwind of other collectors showed large decreases in wind load.
5. Wind loads on a collector in an array field directly exposed to winds decreased dramatically with inclusion of an appropriately designed fence upwind.
6. Gap spacing between collectors in a row did not affect collector loads significantly.
7. Row spacing in an array field had a slight influence on collector loads especially at the pitch angle which gives maximum lift.

REFERENCES

1. McBride, D. P., Static Force Tests on Parabolic Trough Solar Collectors, Pretest Information Report No. 395, Sandia Laboratories, Albuquerque, New Mexico.

2. Cermak, J. E., Aerodynamics of Buildings, Annual Review of Fluid Mechanics, Vol. 8, 1976.

3. Cermak, J. E., Laboratory Simulation of the Atmospheric Boundary Layer, AIAA Jl., Vol. 9, September 1971.

4. Cermak, J. E., Applications of Fluid Mechanics to Wind Engineering, A Freeman Scholar Lecture, ASME Jl. of Fluids Engineering, Vol. 97, No. 1, March 1975.

5. Bearman, P. W., Turbulence Effects on Bluff Body Mean Flow, Third U.S. National Conference on Wind Engineering Research, pp. 265-272, 1978.

6. Bearman, P. W., An Investigation of the Forces on Flat Plates Normal to a Turbulent Flow, Jl. Fluid Mechanics, Vol. 46, pp. 177-198, 1971.

7. Nakamura, Y. and Tomonari, Y., The Effect of Turbulence on the Drag of Rectangular Prisms, Transactions Japan Society of Aeronautical and Space Science, Vol. 19, pp. 81-86, 1976.

8. American National Standards Institute, American National Standard Building Code Requirements for Minimum Design Loads in Buildings and Other Structures, ANSI Standard A58.1, 1972.

FIGURES

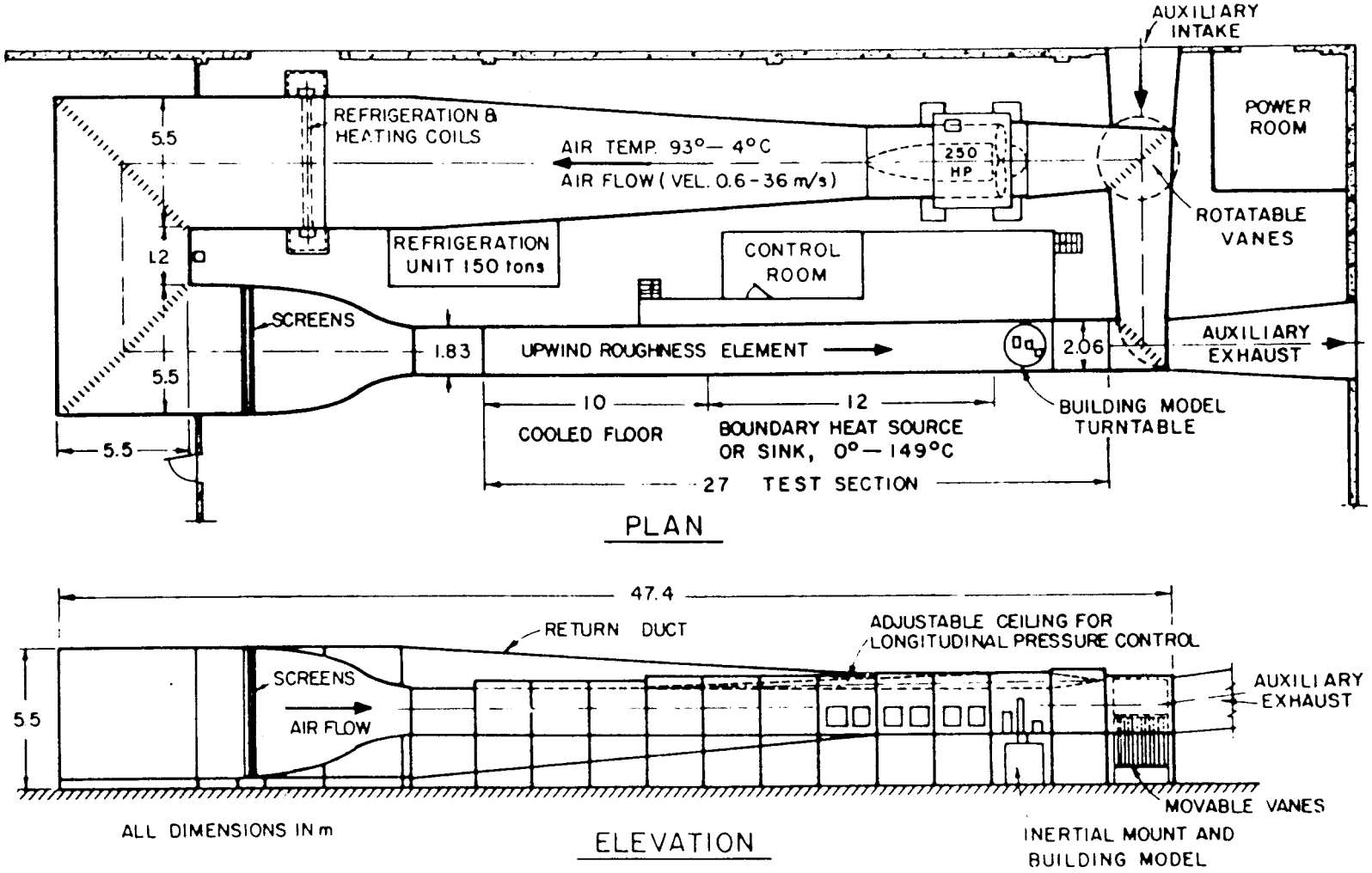

Figure 1. Meteorological wind tunnel.

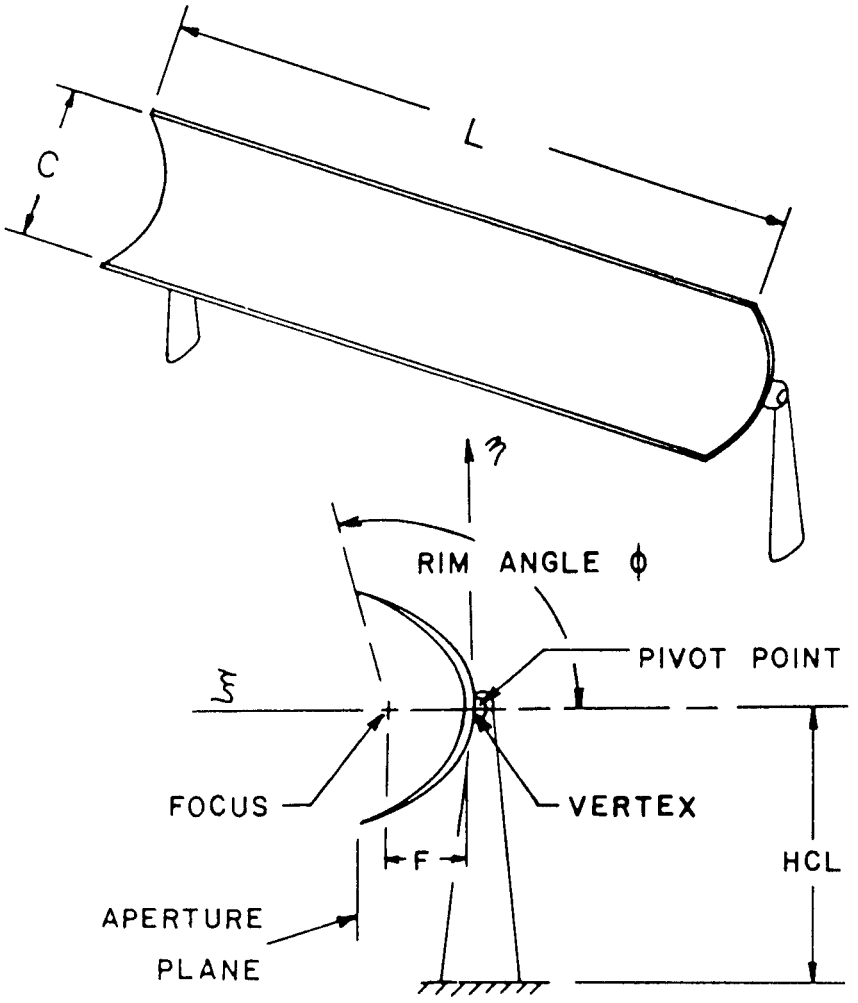

Figure 2a. Collector shapes for configurations 1-4.

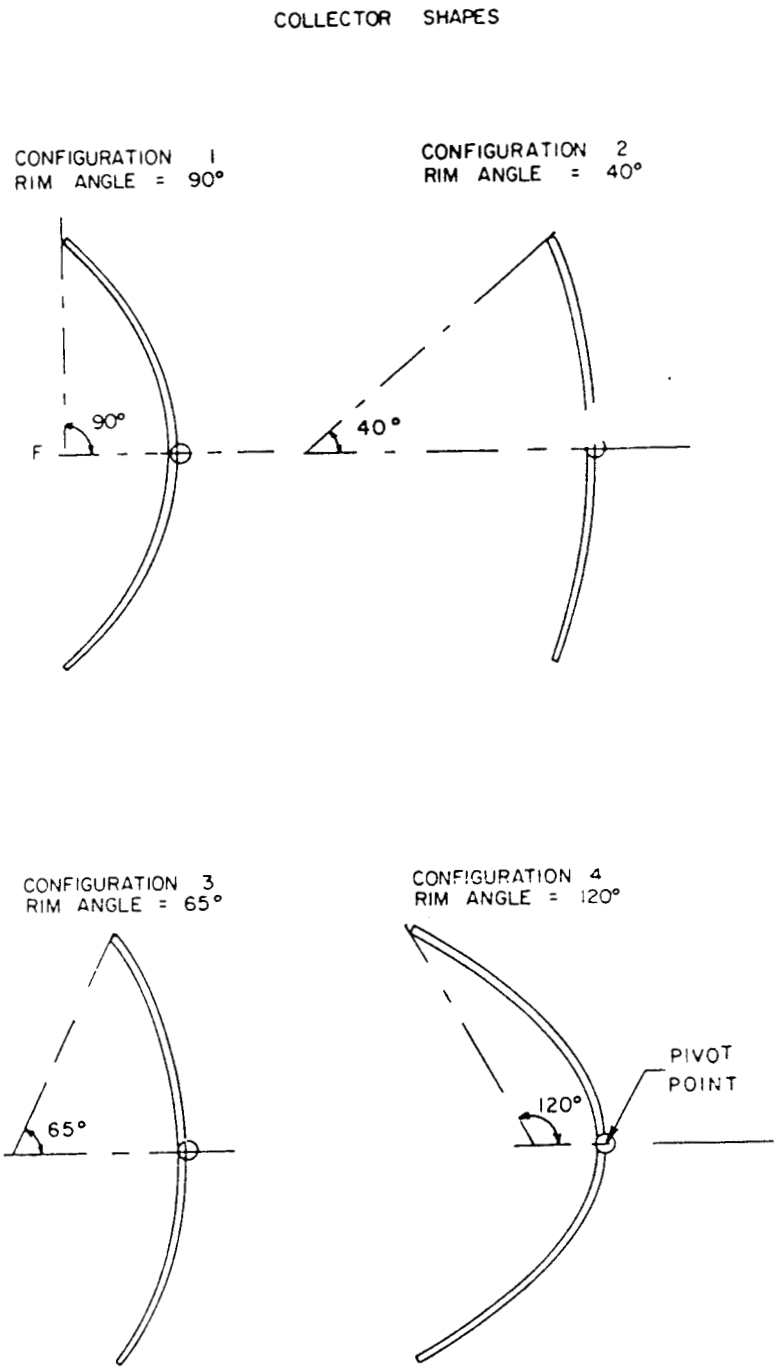

Figure 2b. Collector shapes for configurations 1-4.

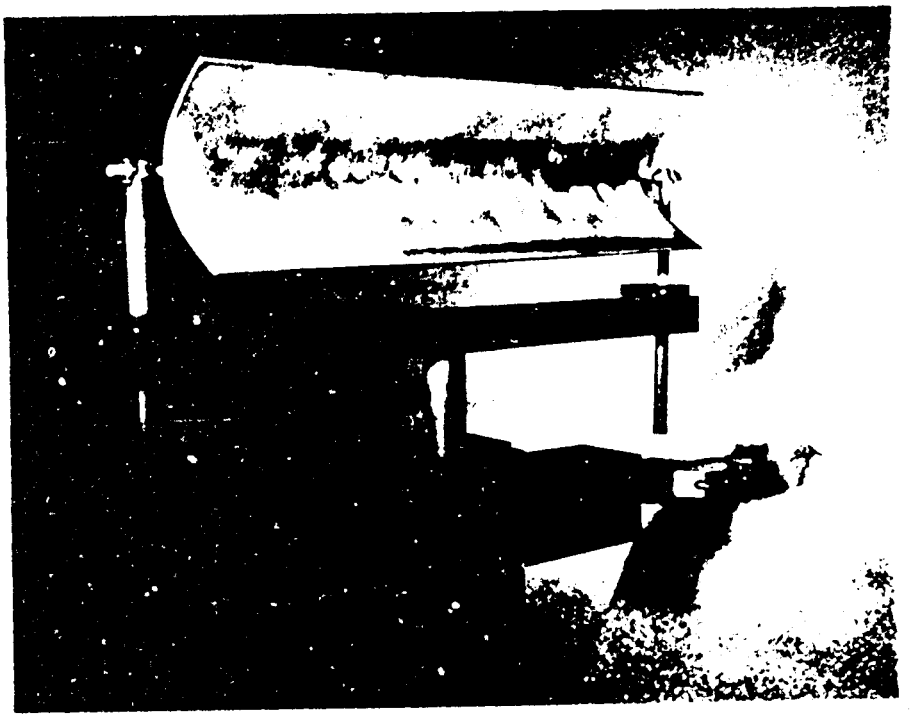

Collector 4

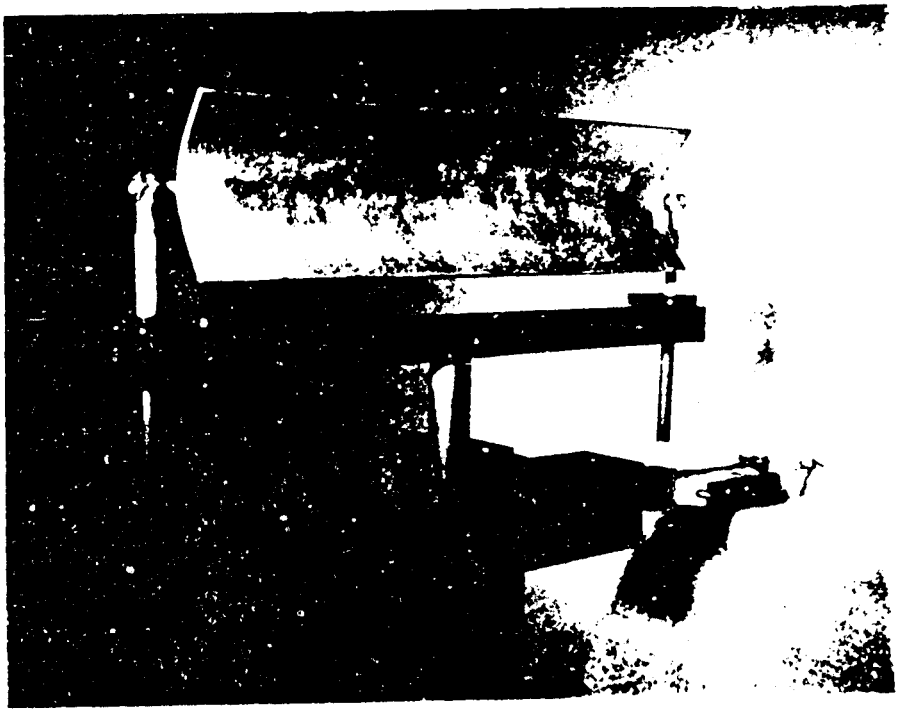

Collector 1

Figure 3. Collector mounted on force balance.

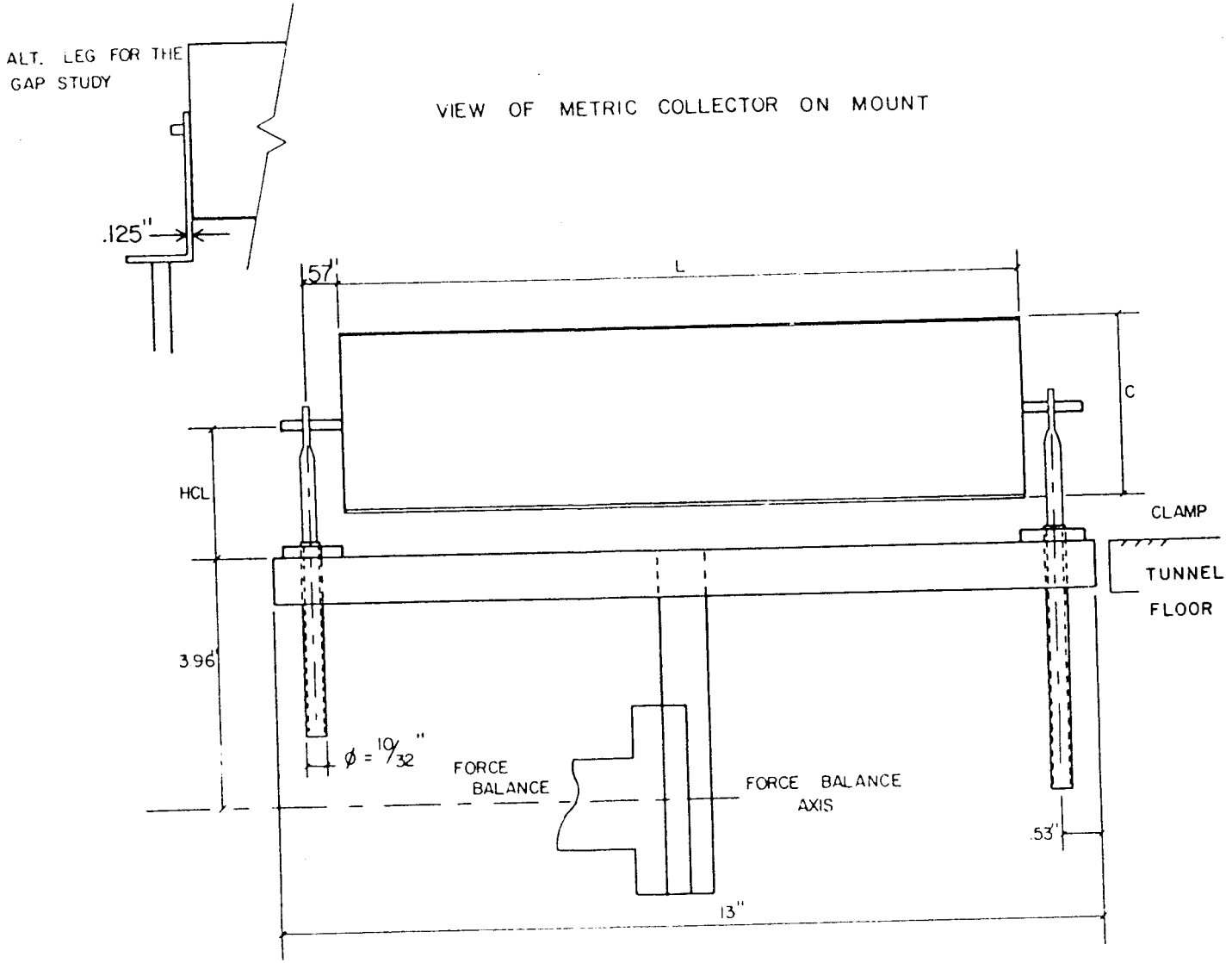

Figure 4. Collector and force balance mount.

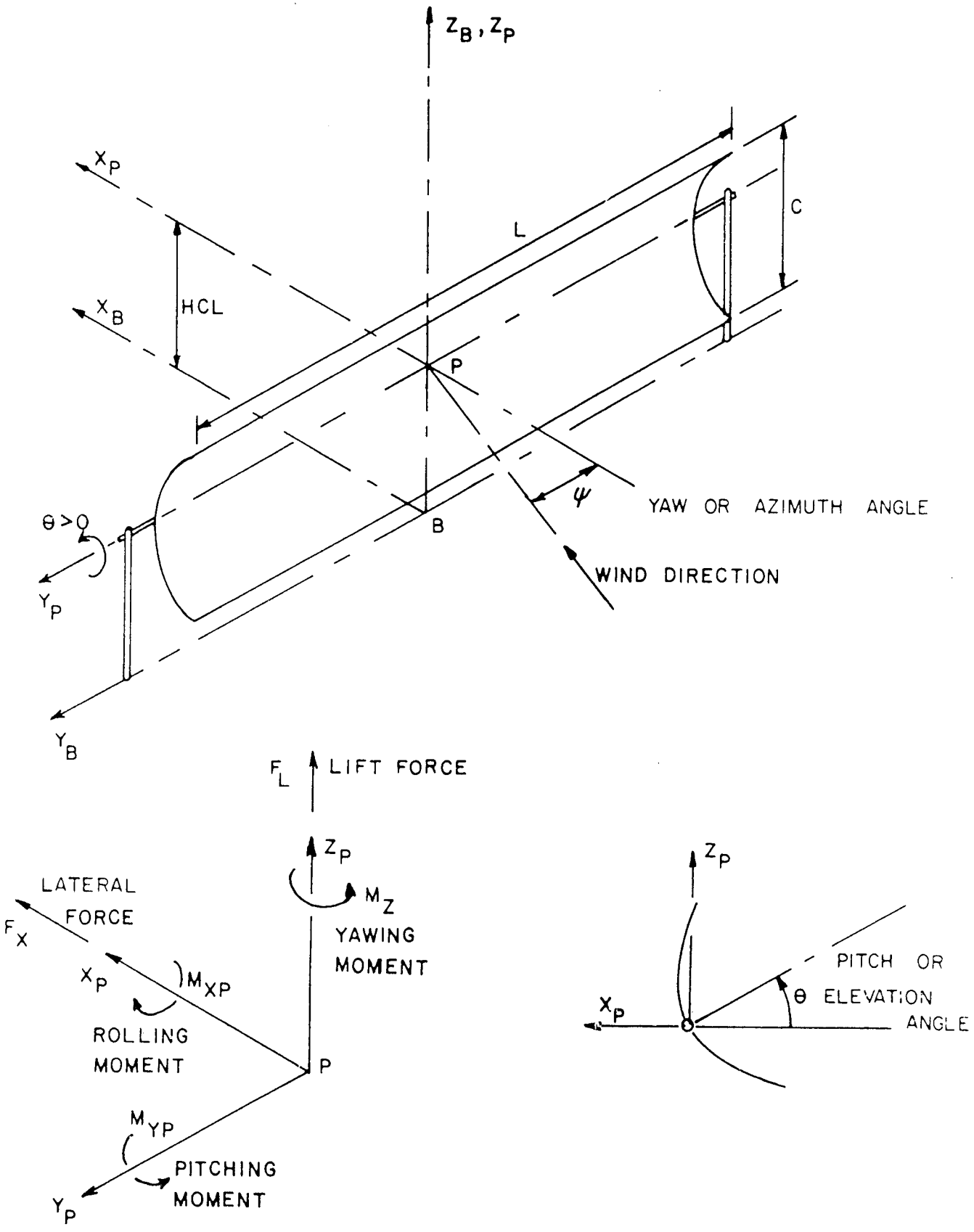

Figure 5a. Coordinate system.

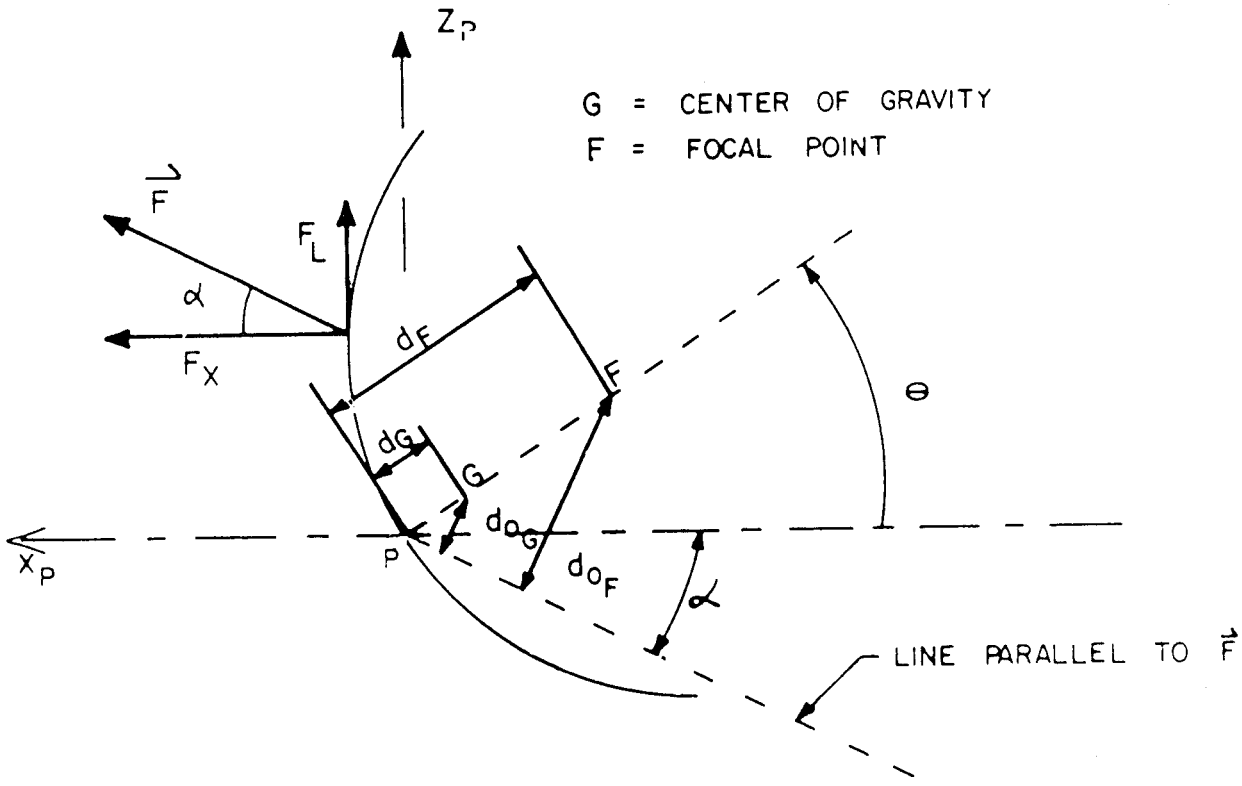

Figure 5b. Coordinate system.

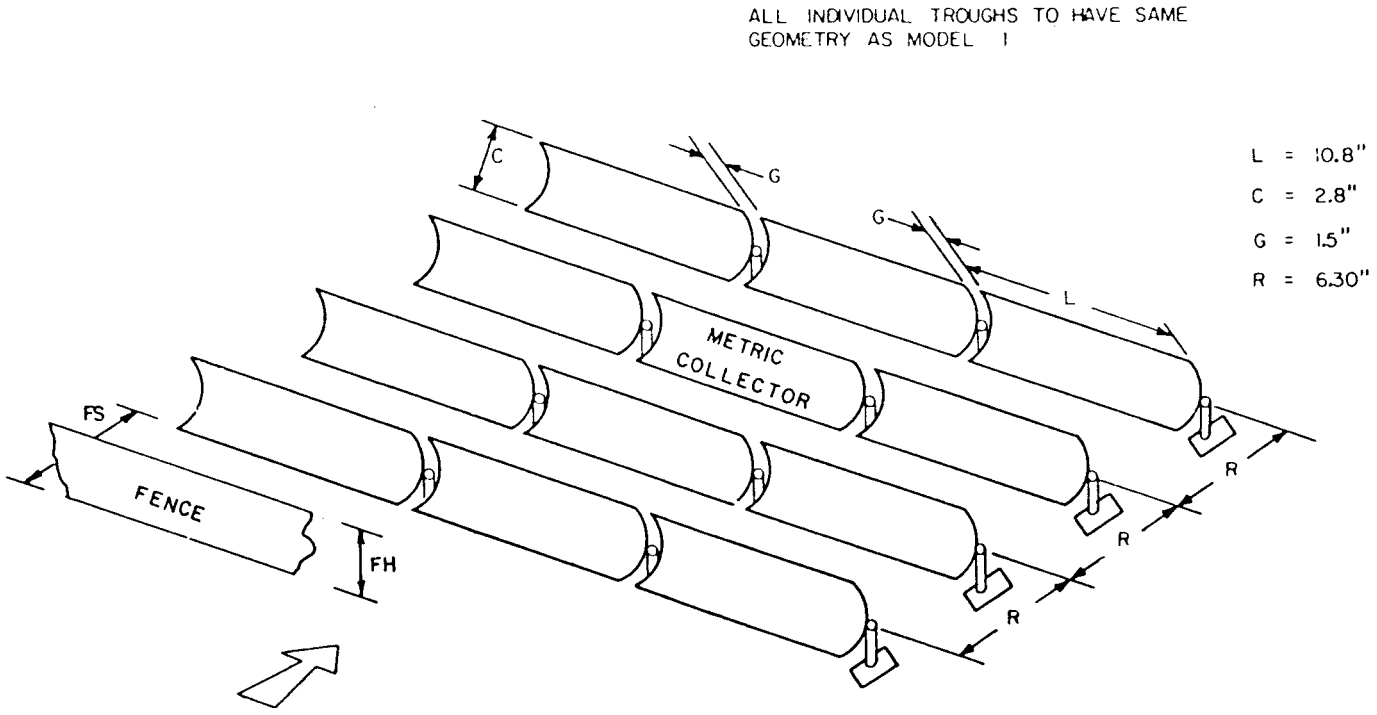

CONFIGURATION NUMBER	ROWS AHEAD	ROWS BEHIND
V	0	0
VI	0	1
VII	1	1
VIII	2	1
IX	4	1

Figure 6a. Collector in arrays for configurations 5-9.

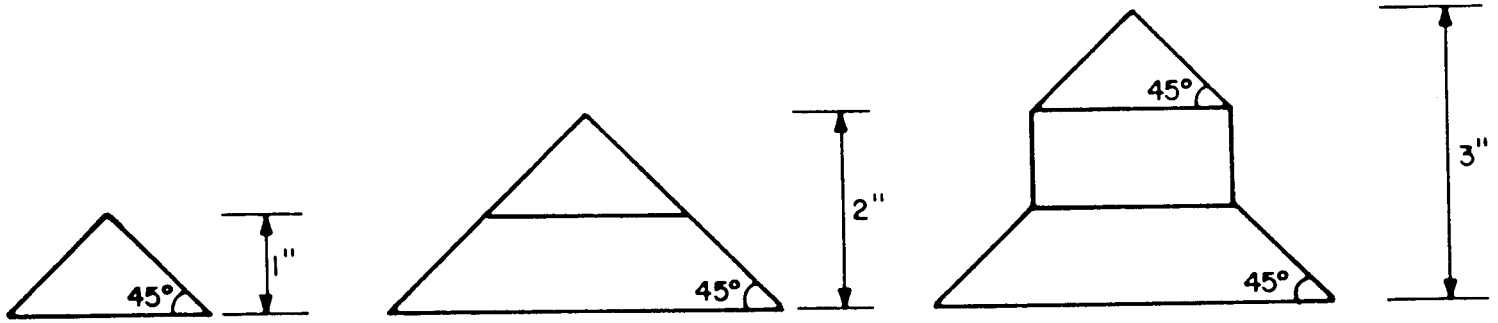

Figure 6b. Berm arrangement.

Figure 7. Array field in the wind tunnel.

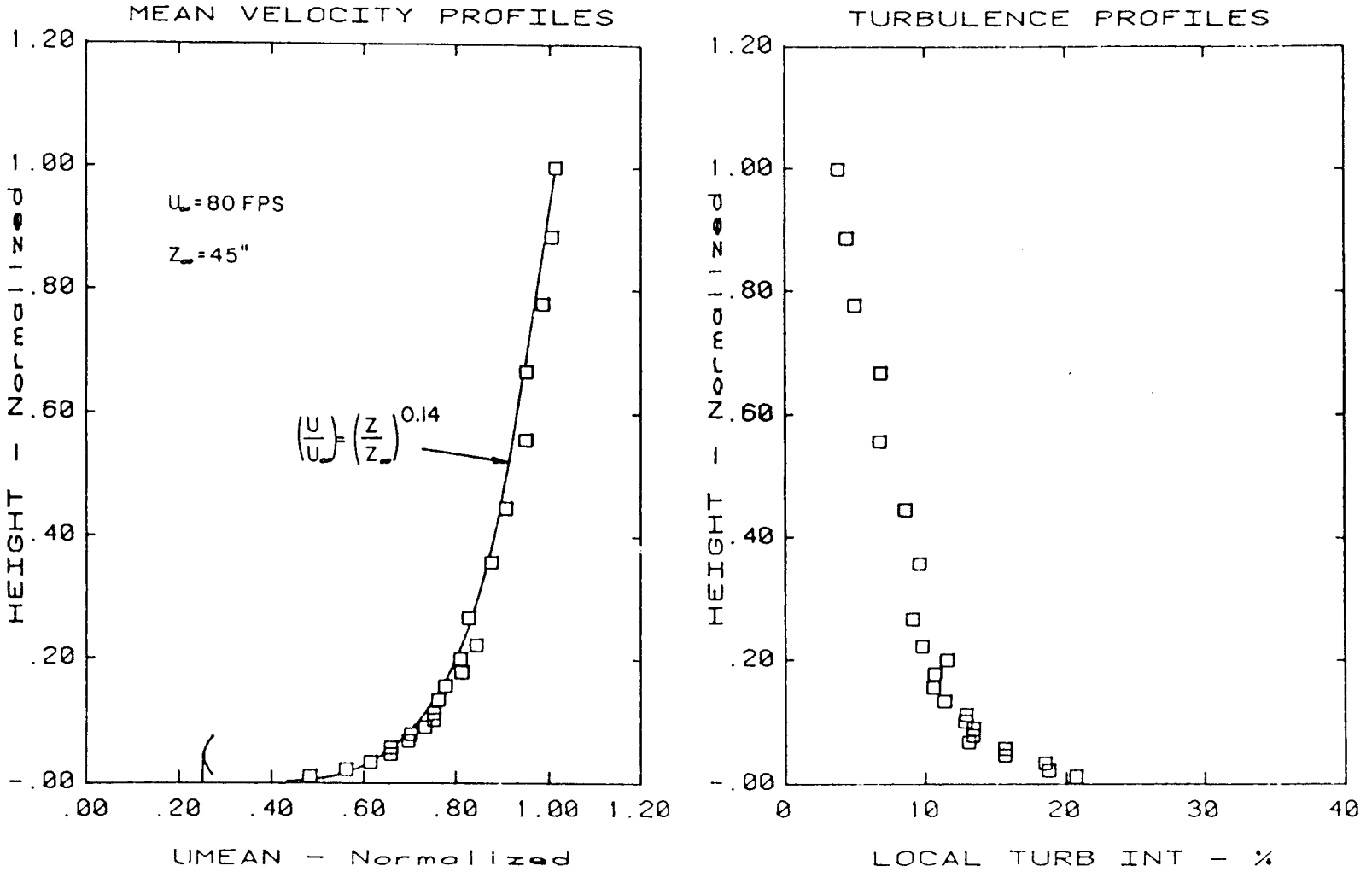

Figure 8. Approach velocity and turbulence profile.

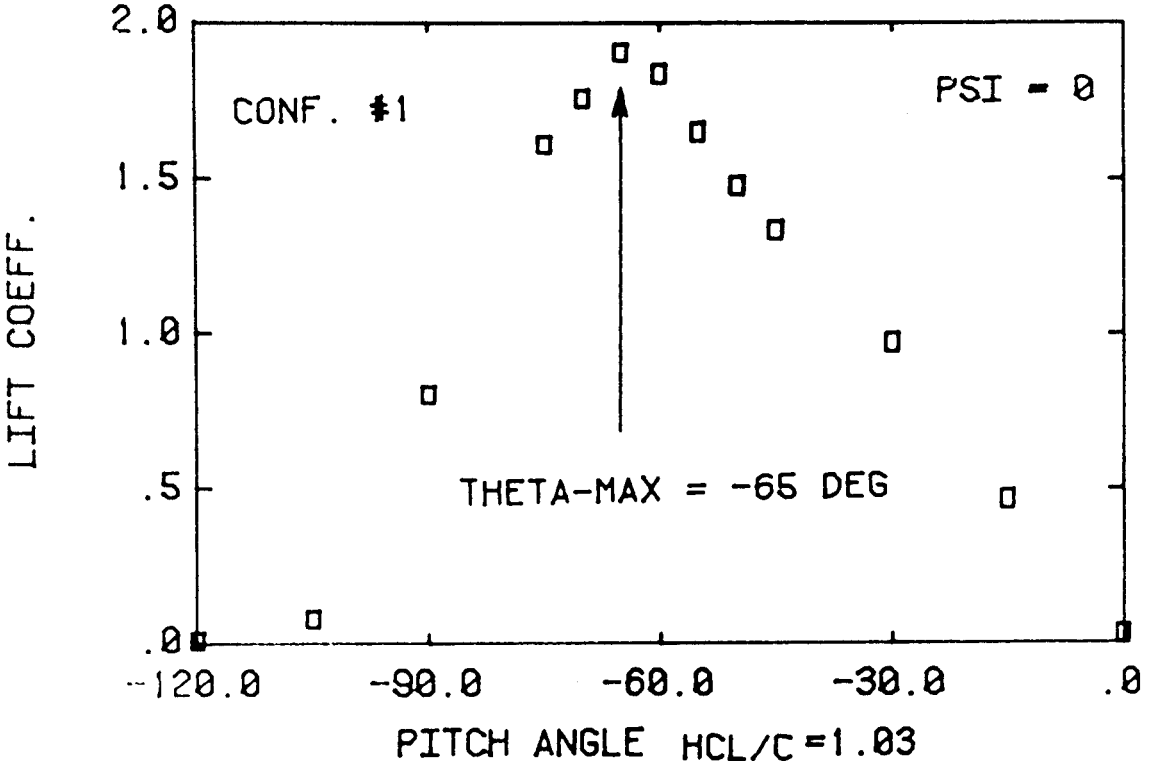

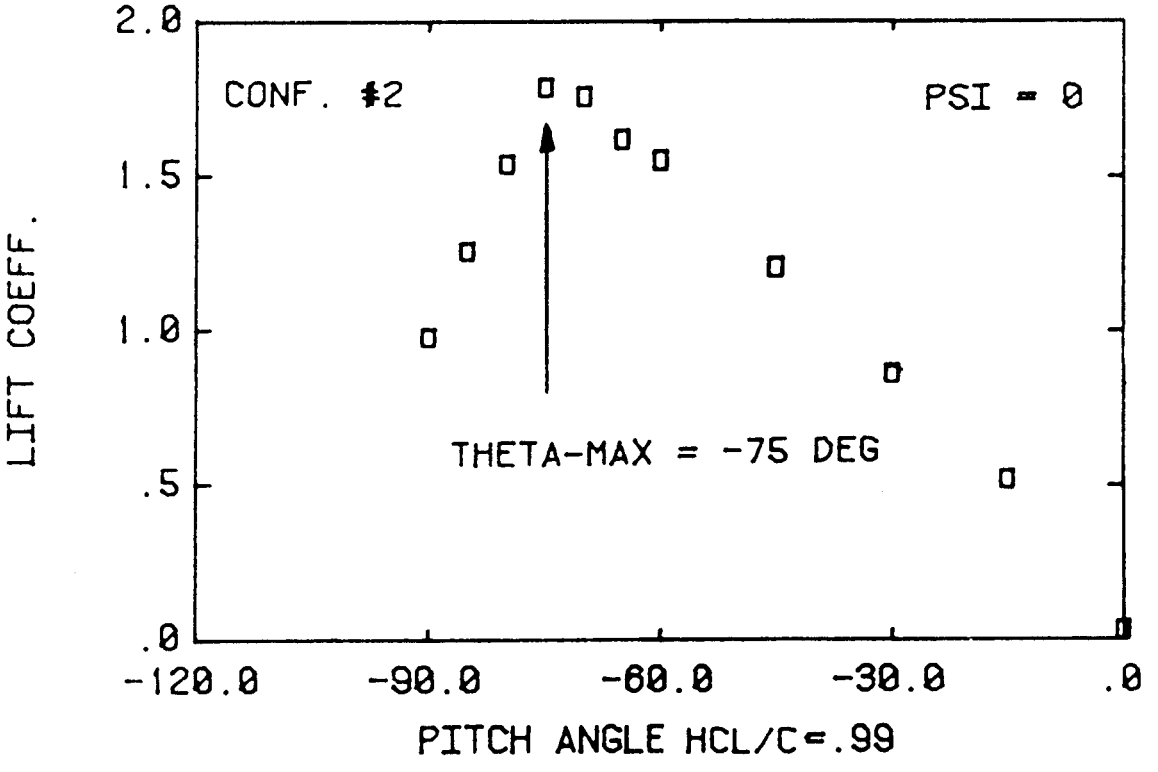

Figure 9a. Determination of θ_{max} (configurations 1-4).

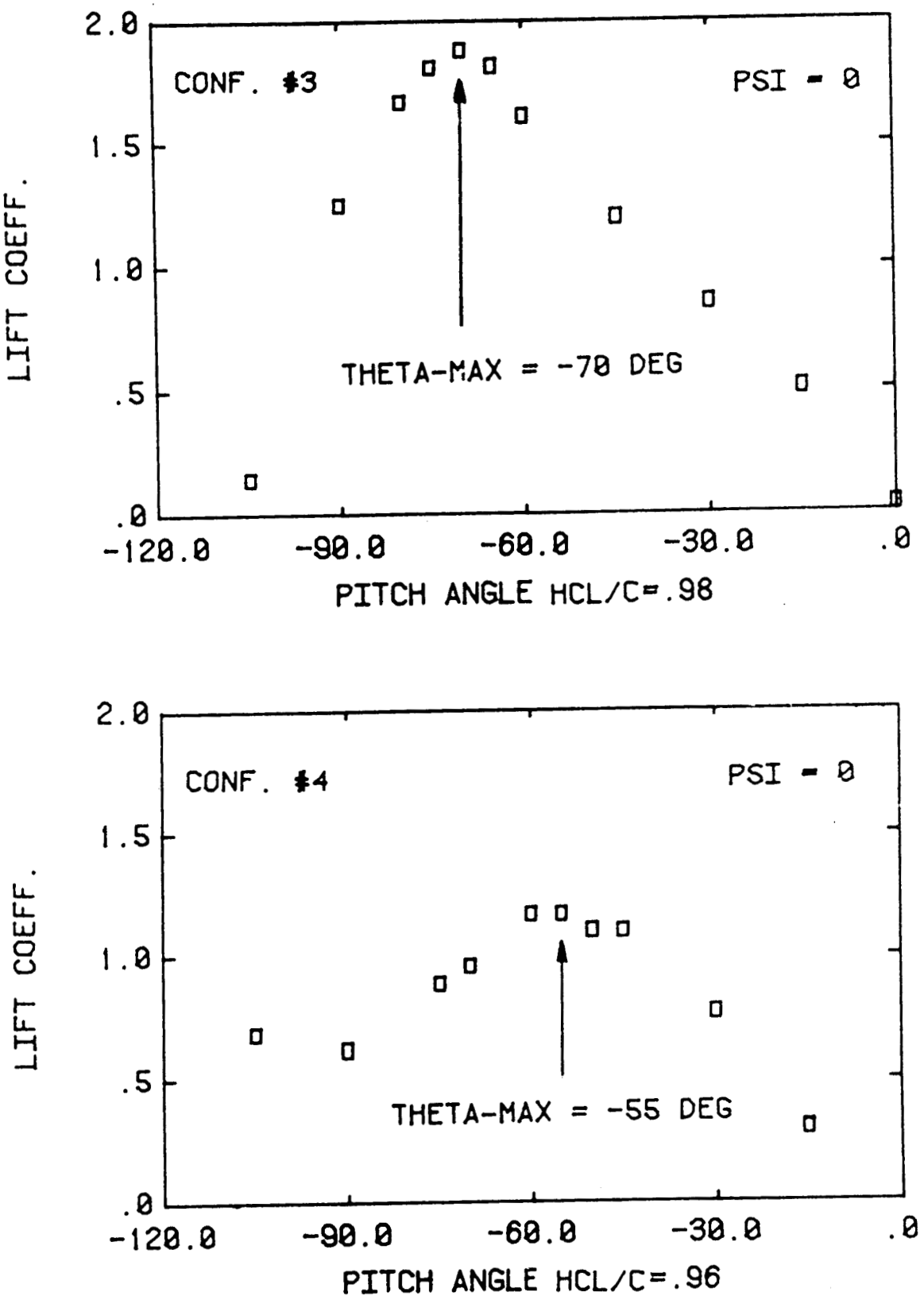

Figure 9b. Determination of θ_{max} (configurations 1-4).

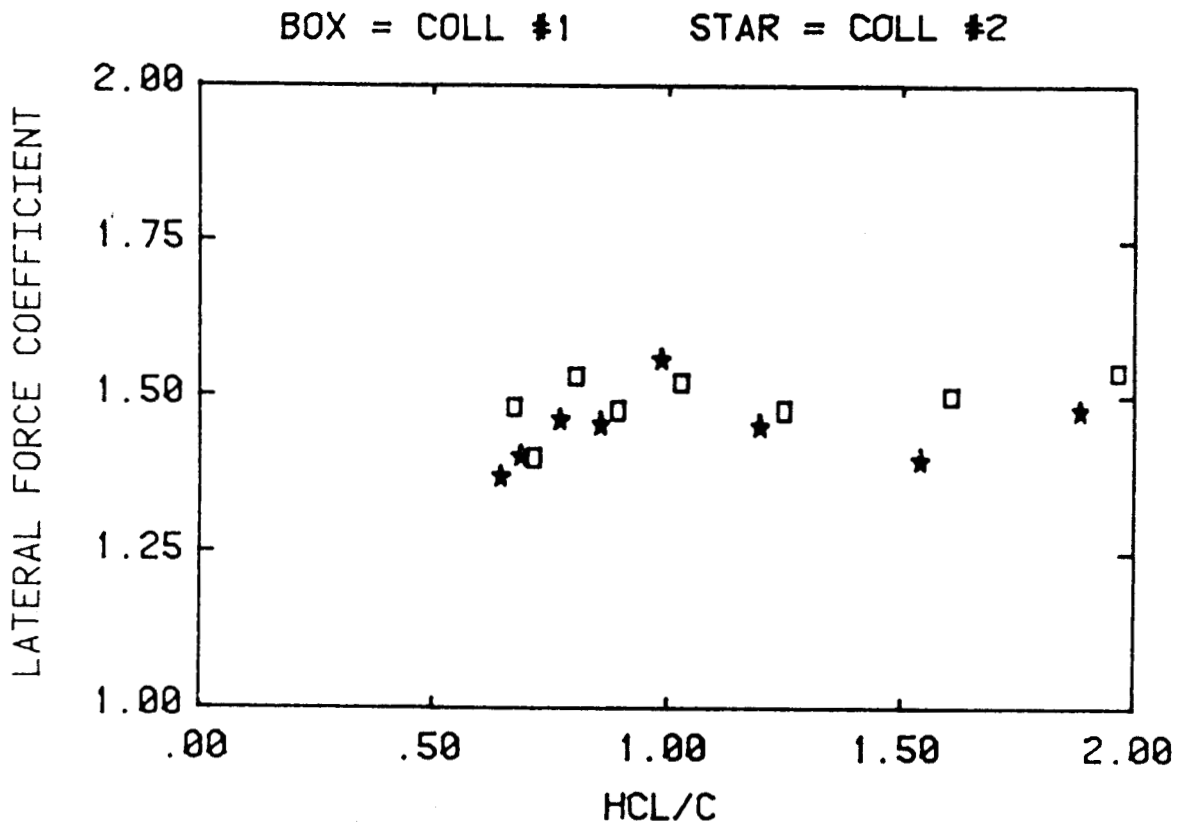

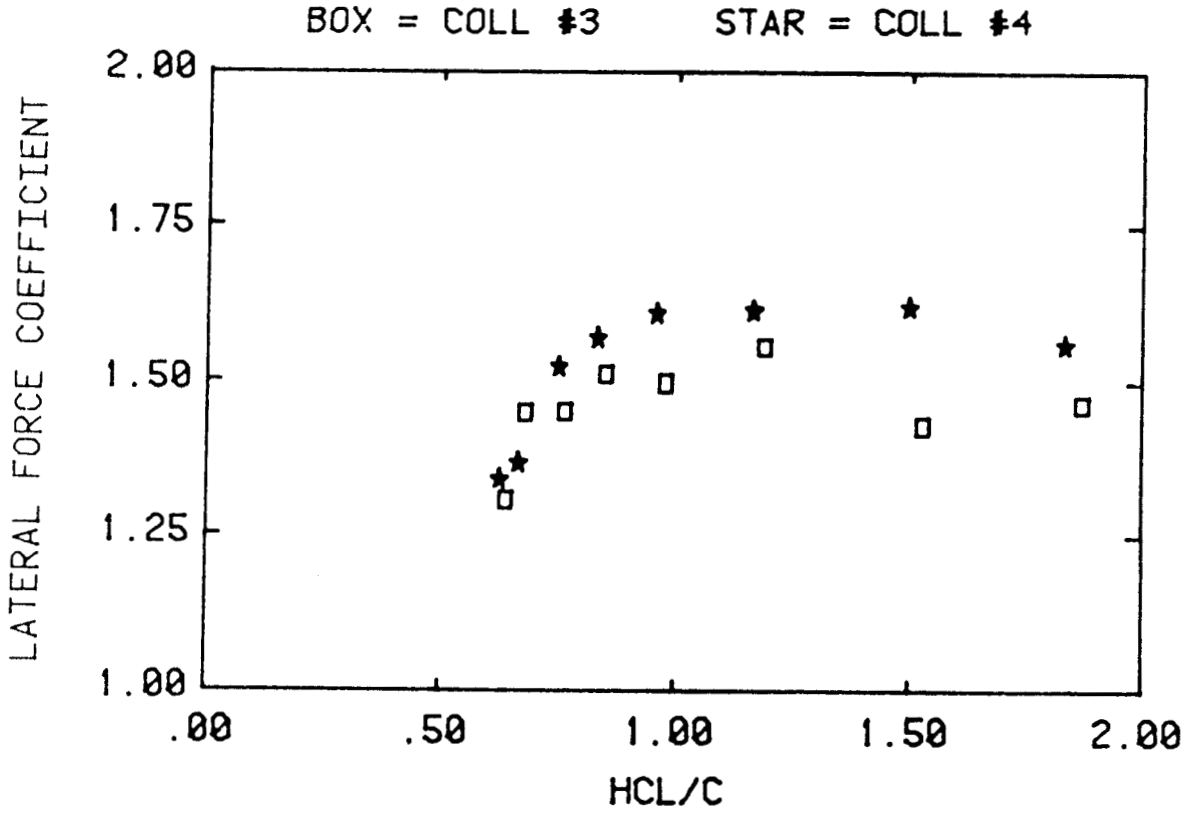

Figure 10a. Effect of height on coefficients at $\theta = 0$, $\psi = 0$ (configurations 1-4).

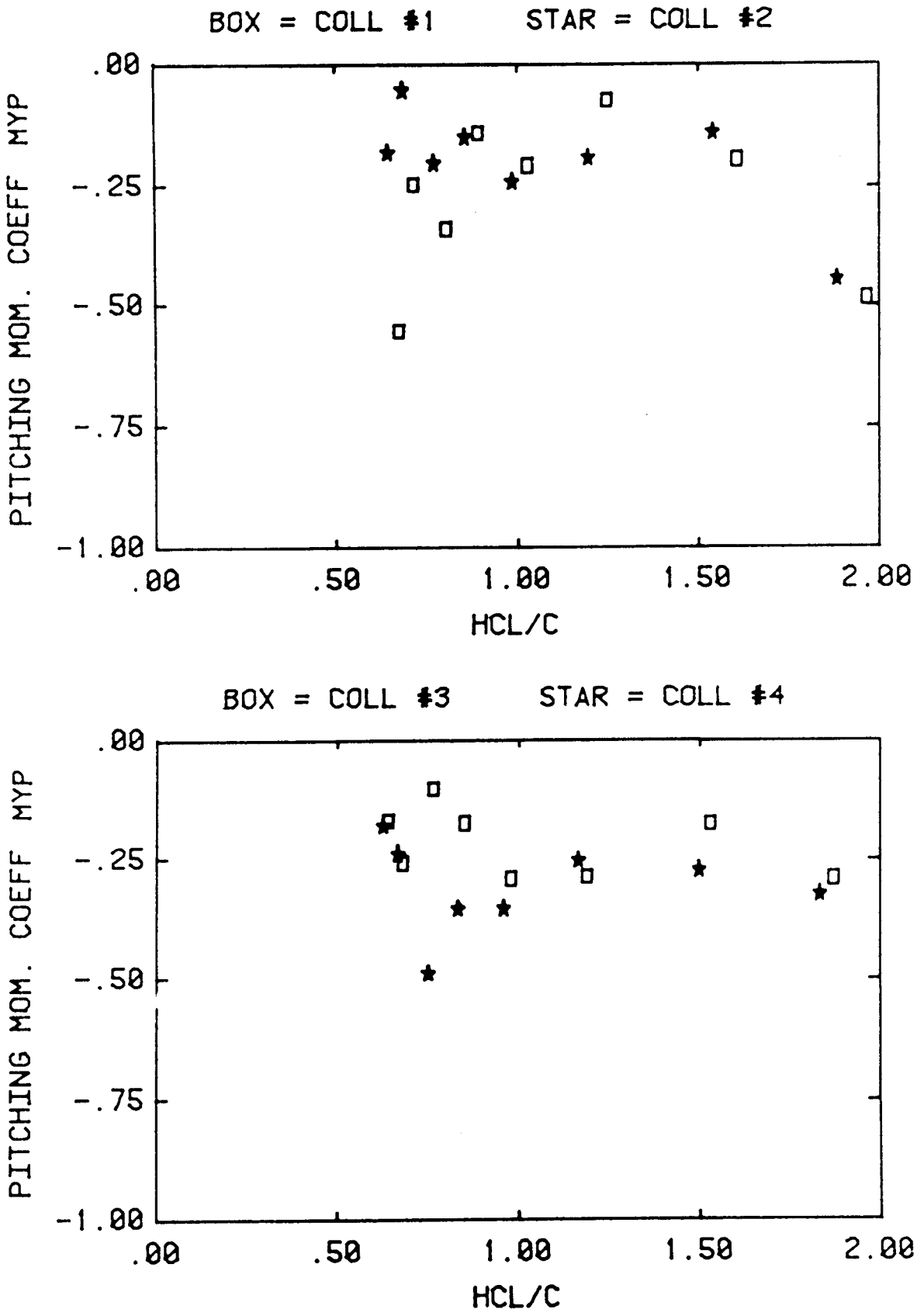

Figure 10b. Effect of height on coefficients at $\theta = 0$, $\psi = 0$ (configurations 1-4).

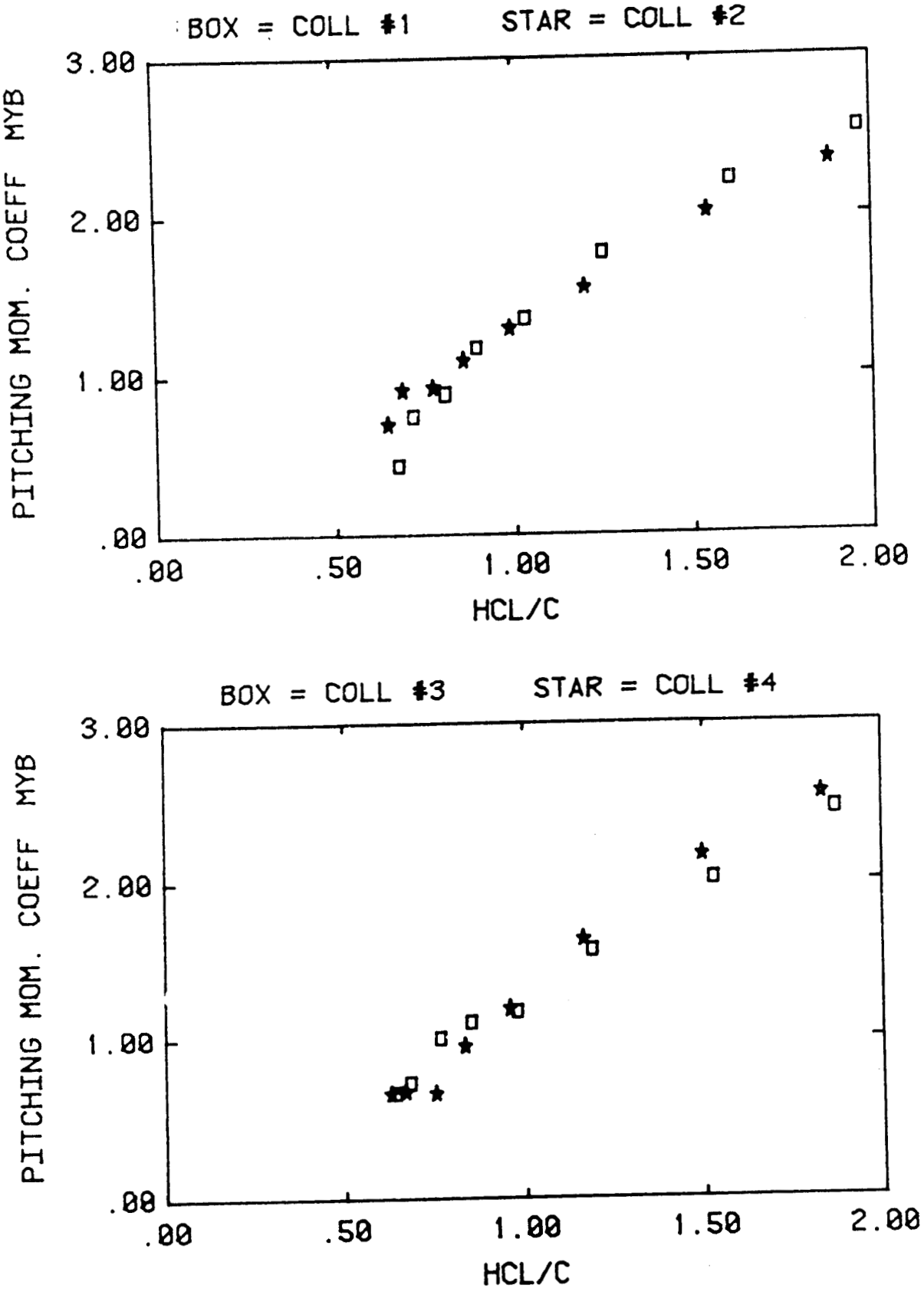

Figure 10c. Effect of height on coefficients at $\theta = 0$, $\psi = 0$ (configurations 1-4).

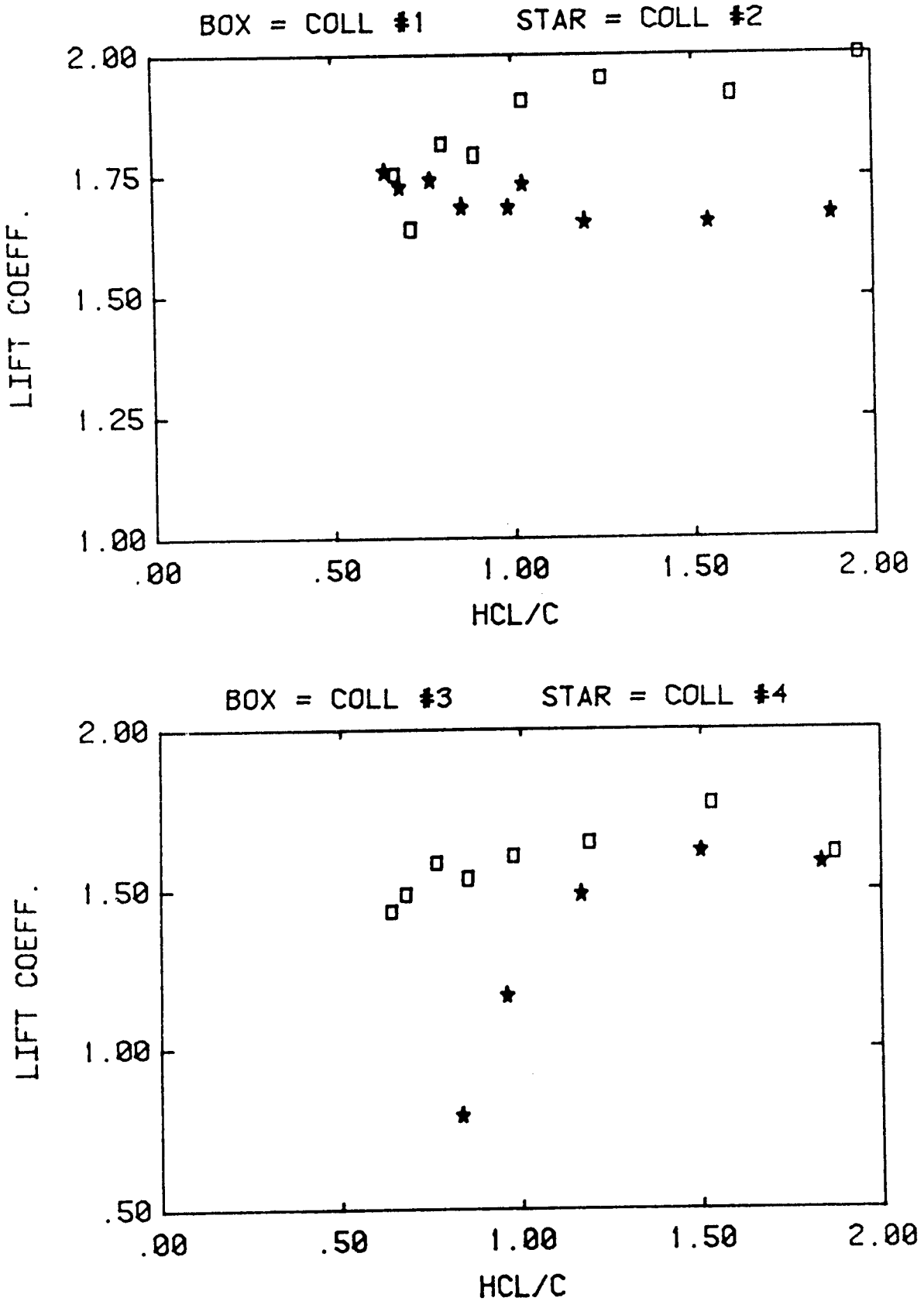

Figure 11. Effect of height on lift at θ_{max}, $\psi = 0$ (configurations 1-4).

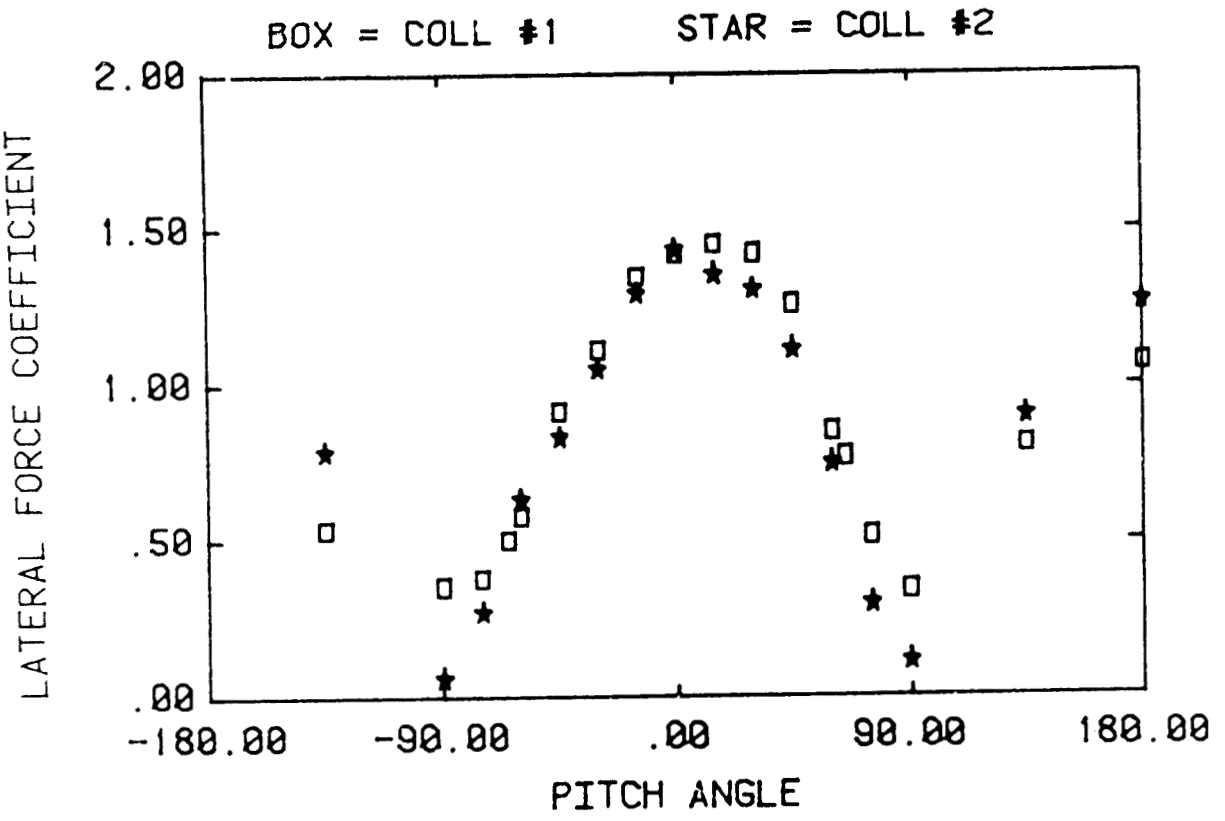

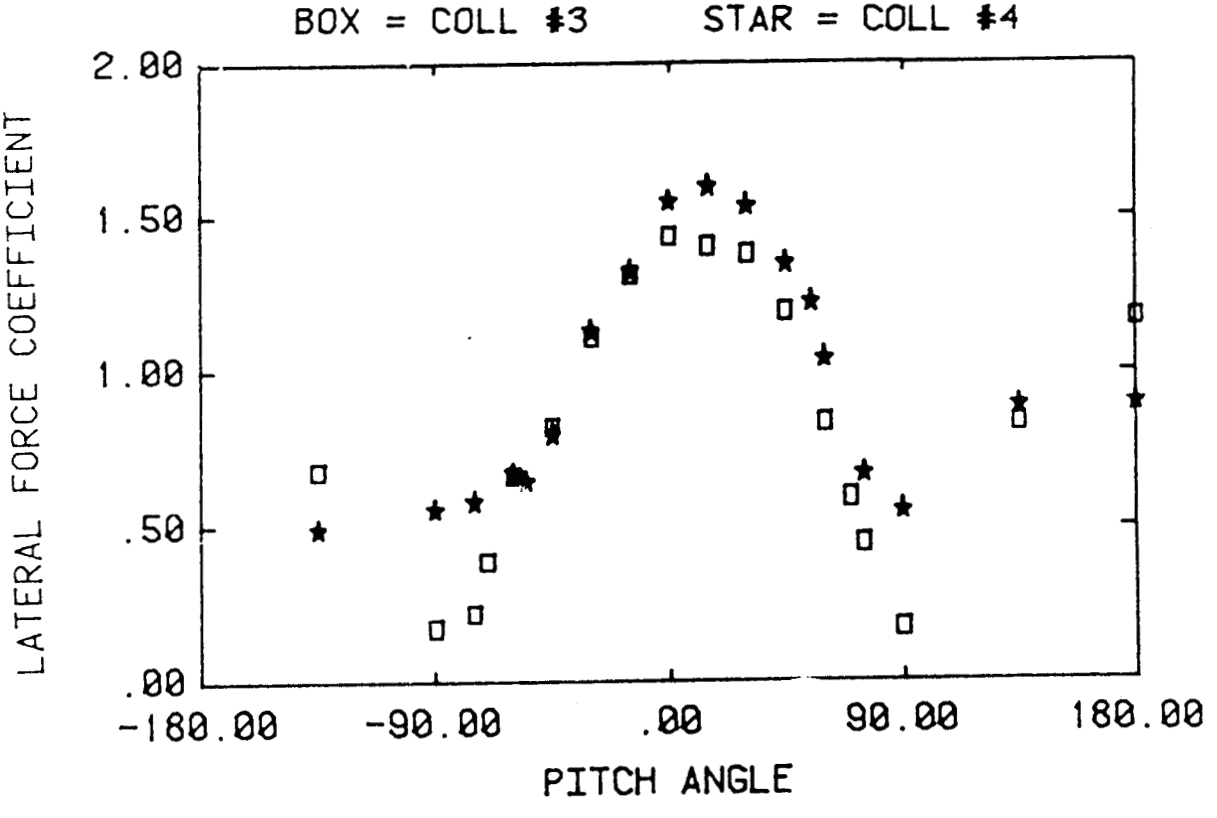

Figure 12a. Variation of single collector loads with pitch angle for HCL/C=K_I, ψ = 0 (configurations 1-4).

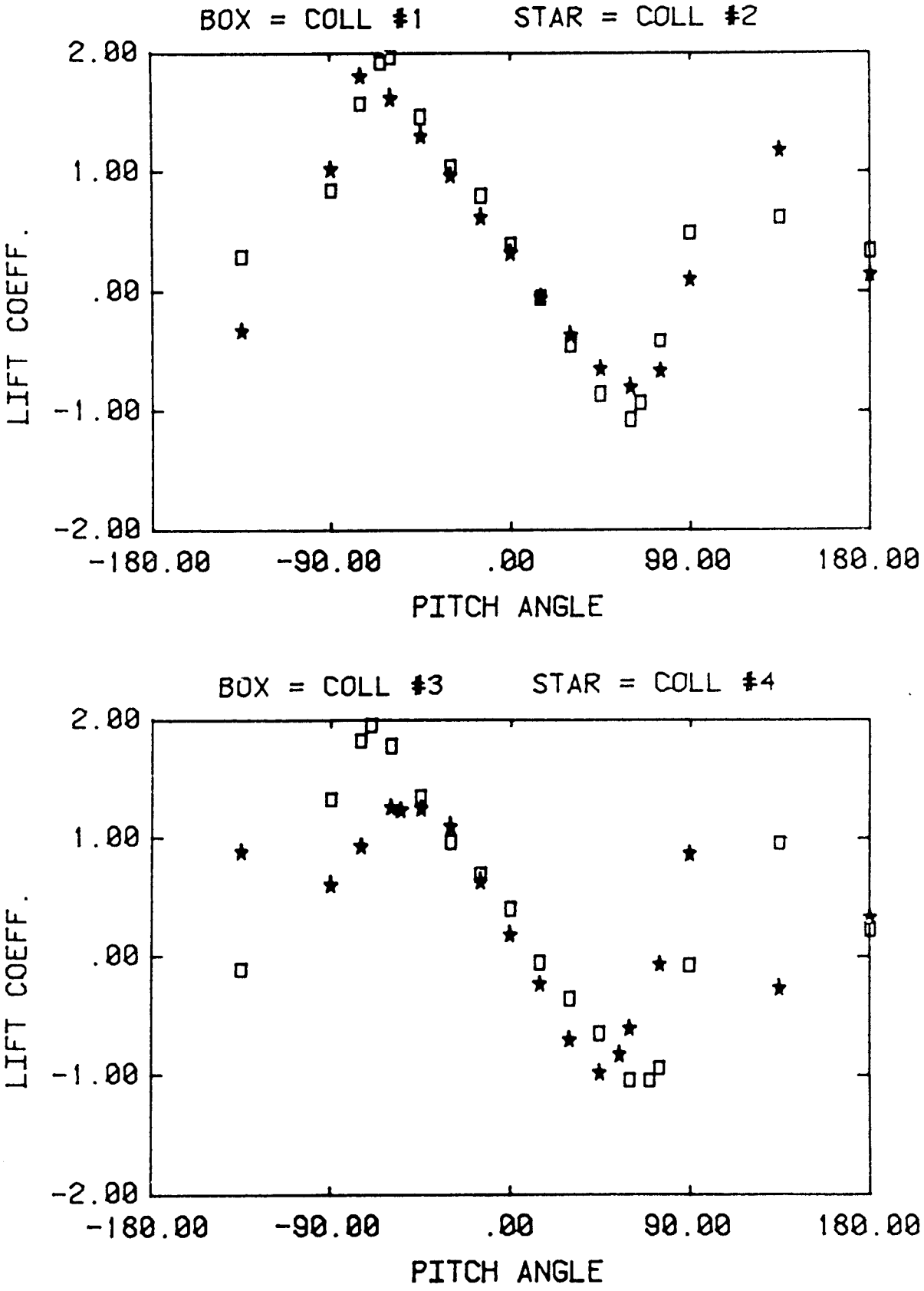

Figure 12b. Variation of single collector loads with pitch angle for HCL/C=K_I, ψ = 0 (configurations 1-4).

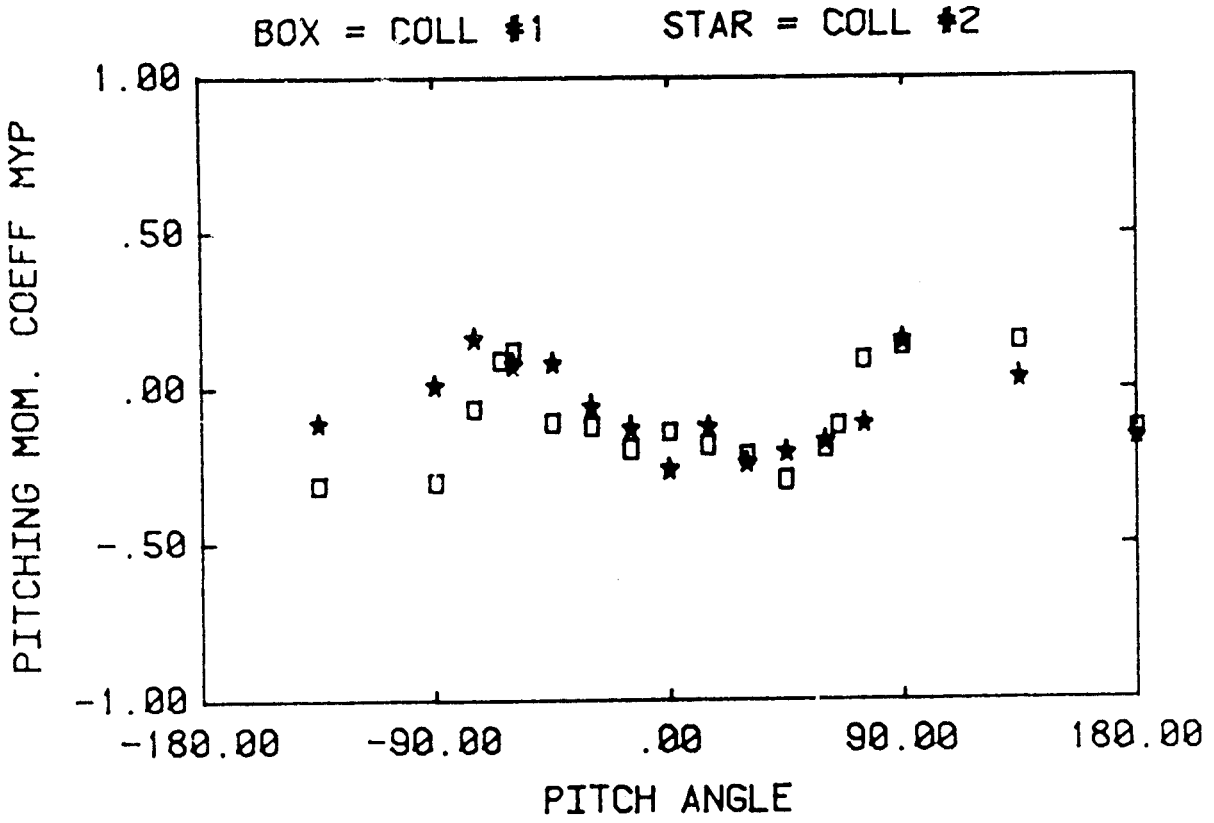

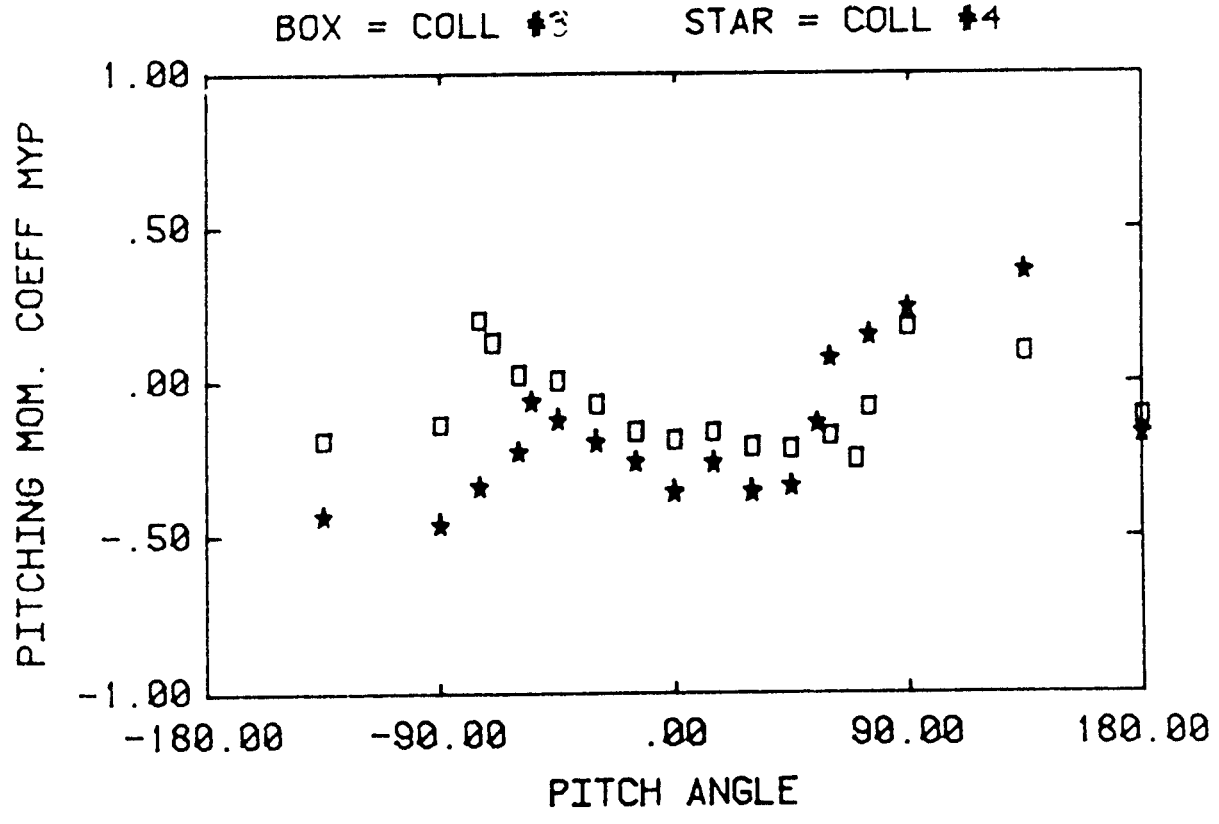

Figure 12c. Variation of single collector loads with pitch angle for HCL/C=K_I, ψ = 0 (configurations 1-4).

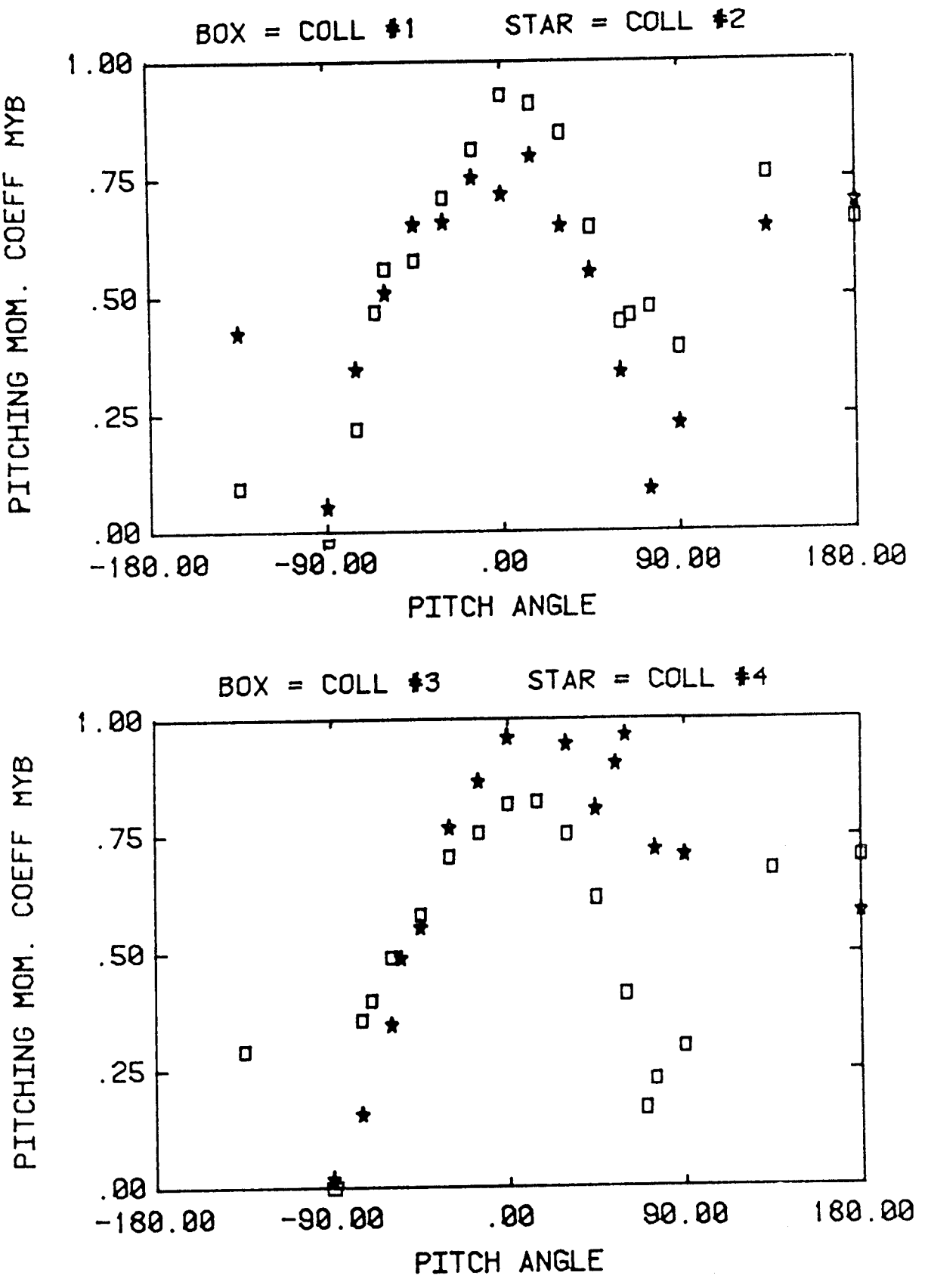

Figure 12d. Variation of single collector loads with pitch angle for HCL/C=K_I, ψ = 0 (configurations 1-4).

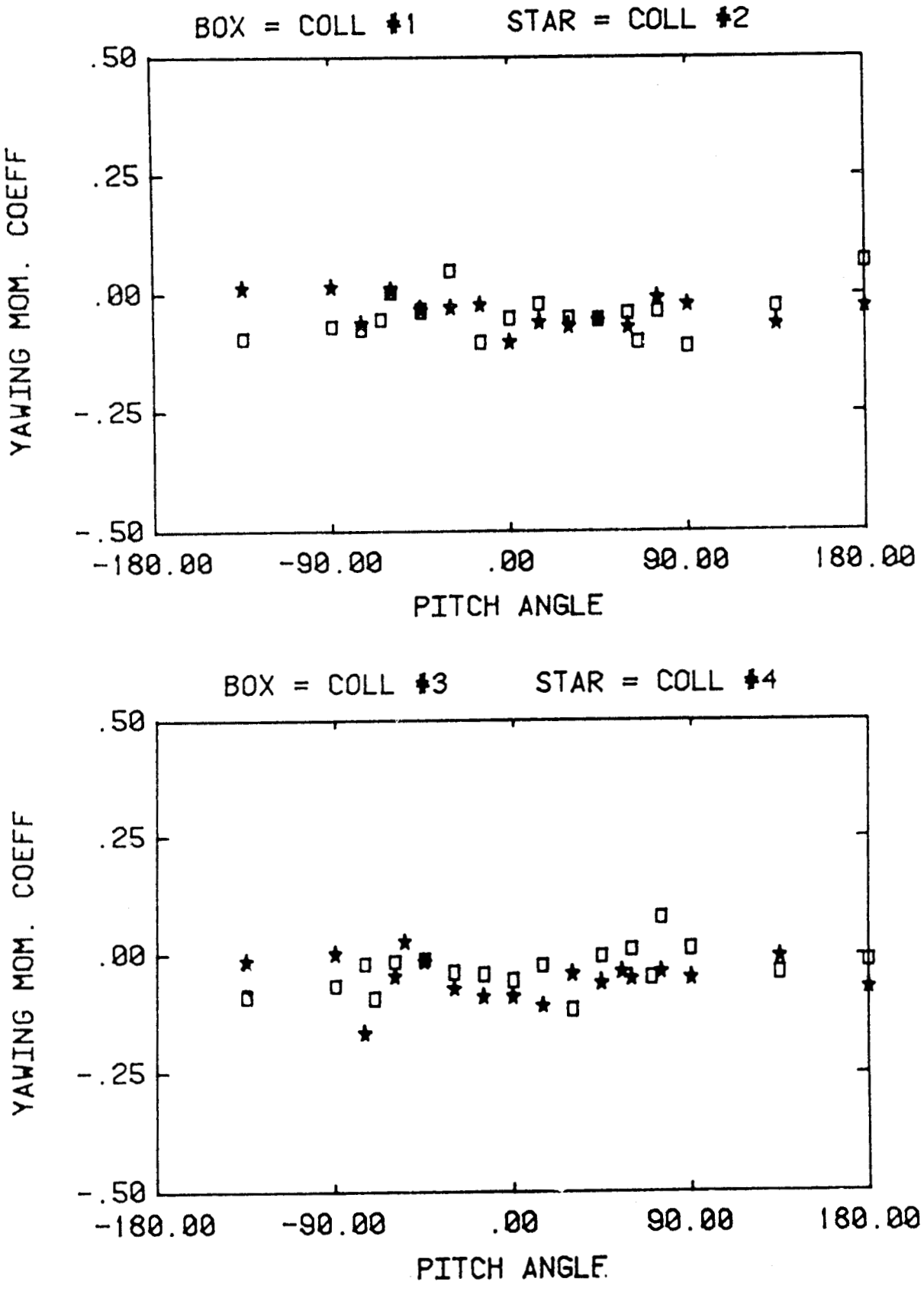

Figure 12e. Variation of single collector loads with pitch angle for HCL/C=K_I, ψ = 0 (configurations 1-4).

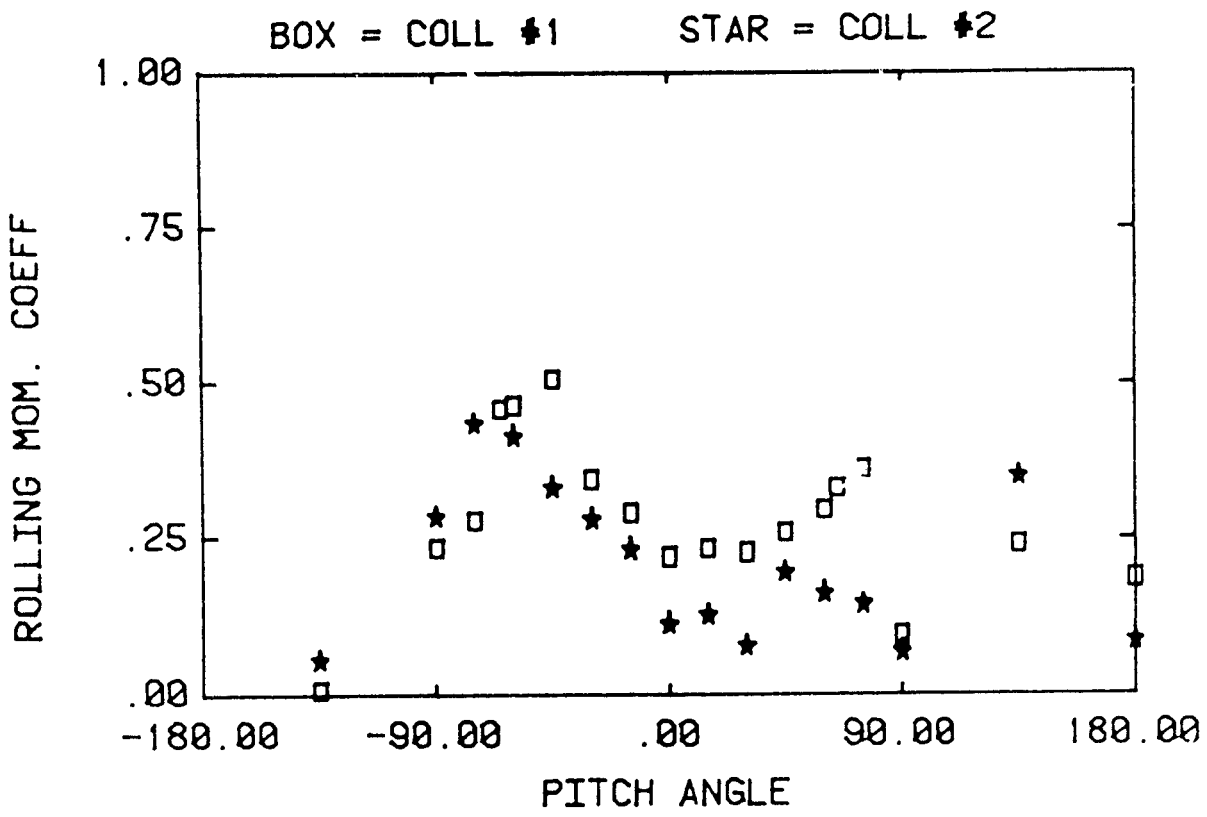

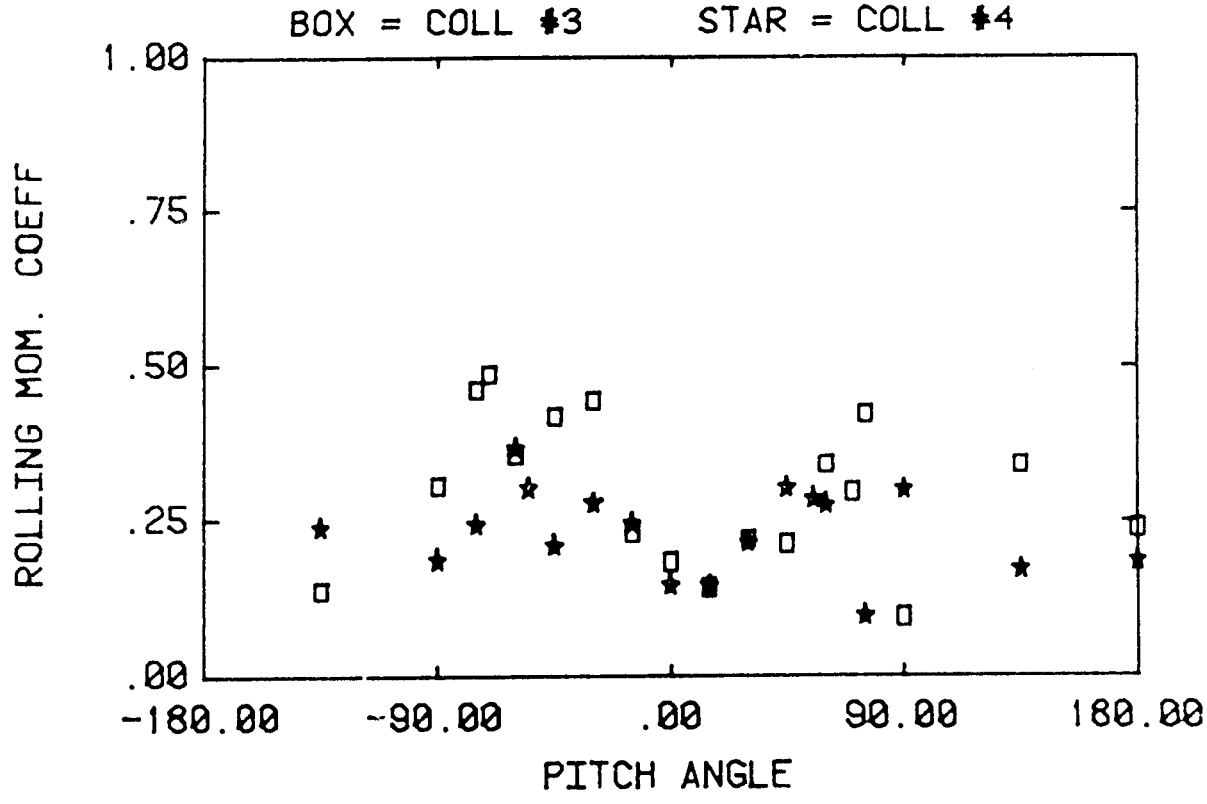

Figure 12f. Variation of single collector loads with pitch angle for HCL/C=K_I, ψ = 0 (configurations 1-4).

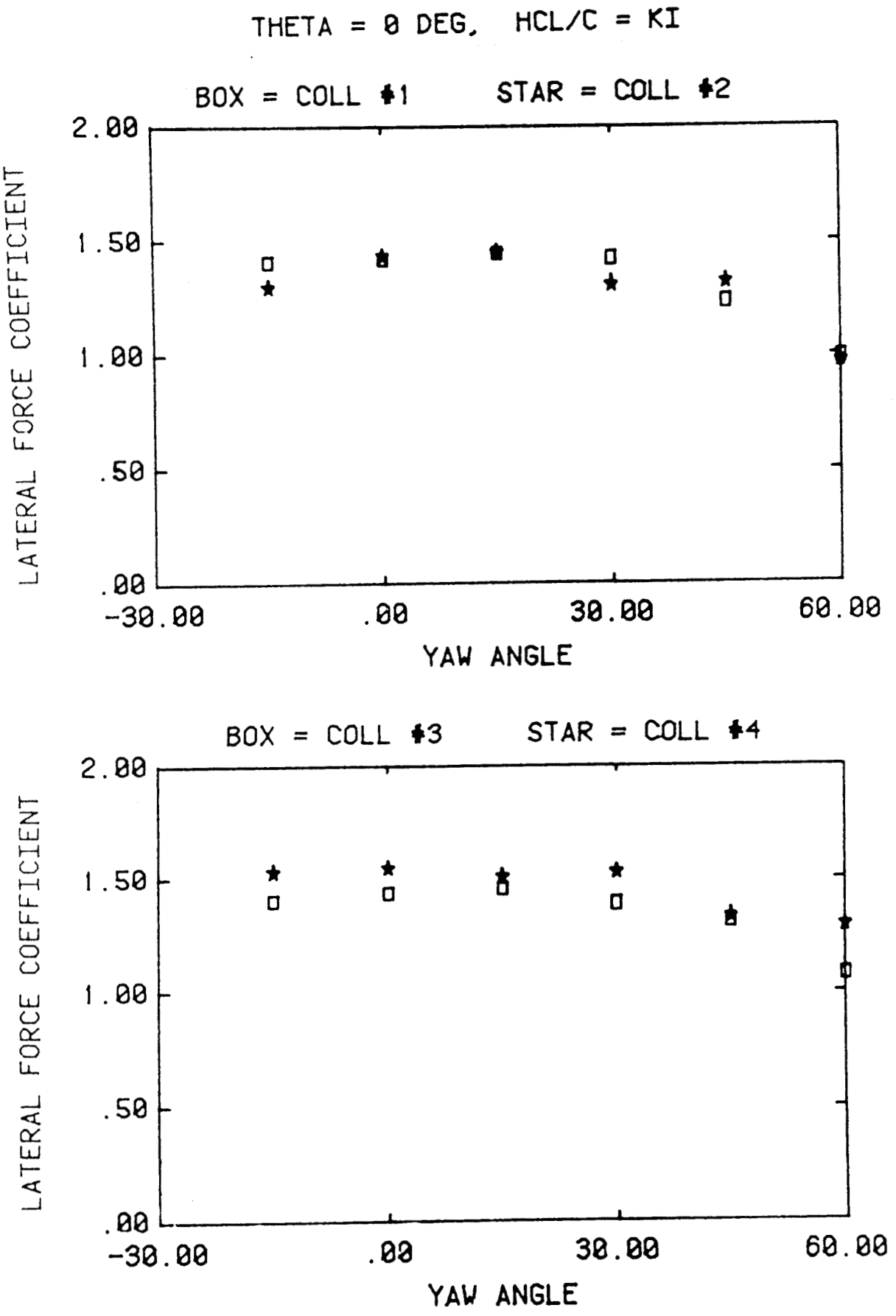

Figure 13a. Variation of single collector loads with yaw angle for HCL/C=K_I, (configurations 1-4).

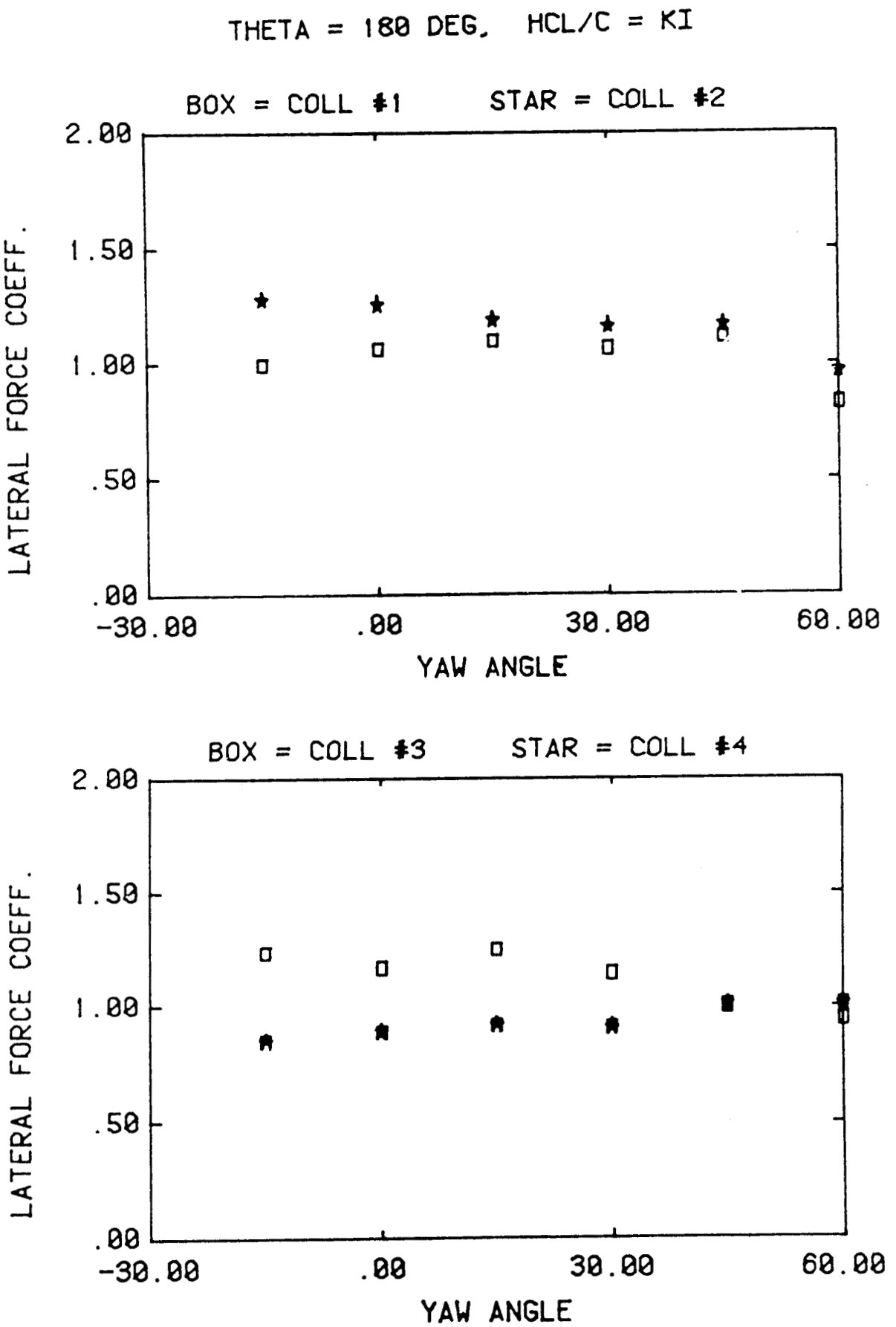

Figure 13b. Variation of single collector loads with yaw angle for HCL/C=K_I, (configurations 1-4).

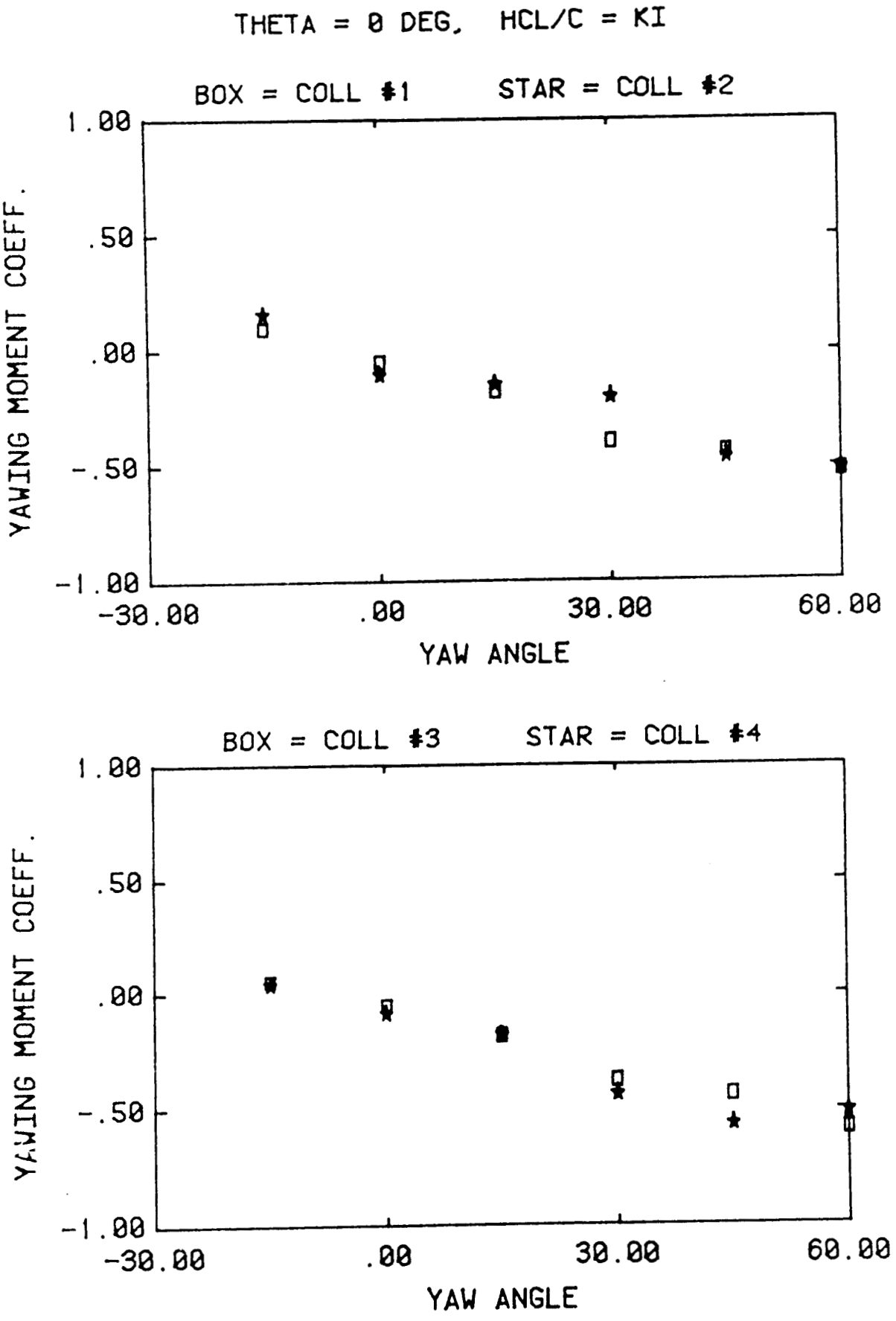

Figure 13c. Variation of single collector loads with yaw angle for HCL/C=K_I, (configurations 1-4).

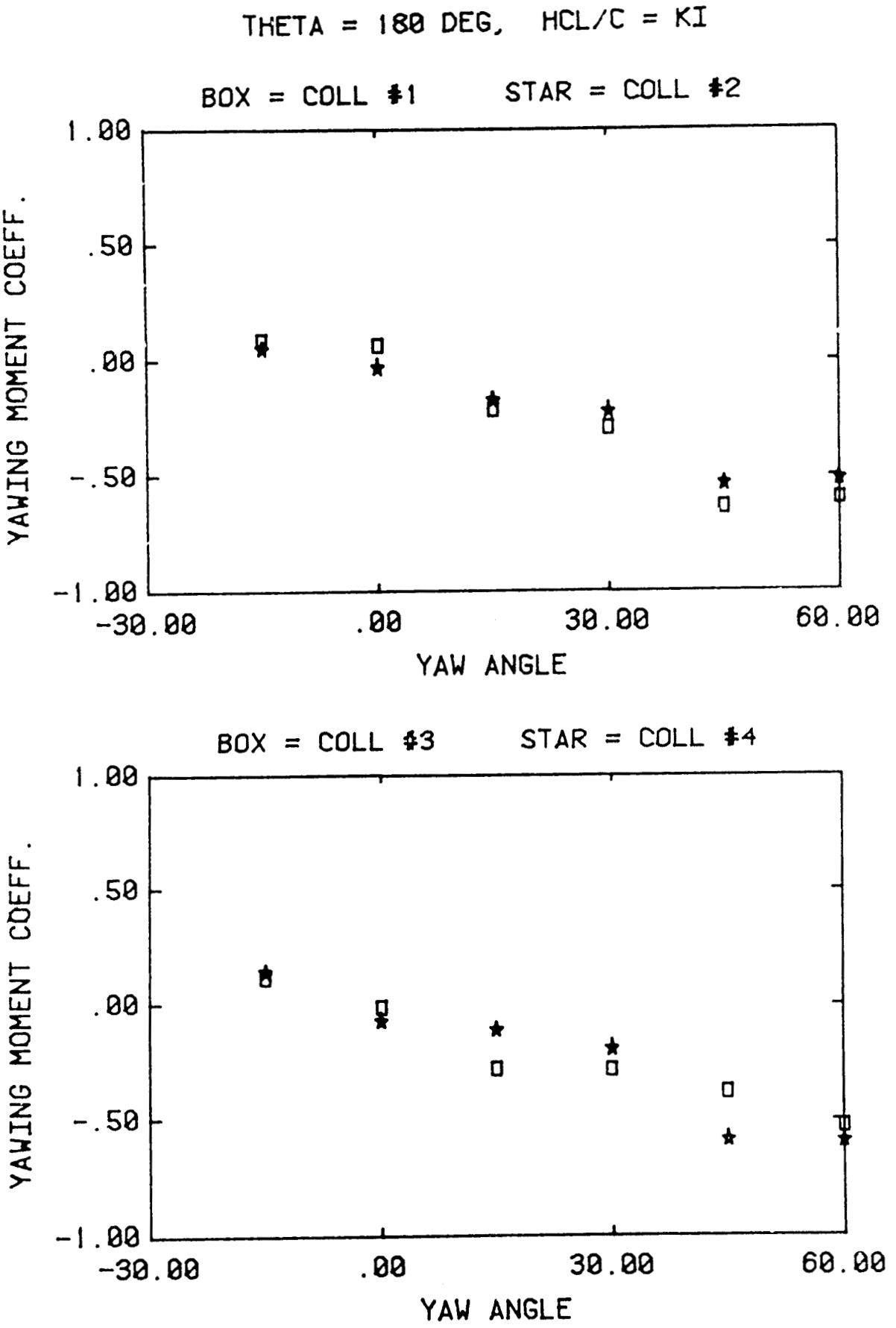

Figure 13d. Variation of single collector loads with yaw angle for HCL/C=K_I, (configurations 1-4).

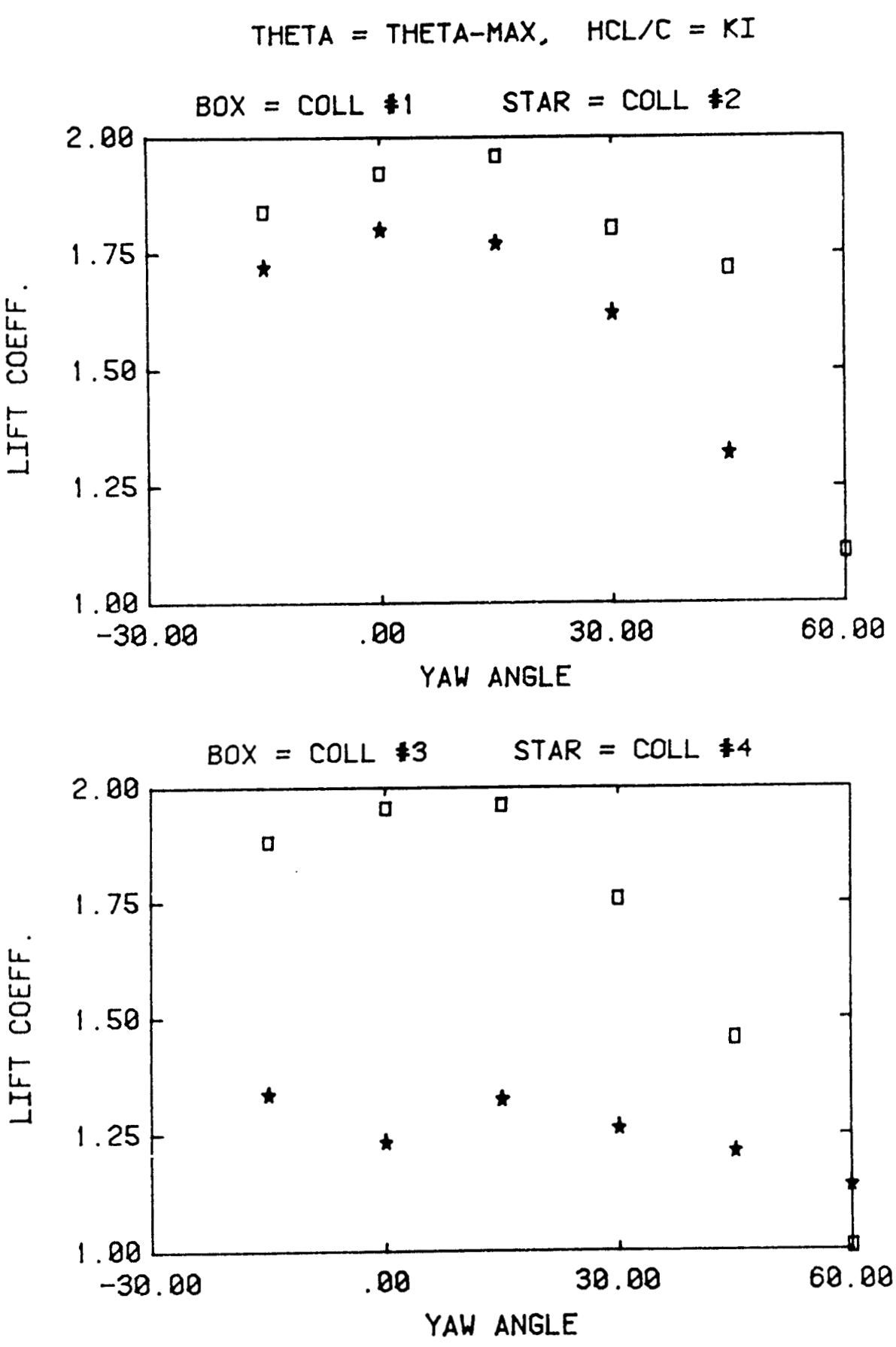

Figure 13e. Variation of single collector loads with yaw angle for HCL/C=K_I, (configurations 1-4).

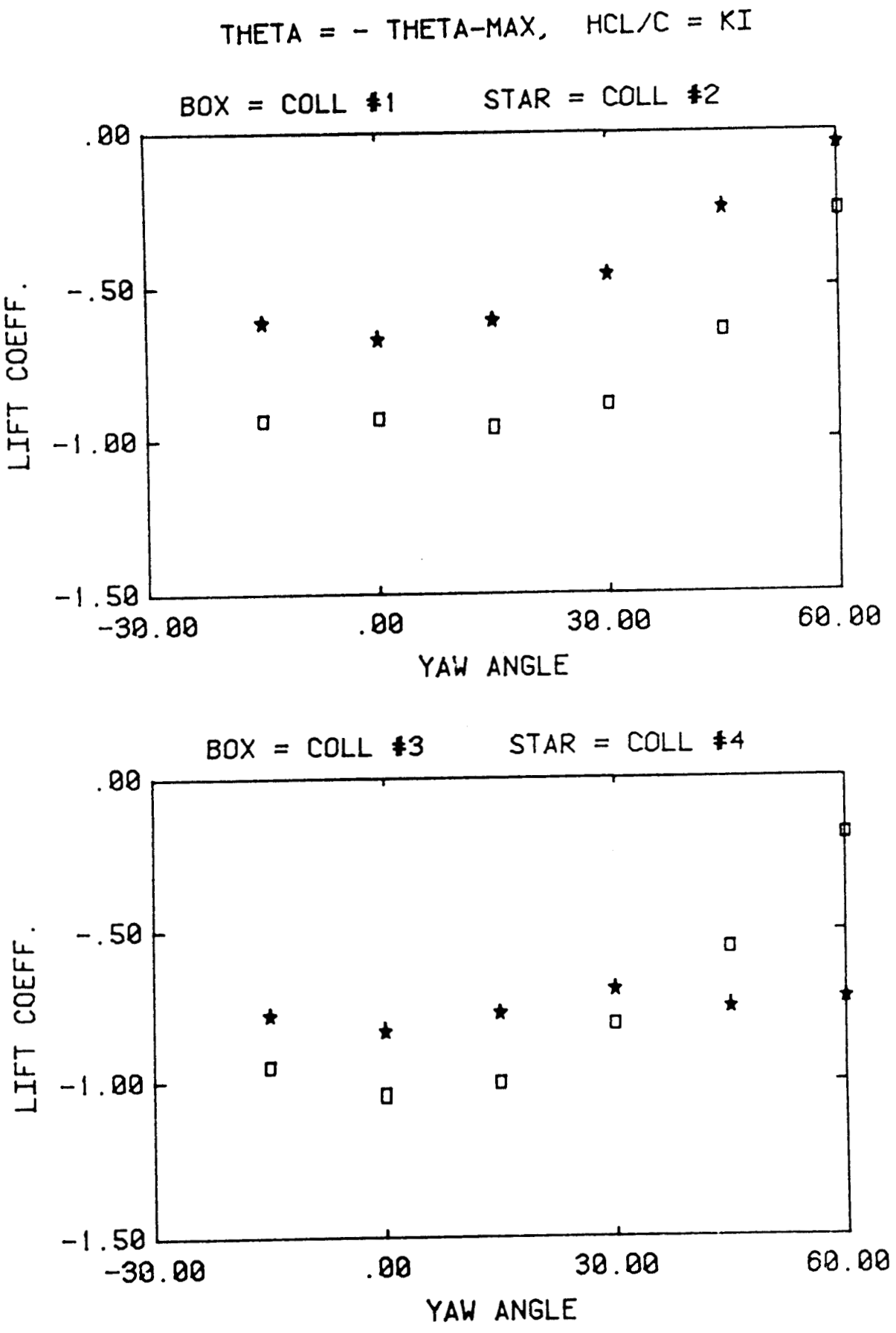

Figure 13f. Variation of single collector loads with yaw angle for HCL/C=K_I, (configurations 1-4).

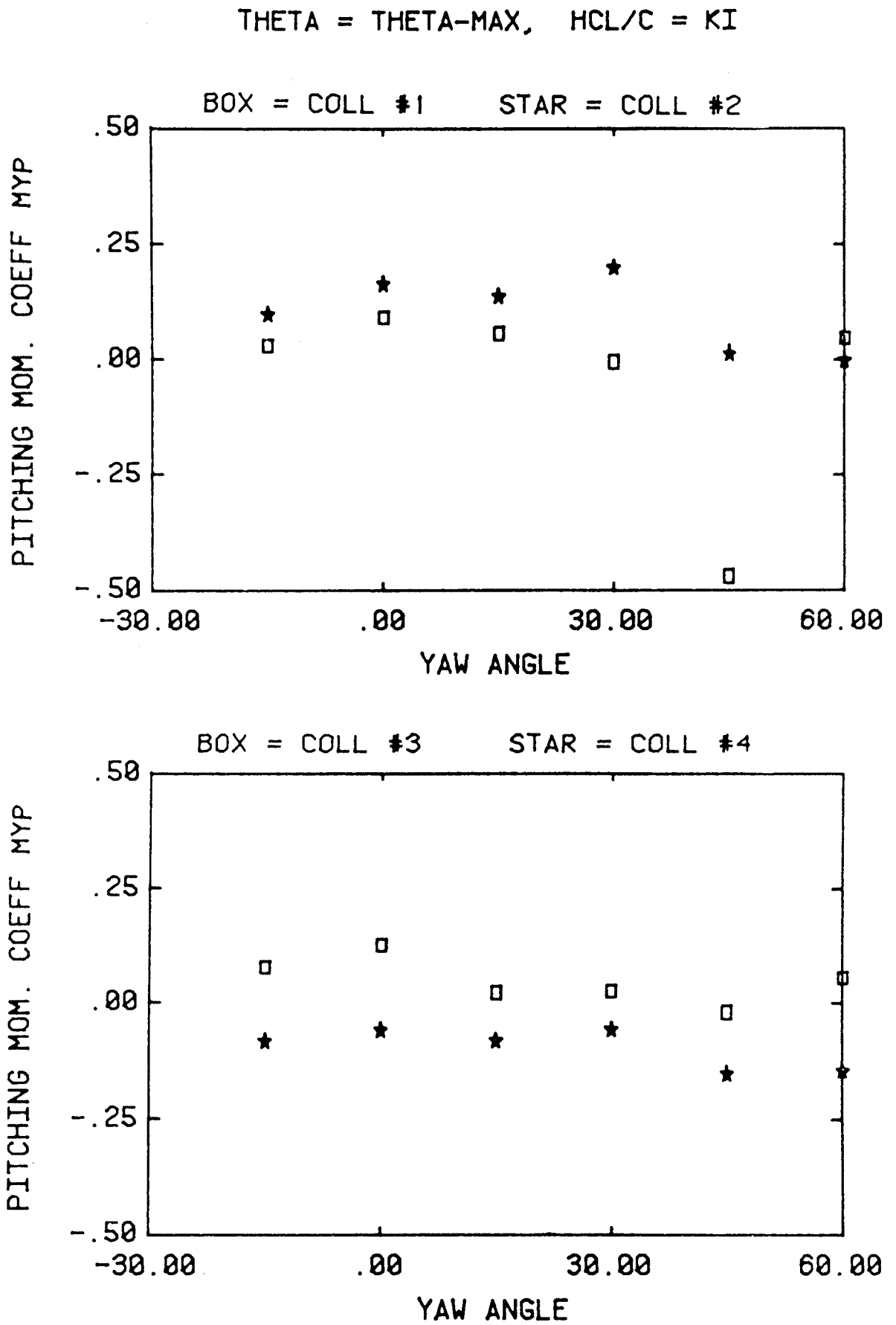

Figure 13g. Variation of single collector loads with yaw angle for HCL/C=K_I, (configurations 1-4).

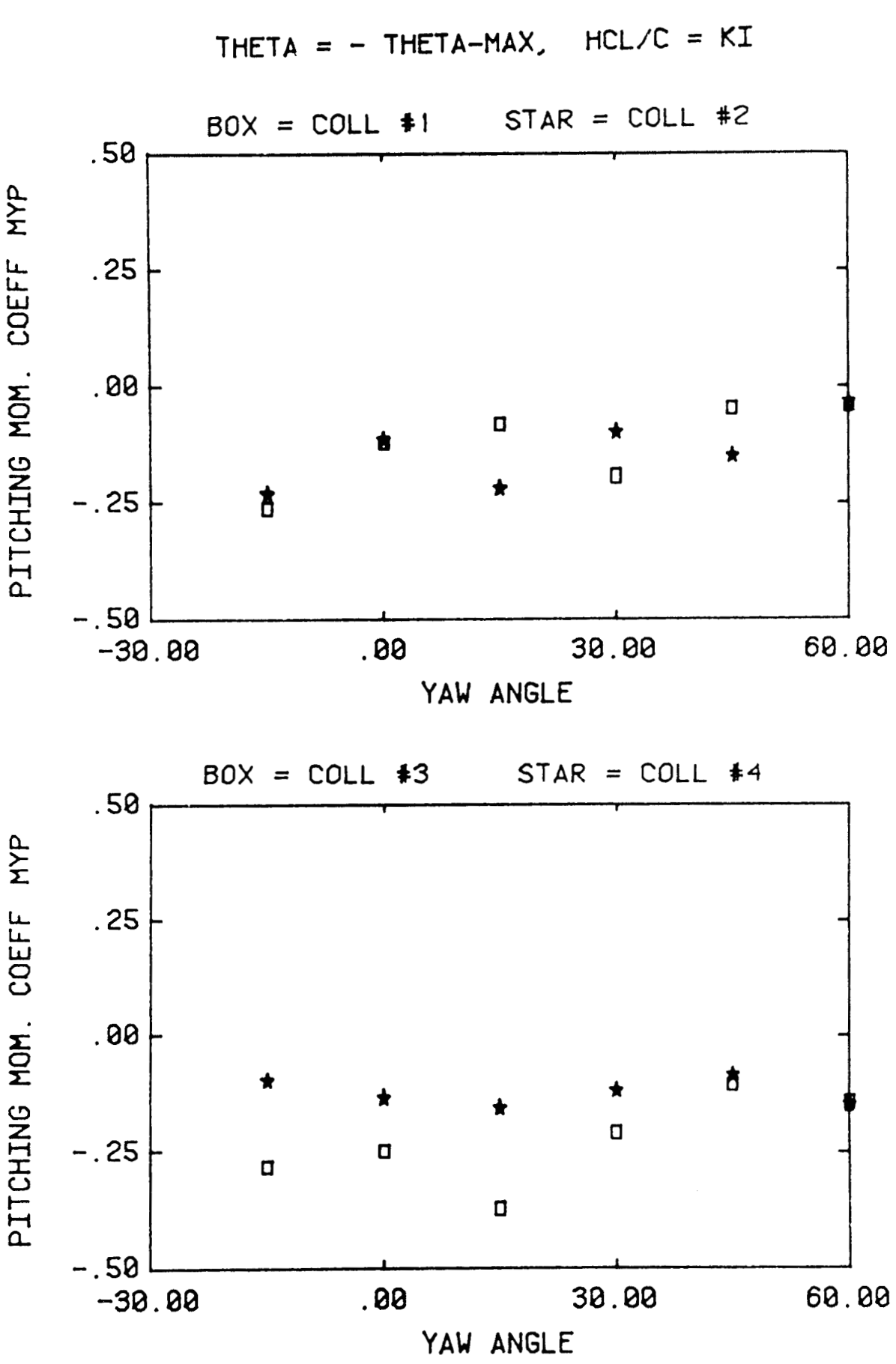

Figure 13h. Variation of single collector loads with yaw angle for HCL/C=K_I, (configurations 1-4).

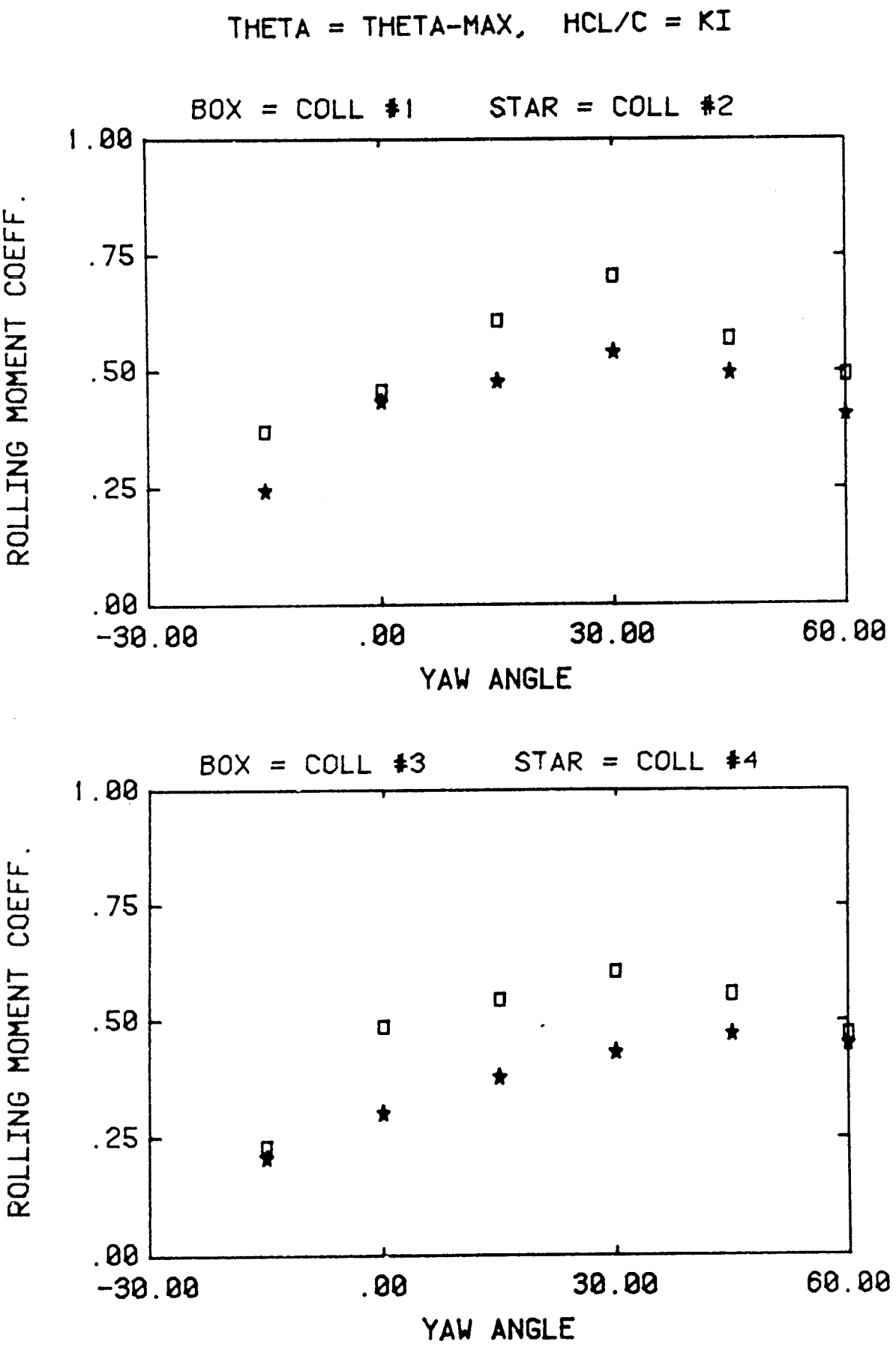

Figure 13i. Variation of single collector loads with yaw angle for HCL/C=K_I, (configurations 1-4).

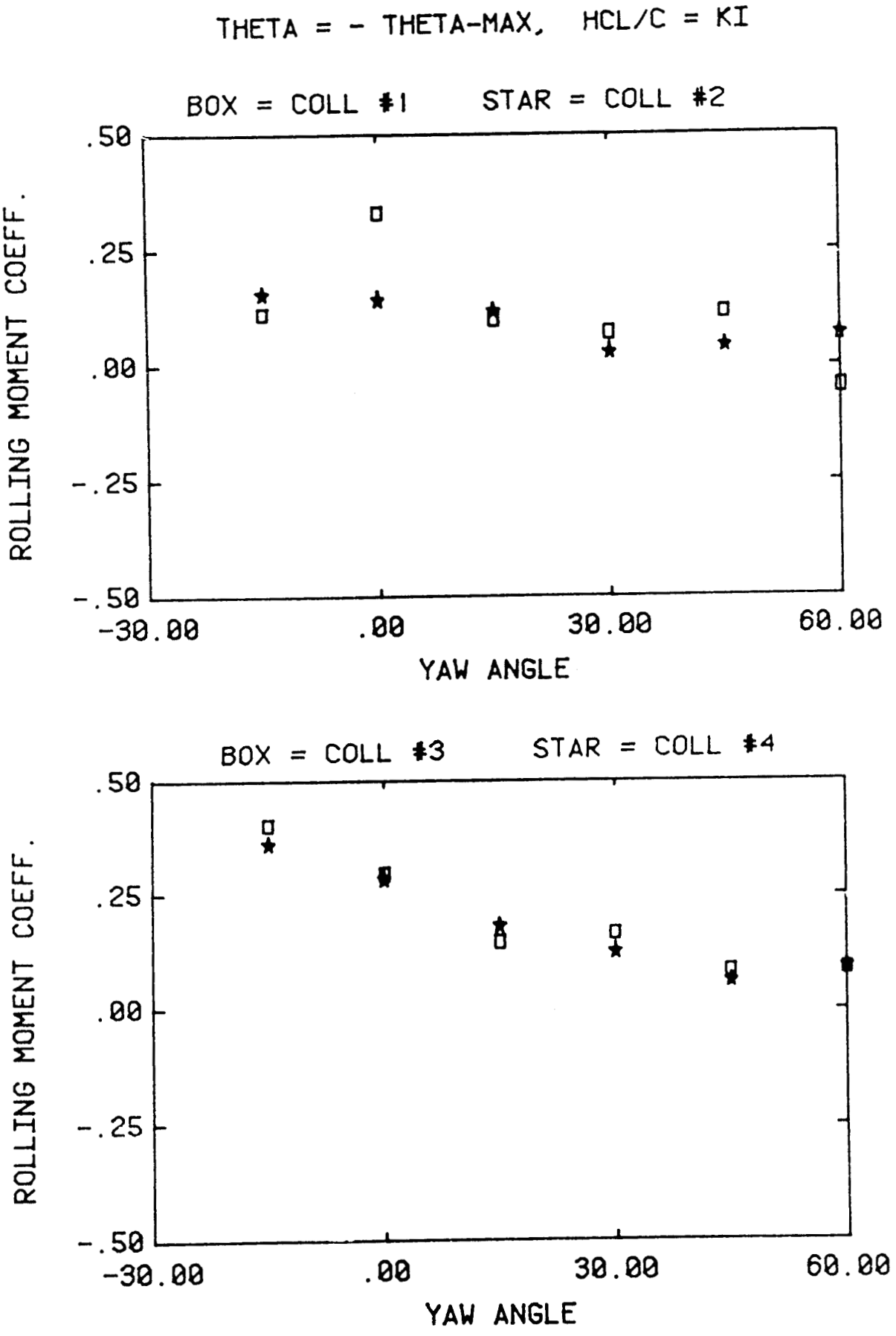

Figure 13j. Variation of single collector loads with yaw angle for HCL/C=K_I, (configurations 1-4).

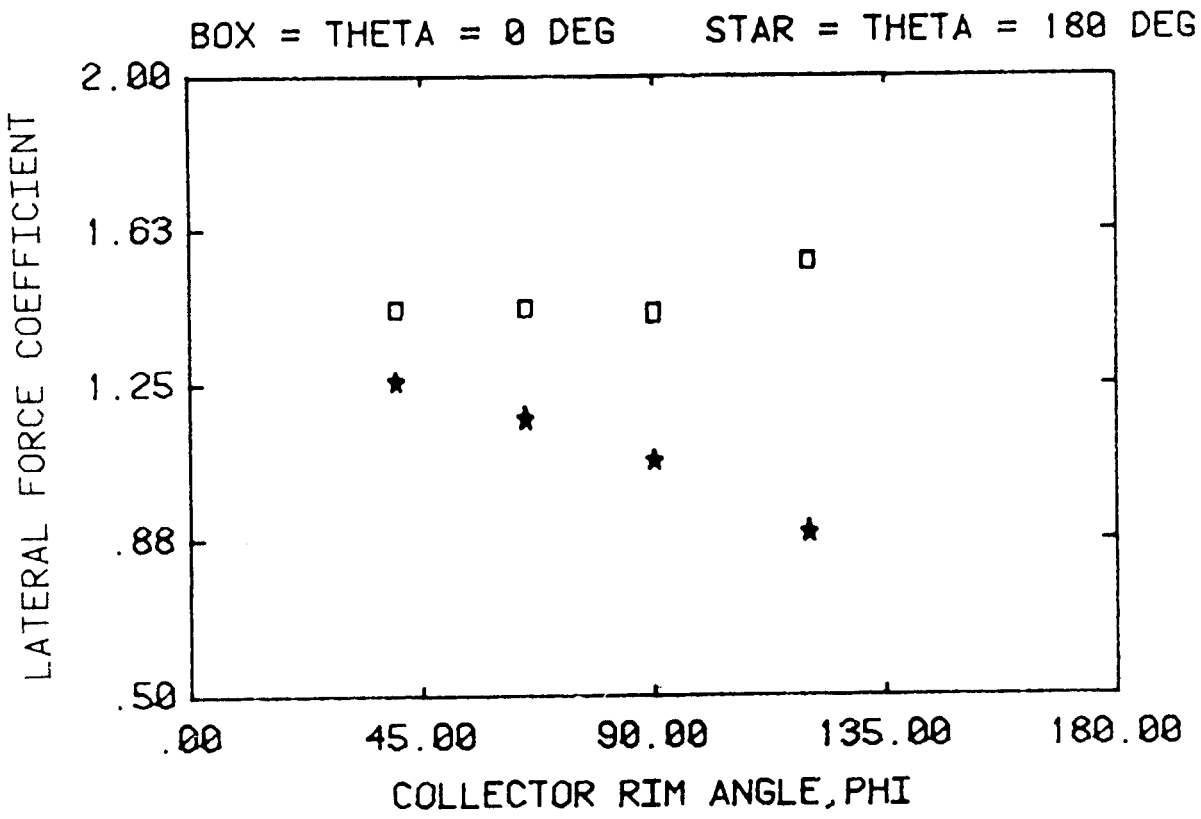

Figure 14a. Effect on the rim angle ϕ on collector loads.

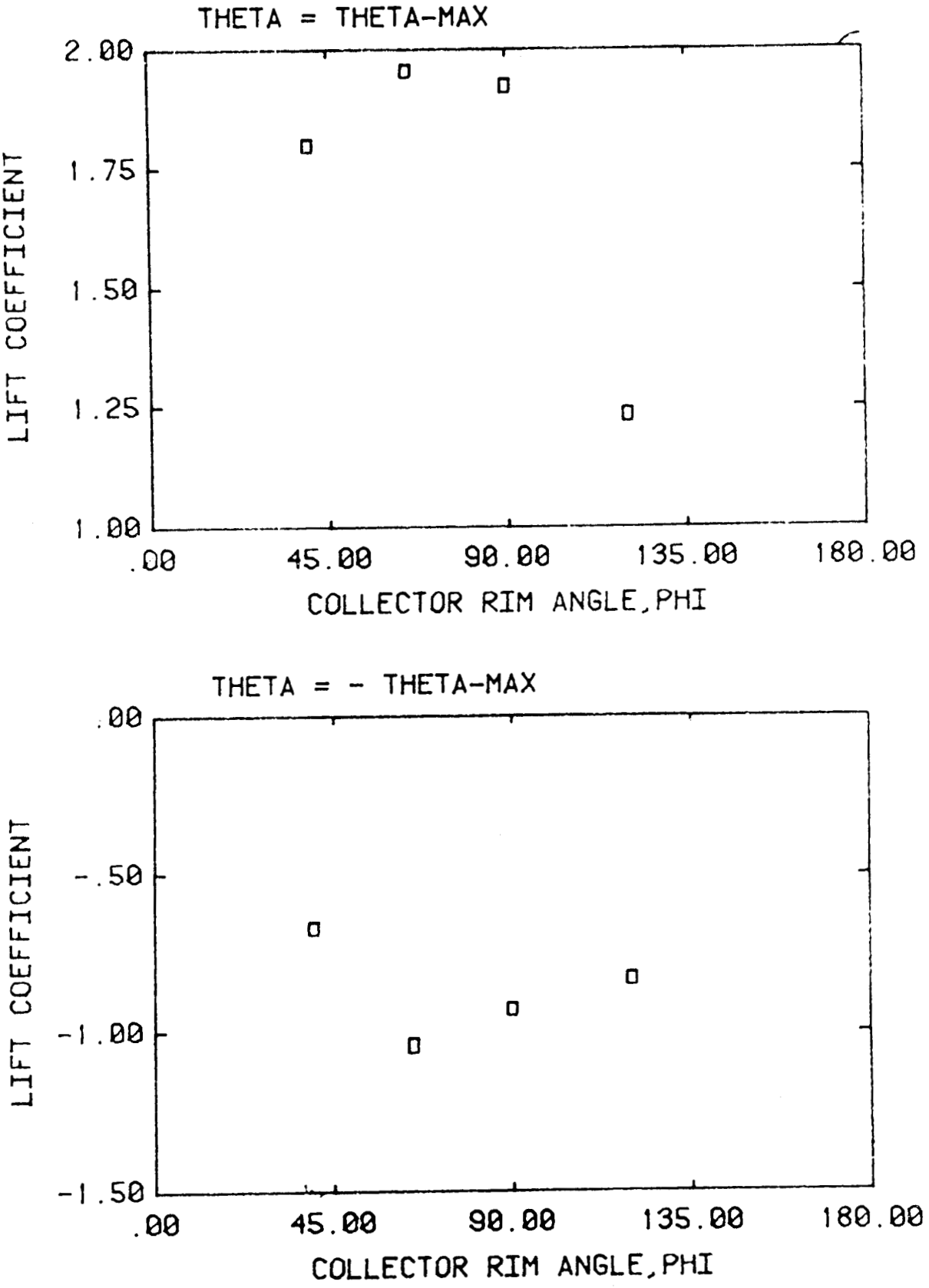

Figure 14b. Effect on the rim angle ϕ on collector loads.

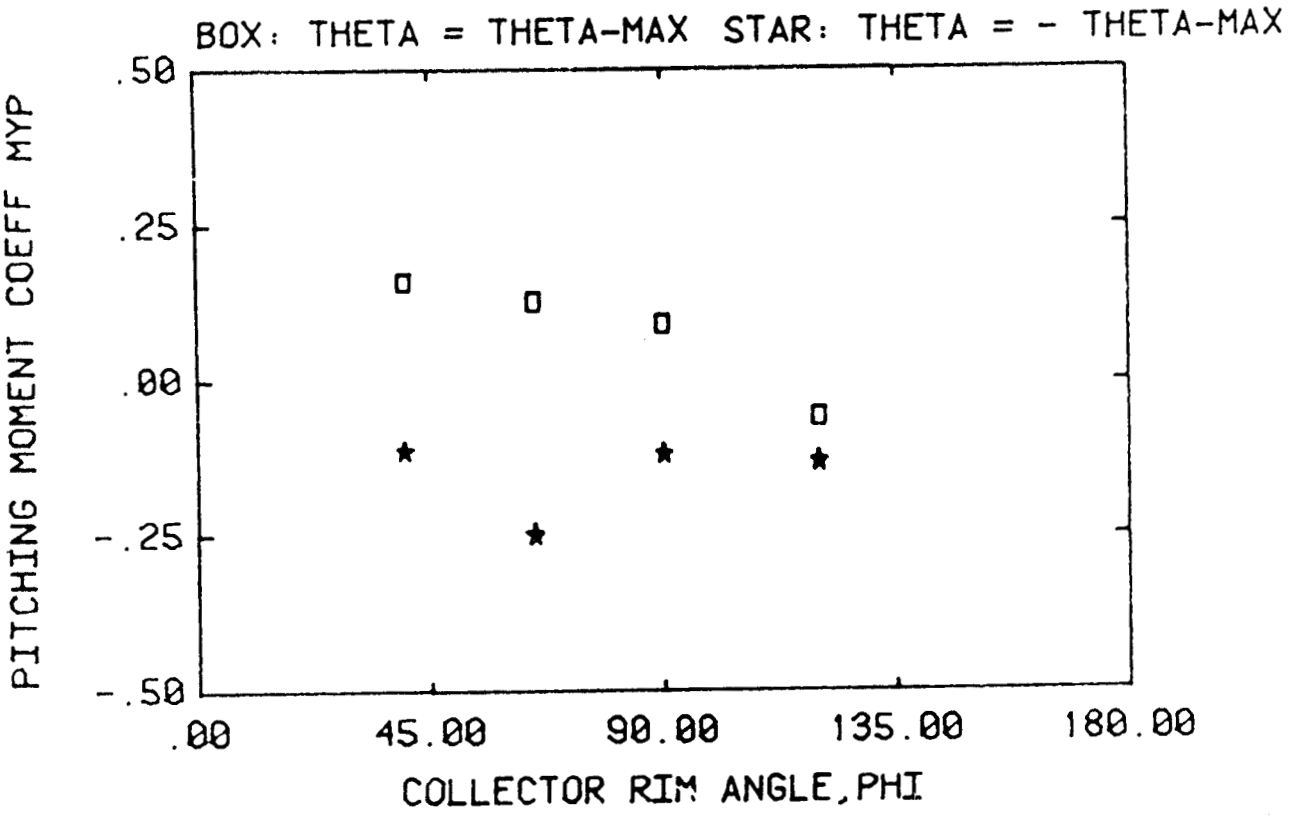

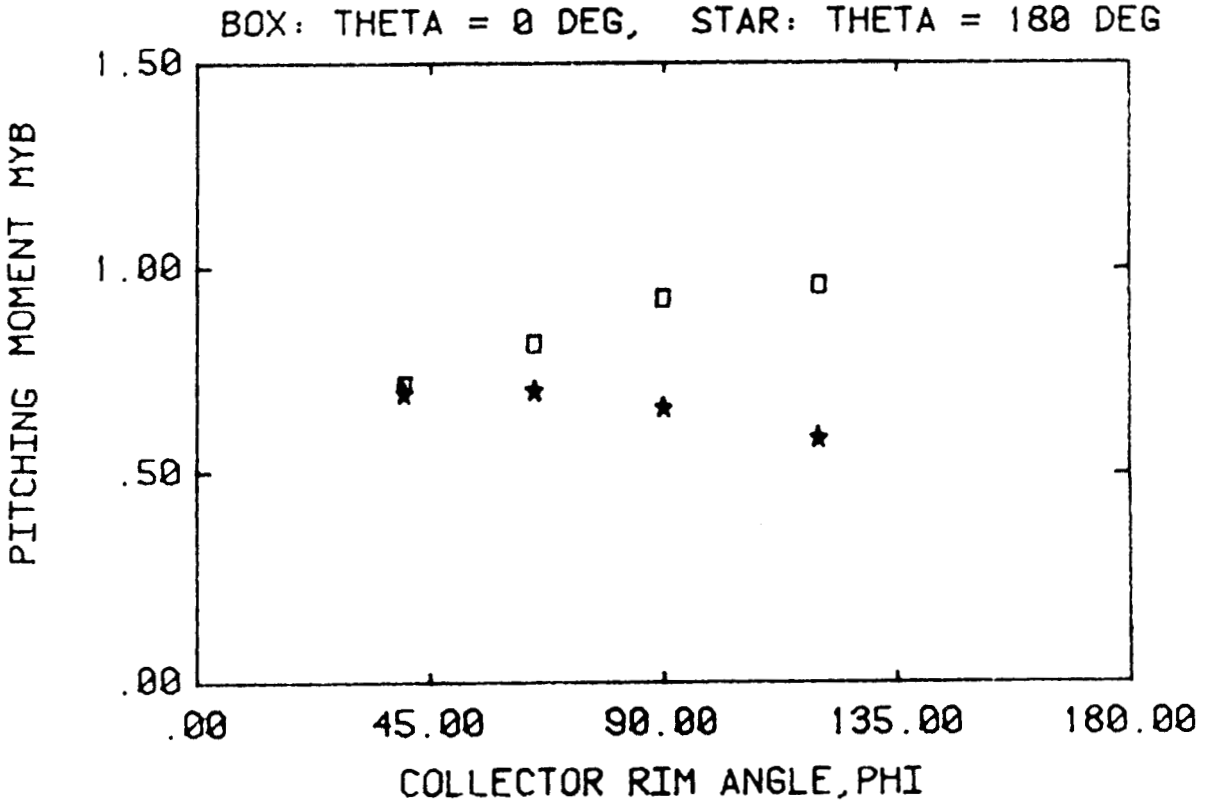

Figure 14c. Effect on the rim angle ϕ on collector loads.

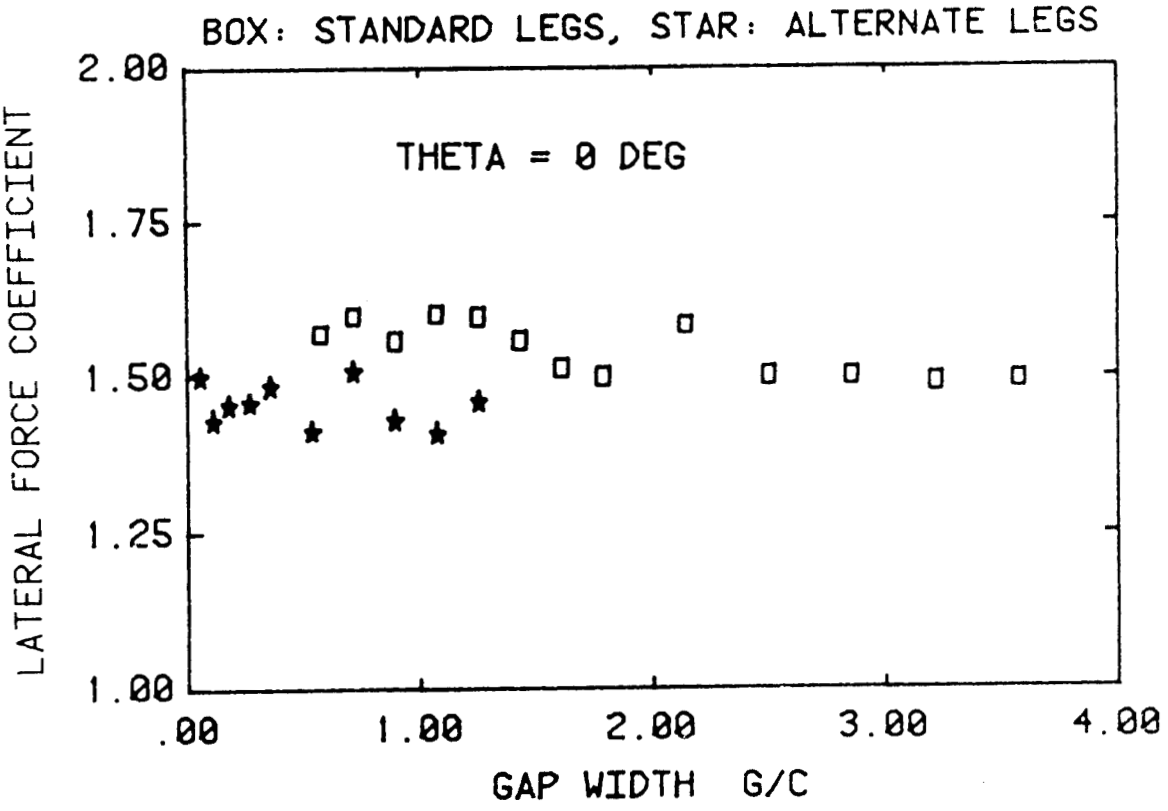

Figure 15a. Effect of gap width on loads for configuration 5.

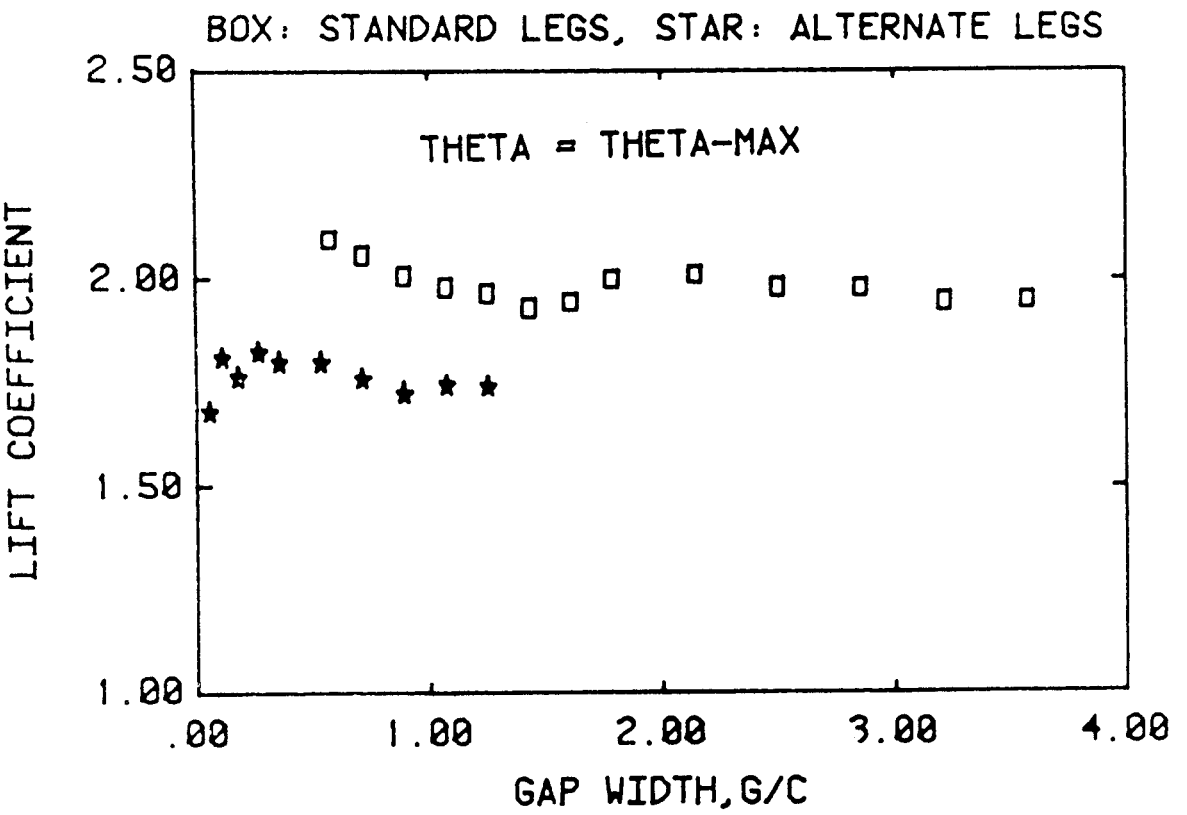

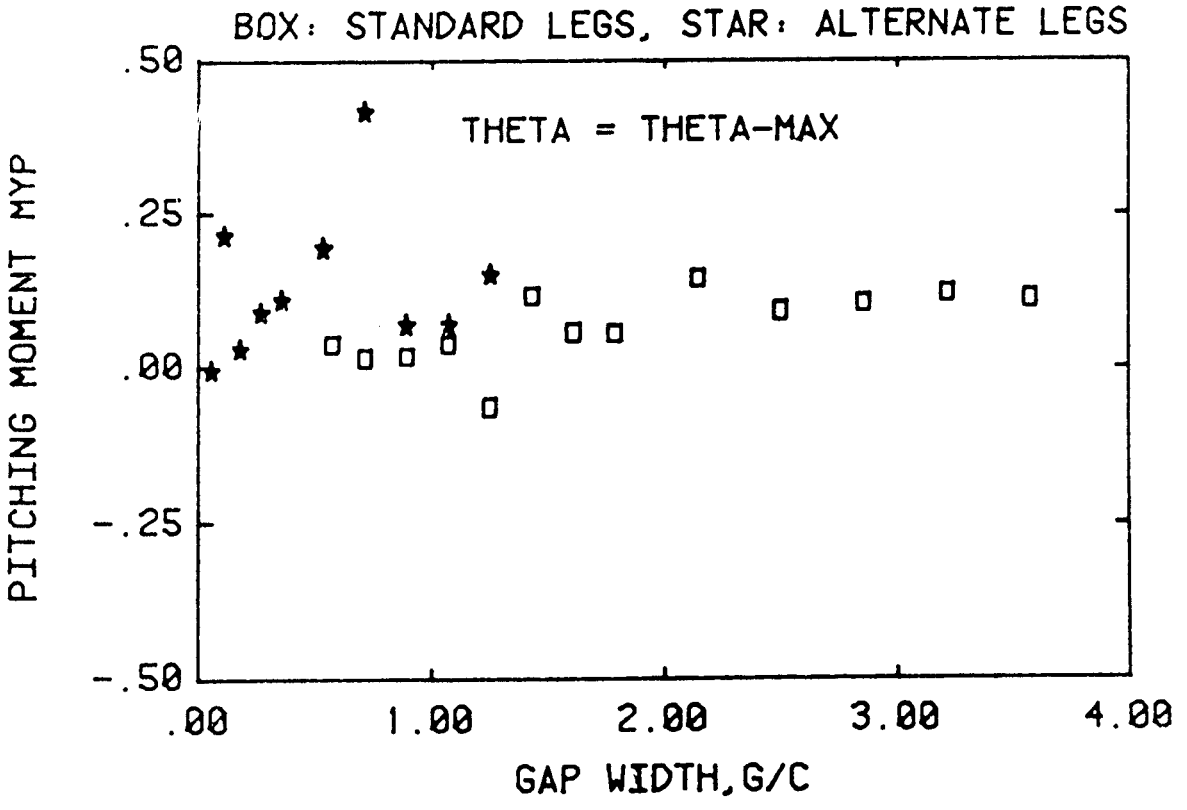

Figure 15b. Effect of gap width on loads for configuration 5.

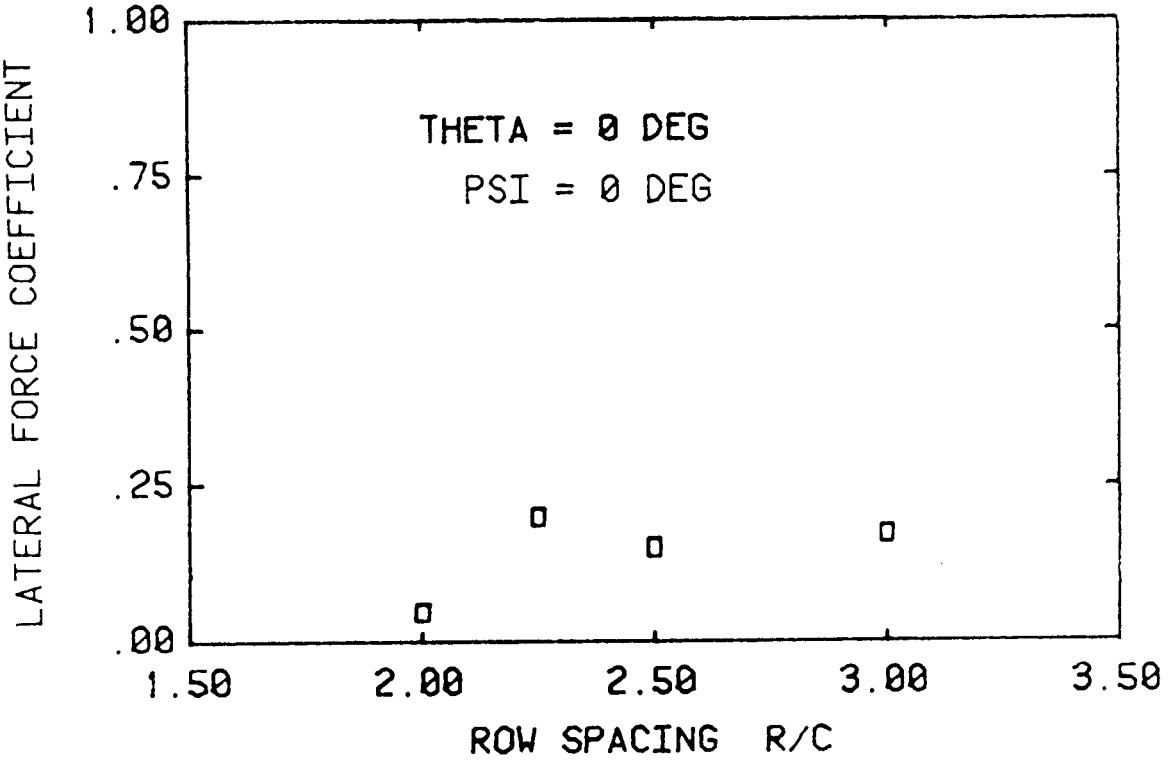

Figure 16a. Effect of row spacing on collector loads (configuration 9).

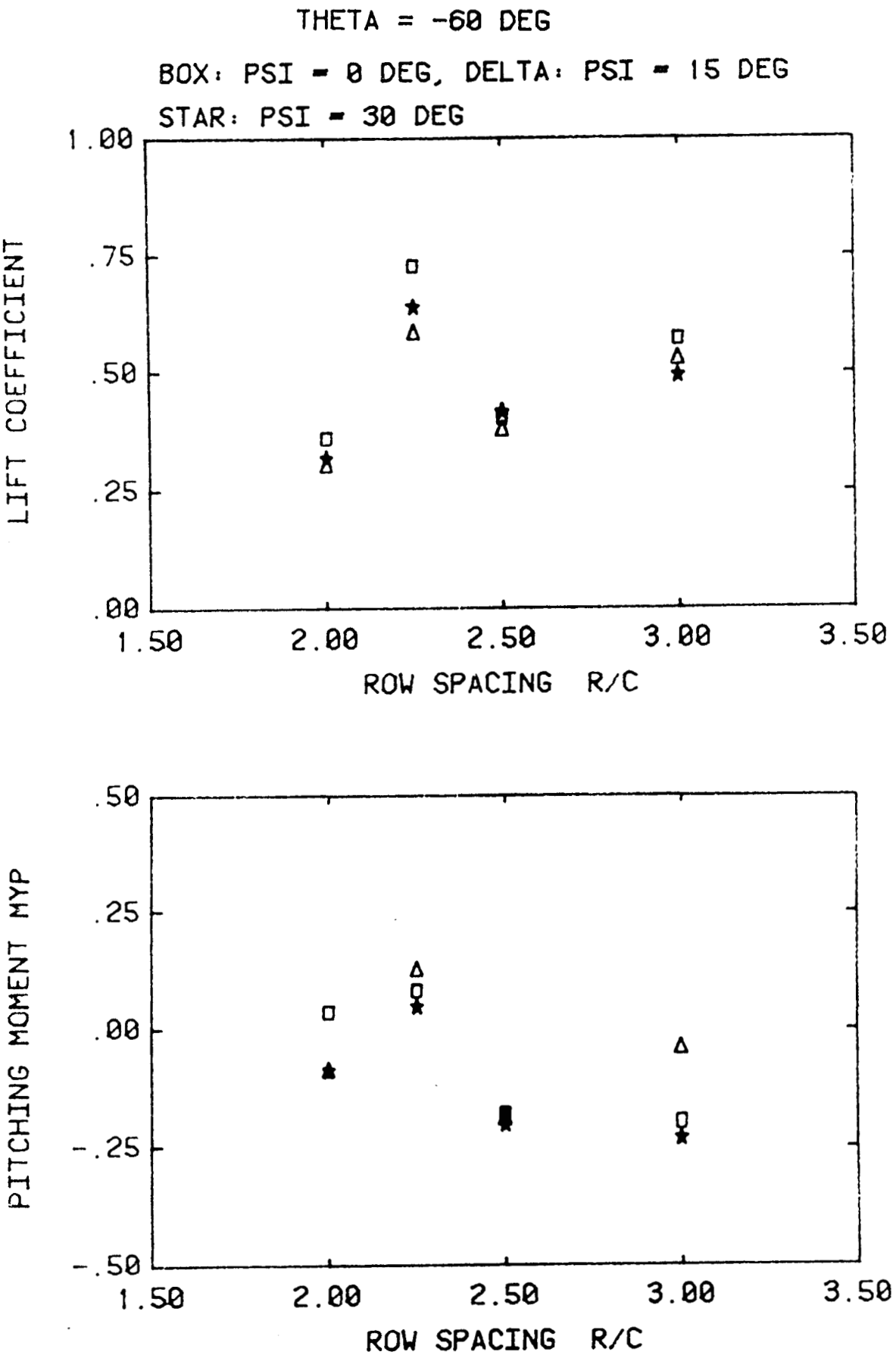

Figure 16b. Effect of row spacing on collector loads (configuration 9).

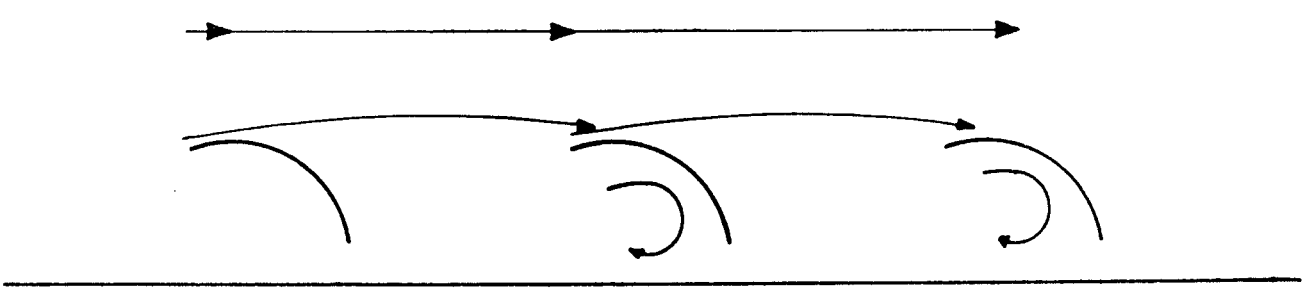

R/C = 2.0 $\theta = \theta_{max}$

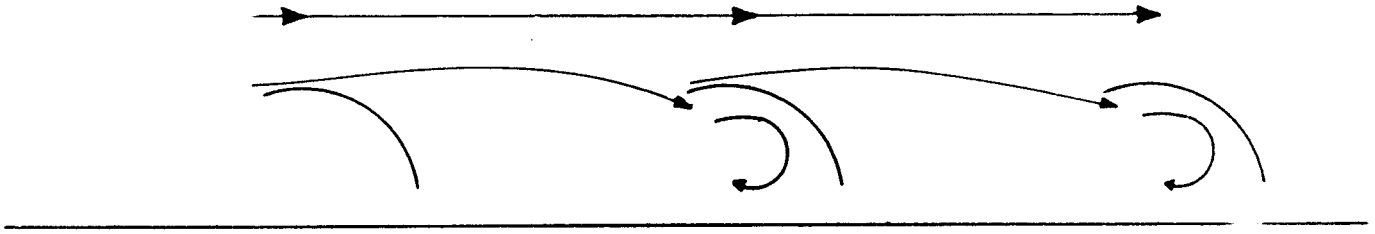

R/C = 2.25 $\theta = \theta_{max}$

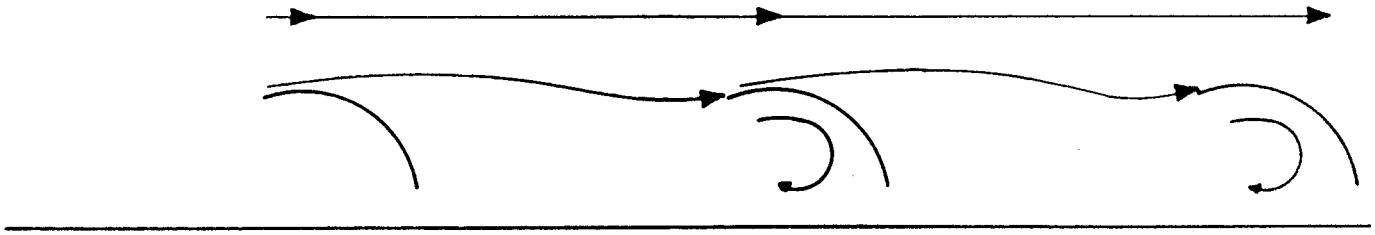

R/C = 2.5 $\theta = \theta_{max}$

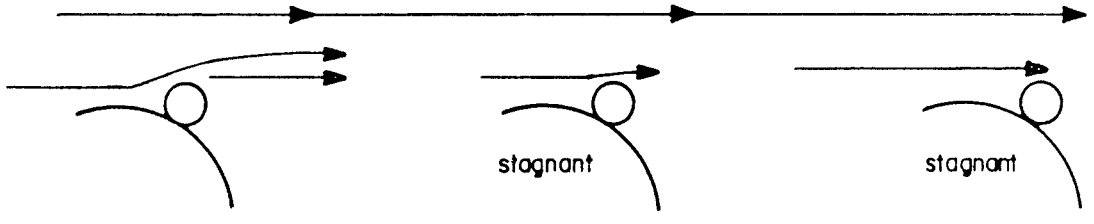

R/C = 2.25 $\theta = \theta_{max}$
WITH TORQUE TUBE

Figure 16c. Effect of the row spacing upon the flow pattern.

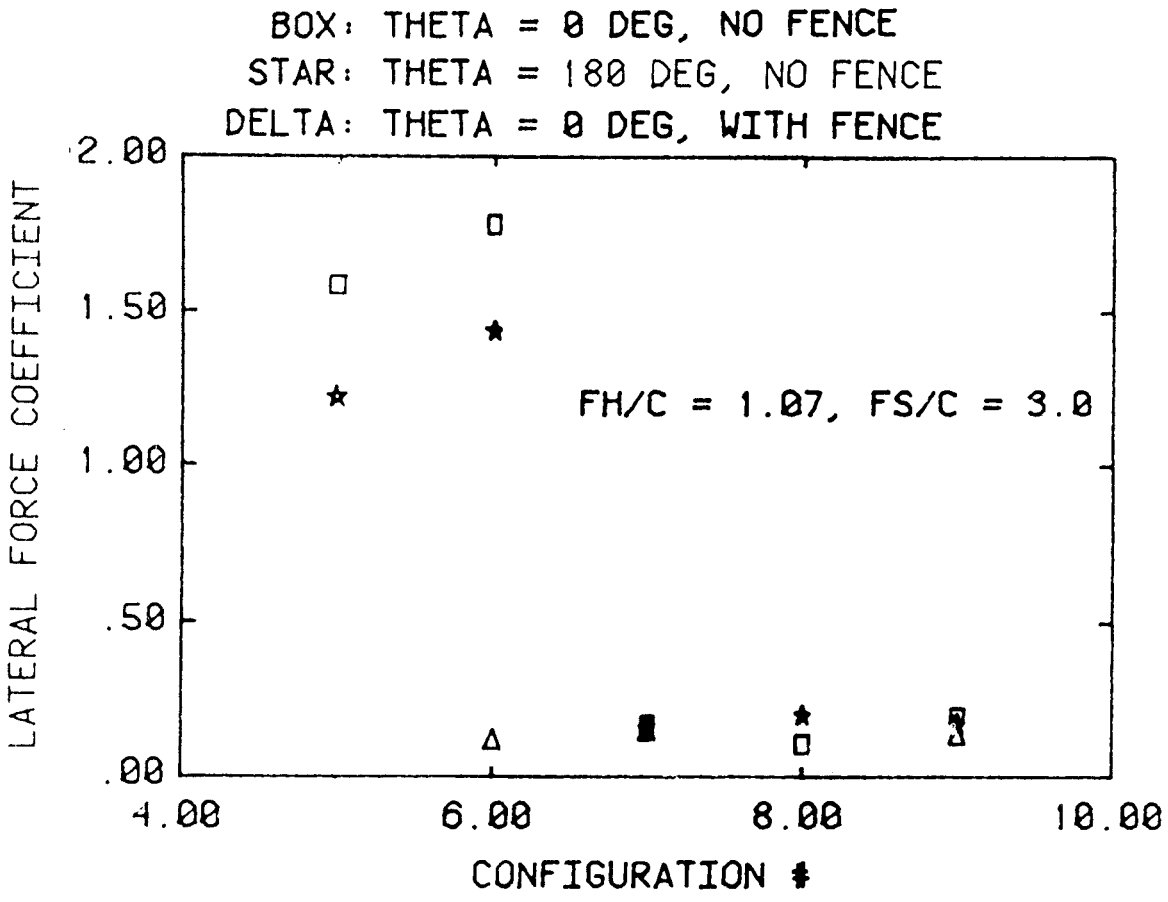

Figure 17a. Influence of array field configuration and fences on collector loads.

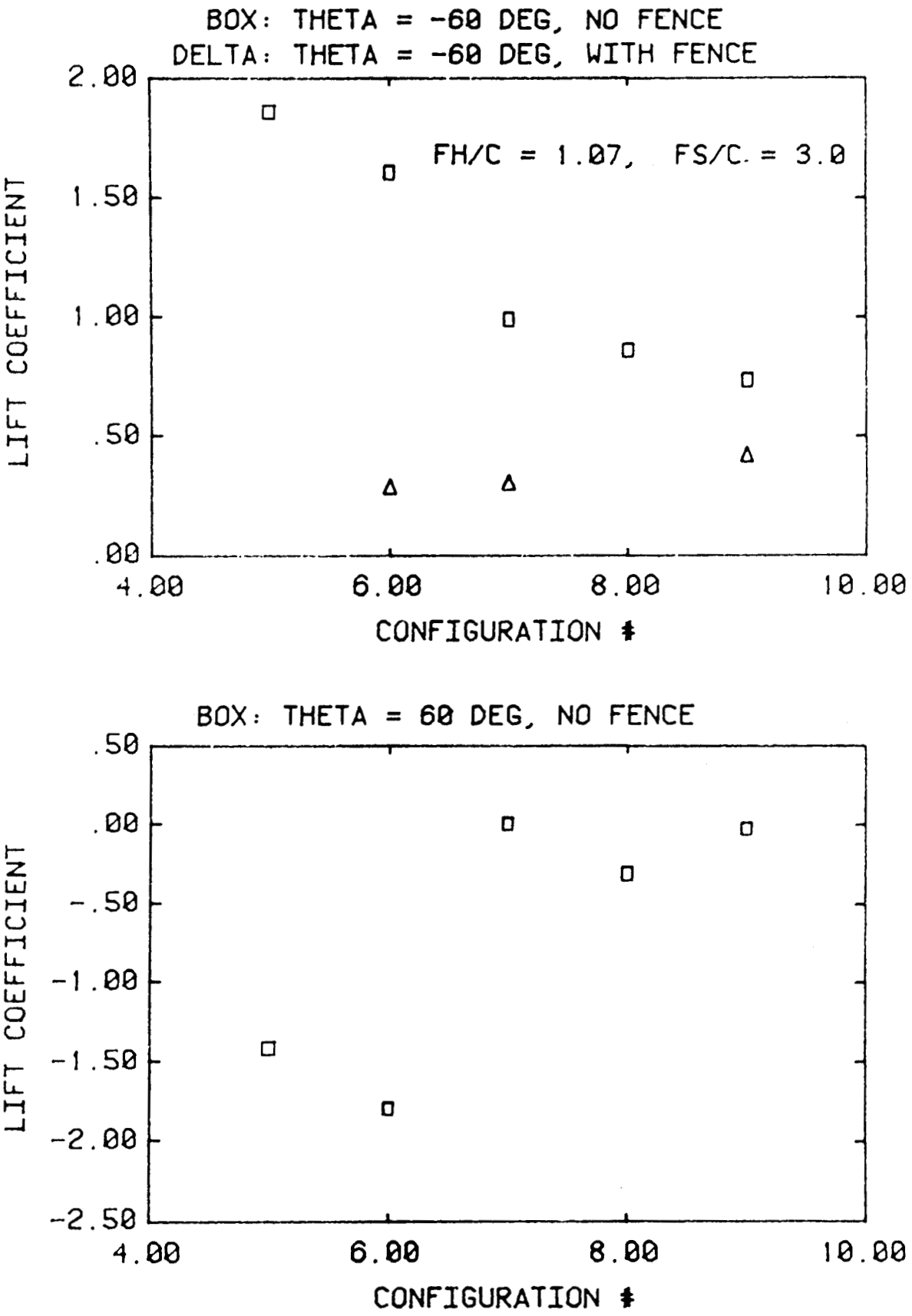

Figure 17b. Influence of array field configuration and fences on collector loads.

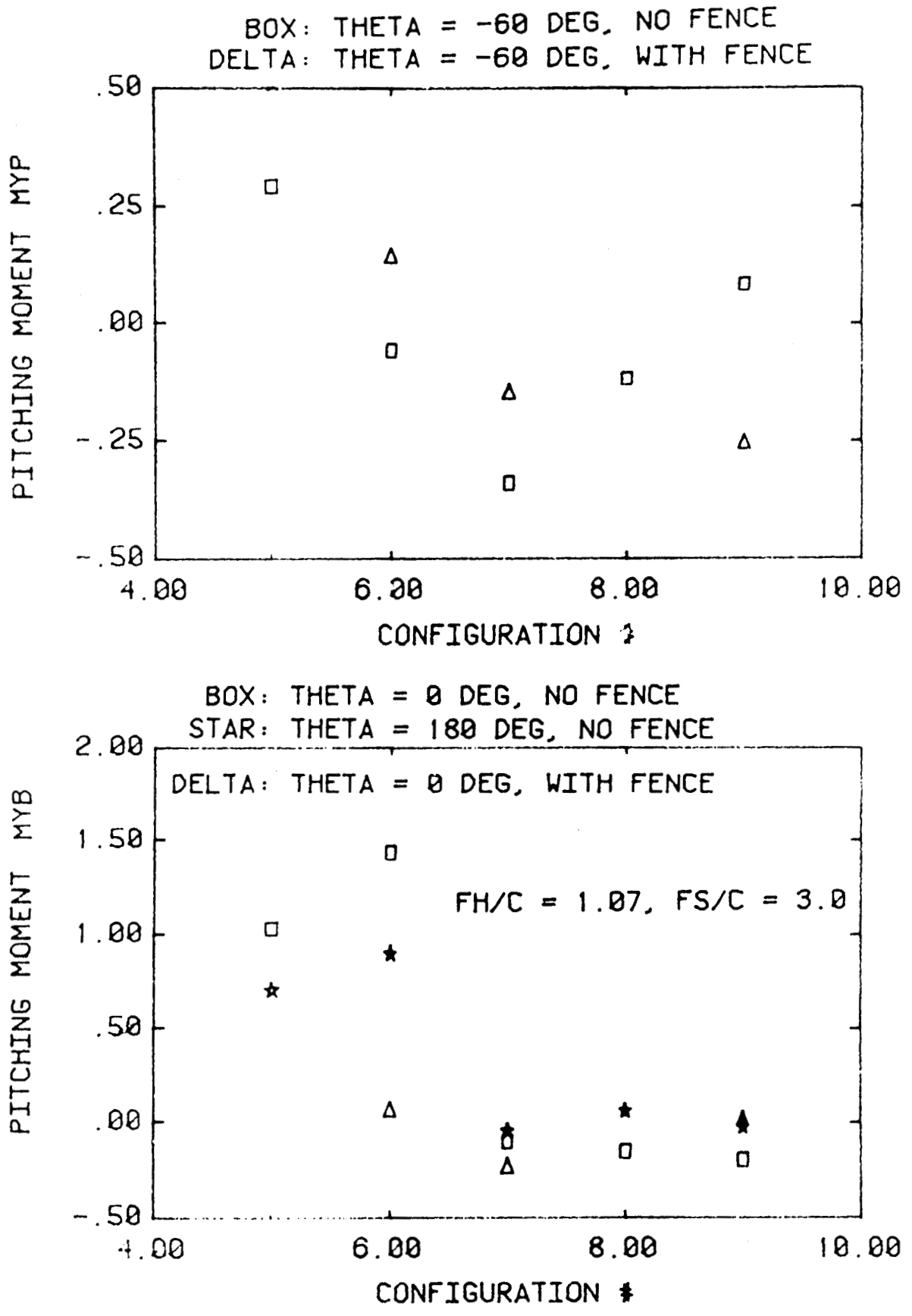

Figure 17c. Influence of array field configuration and fences on collector loads.

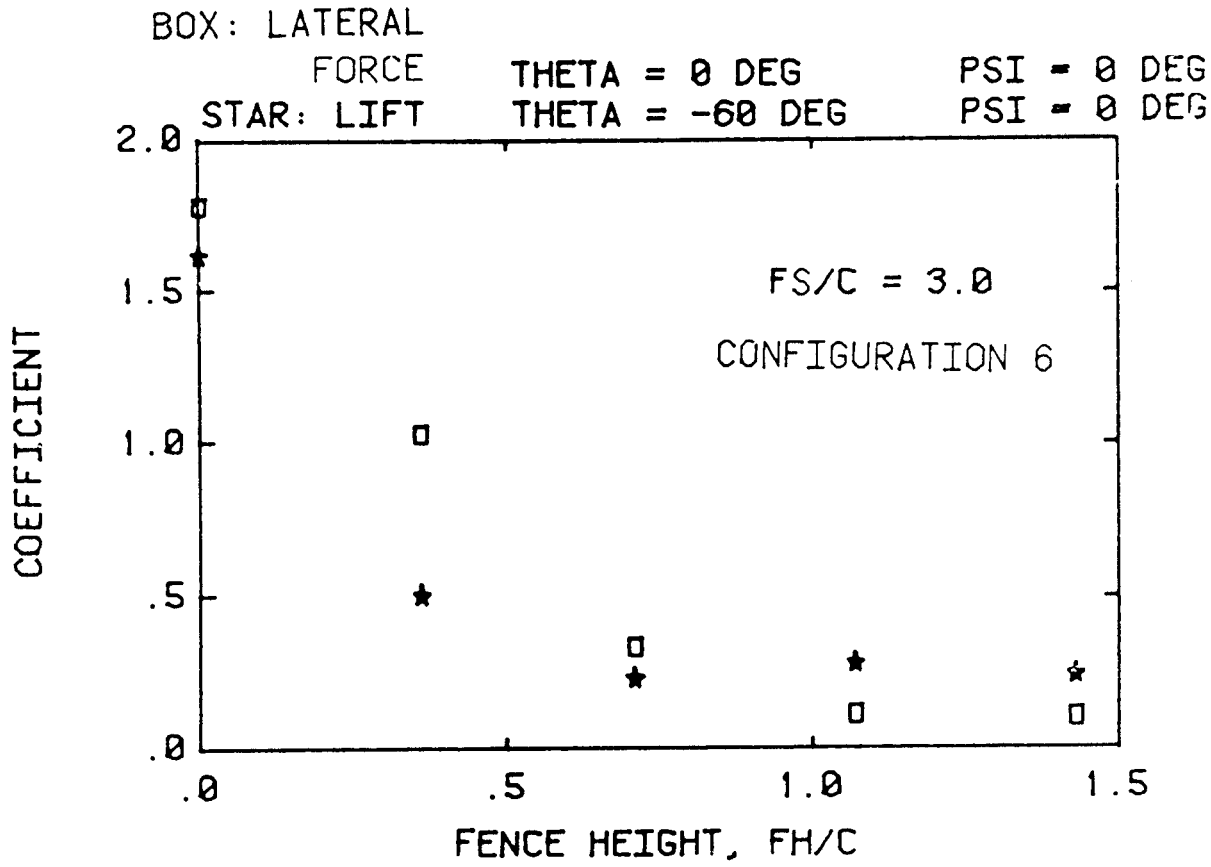

Figure 17d. Influence of array field configuration and fences on collector loads.

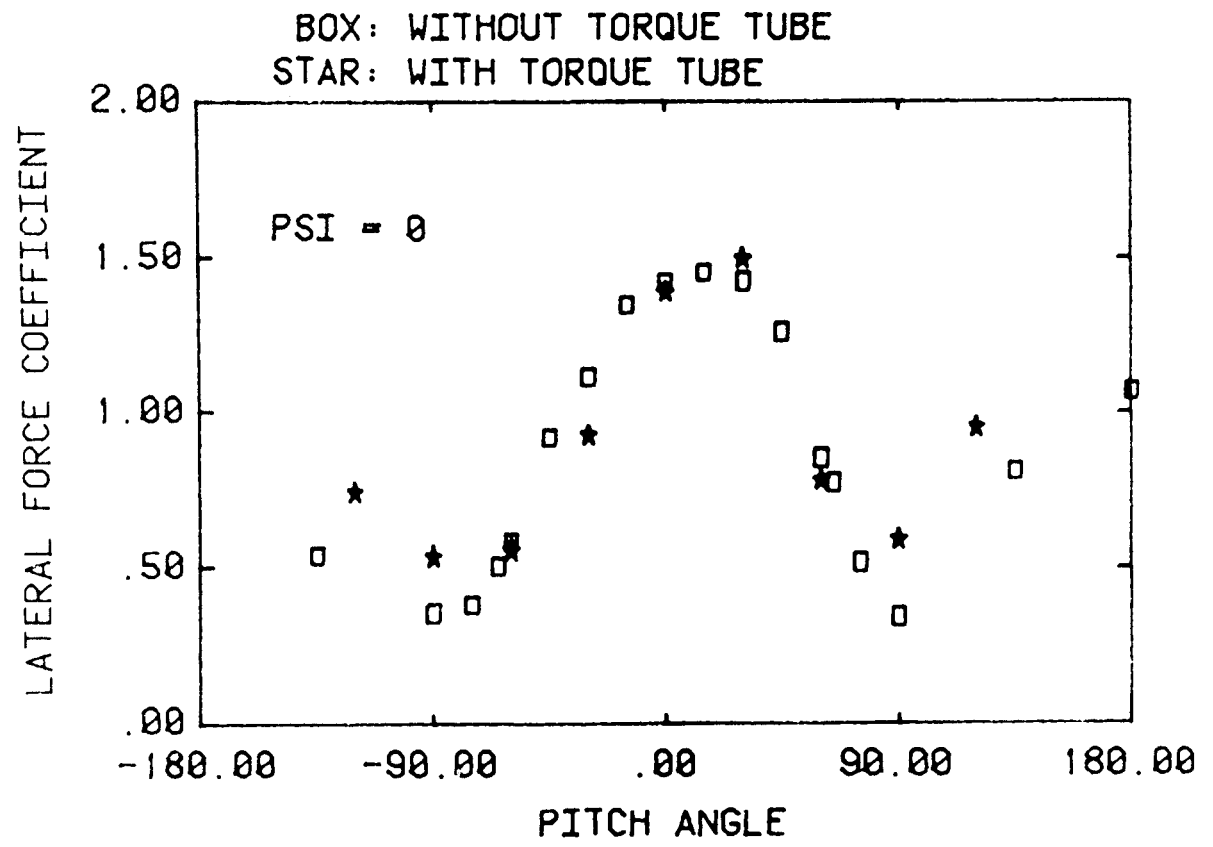

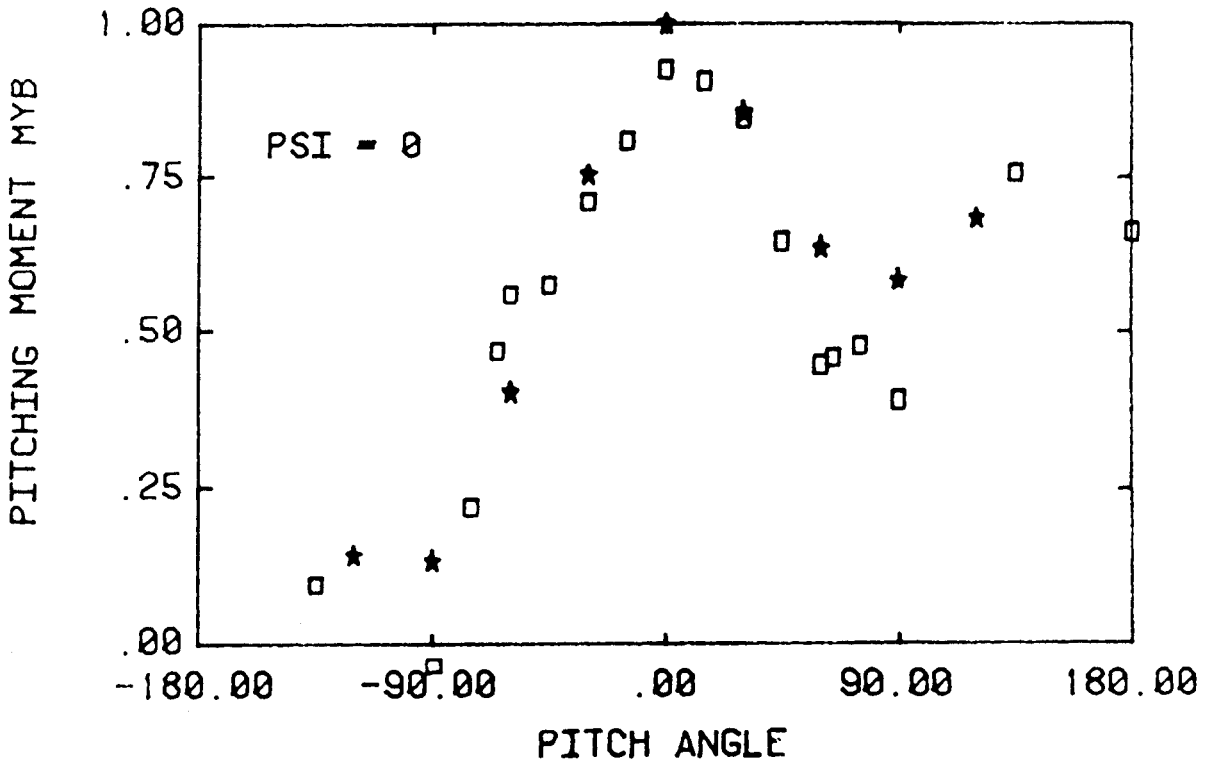

Figure 18a. Effect of torque tube on collector 1 loads.

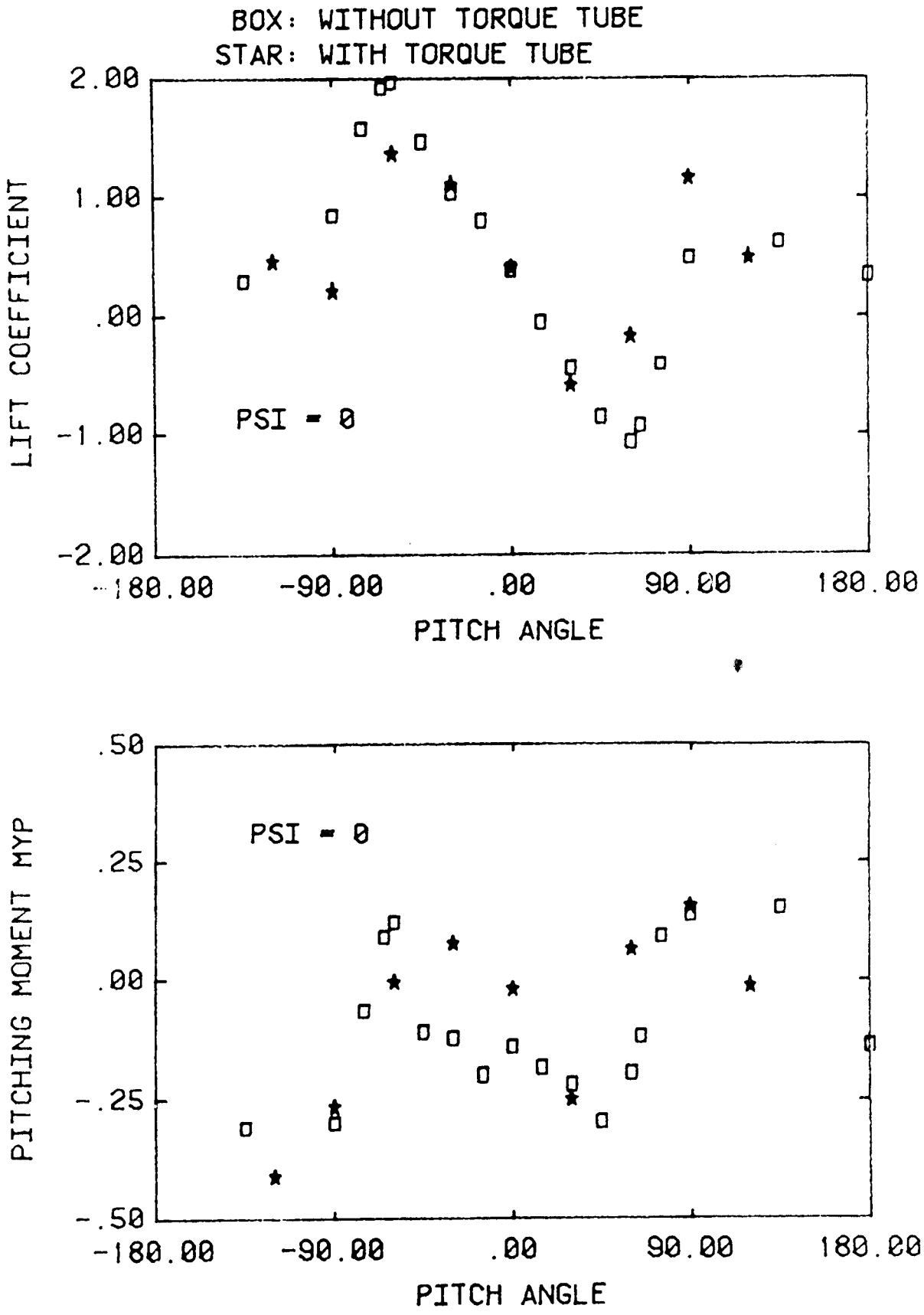

Figure 18b. Effect of torque tube on collector 1 loads.

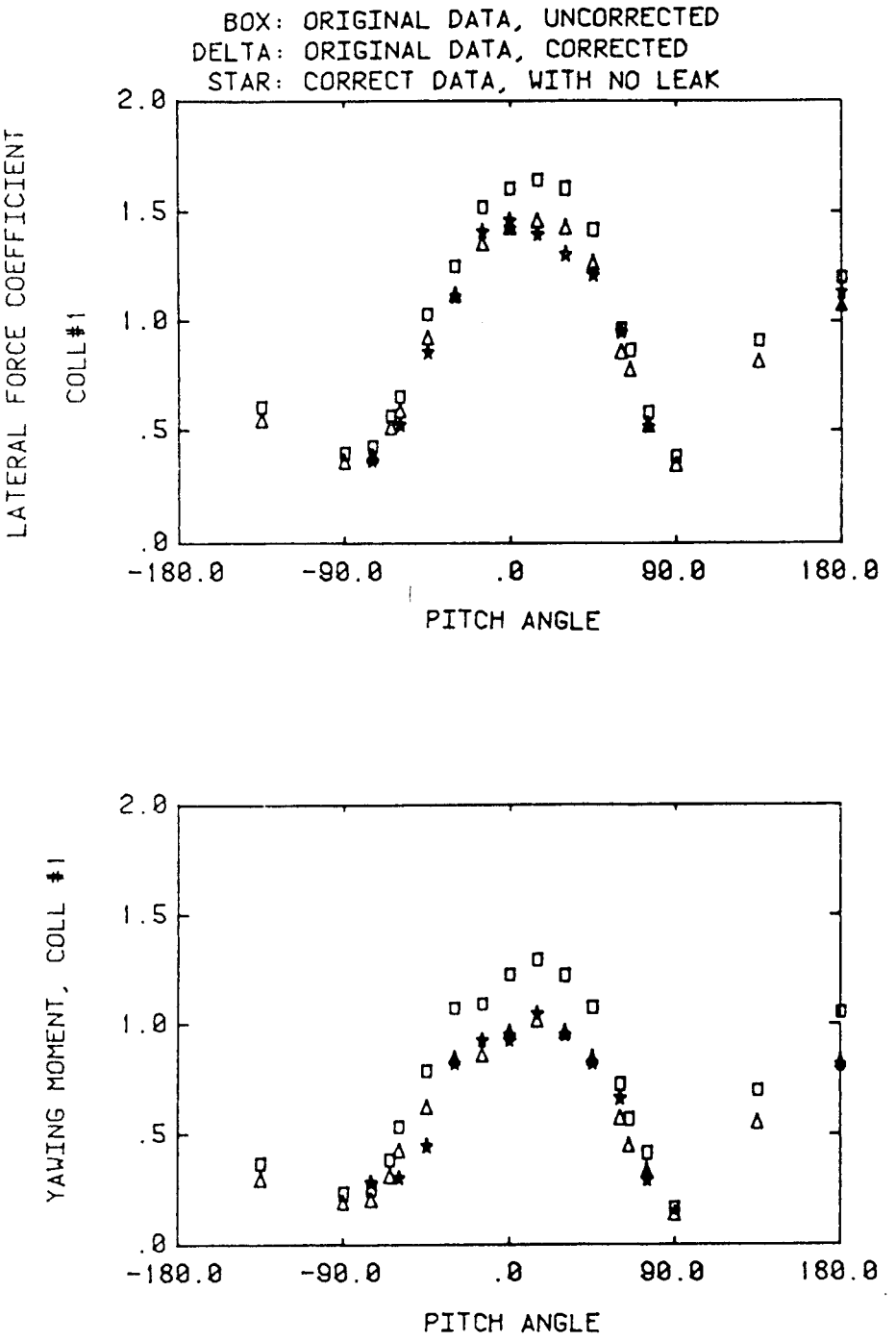

Figure 19. Effect of applying correction to collector 1.

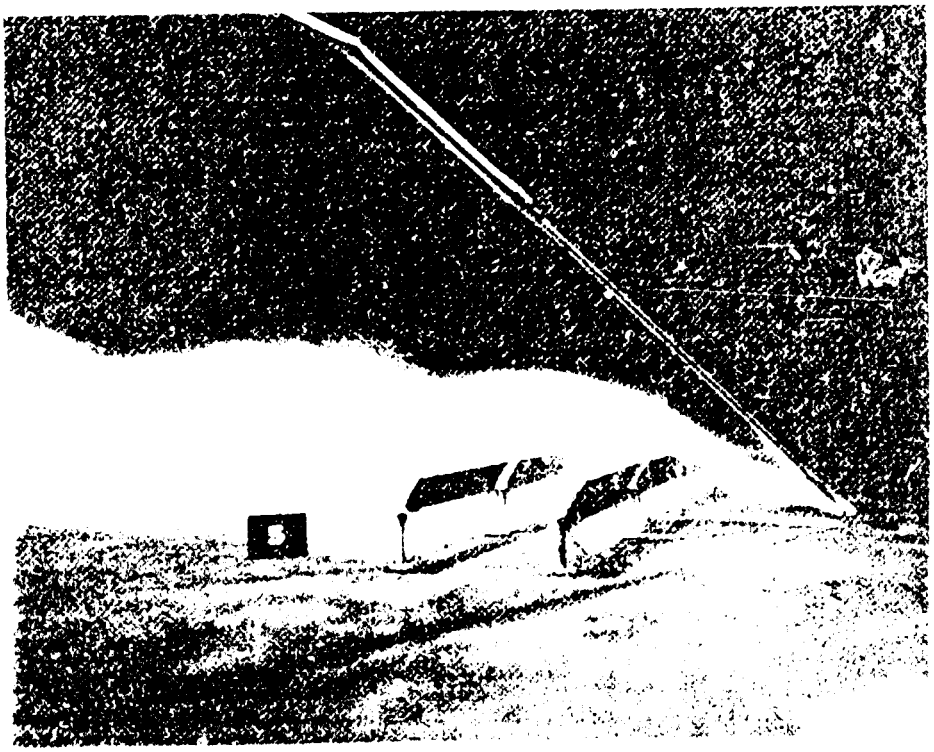

(a)

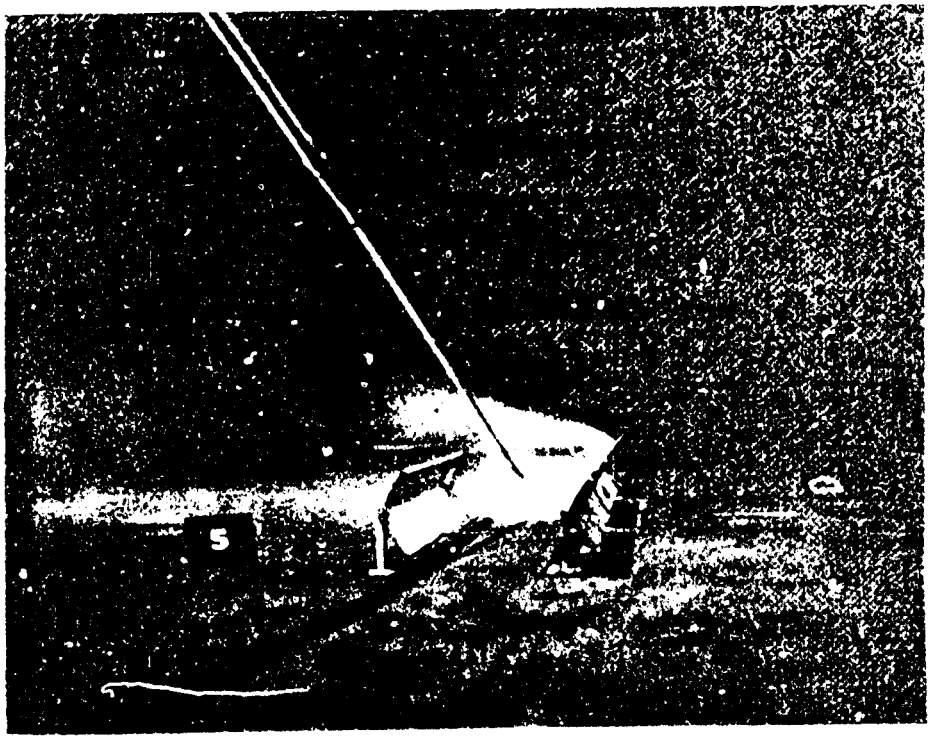

(b)

Figure 20. Smoke visualization of upwind barriers.

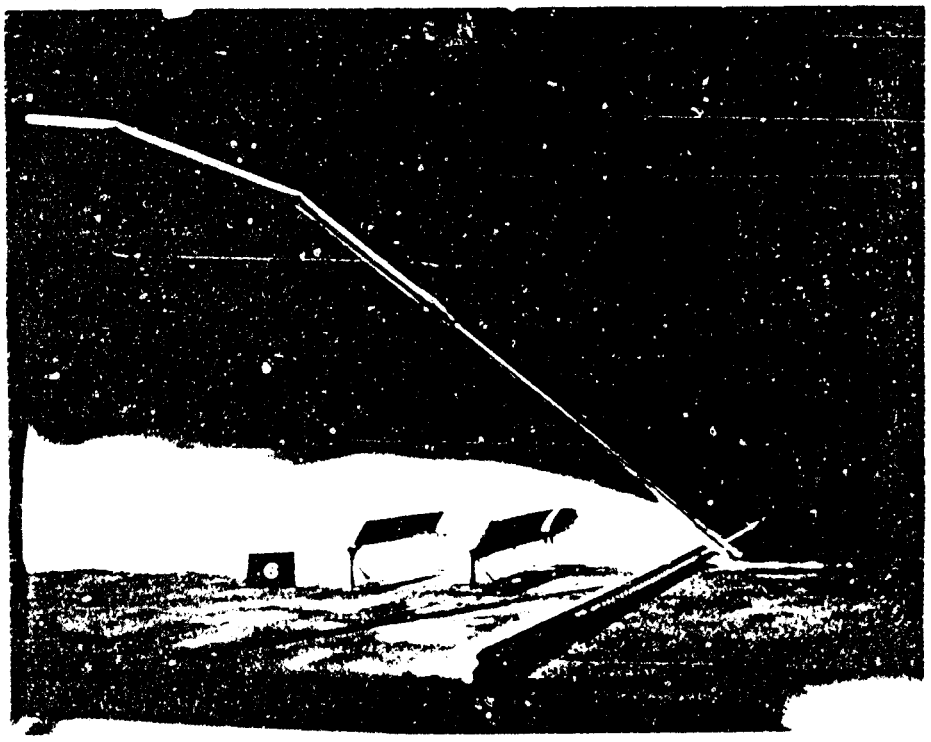

(c)

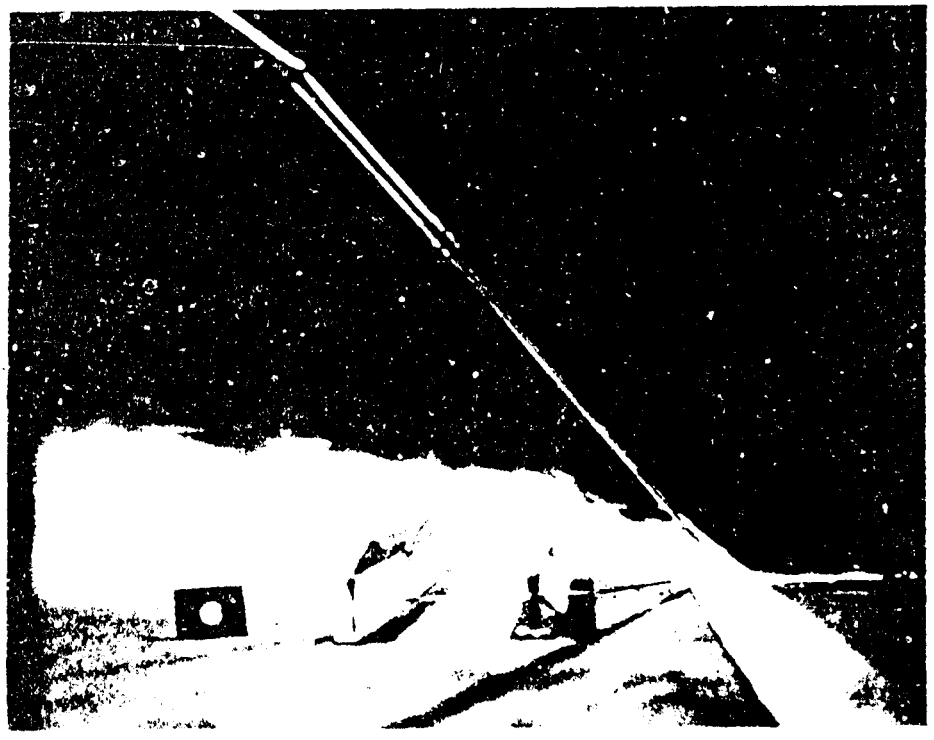

(d)

Figure 20 (continued).

TABLES

Table 1. MOTION PICTURE SCENE GUIDE

RUN #	WIND DIRECTION	CONFIGURATION	PITCH	FENCE	BERM
1	General presentation of the array and the wind tunnel				
2	0	9	0	3-in. fence	no
3	30	9	0	3-in. fence	no
4	0	9	0	no	2-in. berm
5	0	6	0	no	no
6	0	6	0	1-in. fence	no
7	0	6	0	2-in. fence	no
8	0	6	0	3-in. fence	no
9	0	6	-60	2-in. fence	no
10	0	6	120	2-in. fence	no

Table 2. VELOCITY AND TURBULENCE INTENSITY PROFILE

EXPONENT = .1546 UMAX = 80.53

DATA POINT	HEIGHT IN	UMEAN FPS	U-RMS FPS	TURB. INT. PERCENT
1	.50	38.45	7.956	20.69
2	.98	44.63	8.374	18.76
3	1.49	48.81	9.033	18.51
4	2.02	52.33	8.193	15.66
5	2.51	52.30	8.187	15.65
6	3.01	55.36	7.242	13.08
7	3.50	55.86	7.469	13.37
8	4.01	58.26	7.817	13.42
9	4.51	59.81	7.665	12.82
10	5.00	59.83	7.714	12.89
11	6.00	60.61	6.992	11.54
12	7.01	61.77	6.532	10.57
13	8.00	64.53	6.881	10.66
14	9.01	64.35	7.432	11.55
15	10.00	67.05	6.558	9.78
16	12.01	65.67	5.998	9.13
17	16.03	69.55	6.679	9.60
18	20.06	72.12	6.209	8.61
19	25.05	75.44	5.135	6.81
20	30.04	75.60	5.226	6.91
21	35.00	78.41	3.957	5.05
22	39.93	79.97	3.585	4.48
23	44.99	80.53	3.113	3.87

Table 3. DETERMINATION OF C_{max} FOR CONFIGURATIONS 1-4

DATA FOR THE SANDIA PARABOLIC COLLECTOR — FORCE AND MOMENT COEFFICIENTS — FILE-NAME: MDPIM1

CONFIGURATION 1 — C = 2.80 — L = 10.80 INCHES

PITCH	HCL/C	FXP	FZP	MXP	MYP	MZP
0	1.03	1.57	.03	.27	-.31	-.13
-15	1.03	1.49	.46	.21	-.41	.15
-30	1.03	1.29	.97	.33	-.34	.09
-45	1.03	1.04	1.33	.24	-.13	.10
-50	1.03	.99	1.47	.47	-.20	-.17
-55	1.03	.80	1.65	.47	.02	-.13

DETERMINATION OF THETA MAX,COLL#1

PITCH	HCL/C	FXP	FZP	MXP	MYP	MZP
-60	1.03	.74	1.83	.49	-.07	-.08
-65	1.03	.59	1.99	.31	-.09	-.07
-70	1.03	.52	1.96	.45	-.12	-.04
-75	1.03	.41	1.61	.23	-.05	.04
-80	1.03	.37	.81	.17	-.32	-.10
-105	1.03	.38	.03	.03	-.26	-.05
-120	1.03	.49	.01	-.03	-.32	-.02

DATA FOR THE SANDIA PARABOLIC COLLECTOR — FORCE AND MOMENT COEFFICIENTS — FILE-NAME: MDPIM2

CONFIGURATION 2 — C = 2.92 — L = 10.80 INCHES

PITCH	HCL/C	FXP	FZP	MXP	MYP	MZP
0	.99	1.56	.03	.03	-.24	-.15
-15	.99	1.43	.51	.13	-.21	-.03
-30	.99	1.13	.86	.27	-.03	-.01
-45	.99	.89	1.20	.29	.06	-.03
-60	.99	.75	1.55	.42	.07	-.11
-65	.99	.65	1.62	.36	-.11	-.04

DETERMINATION OF THETA MAX,COLL#2

PITCH	HCL/C	FXP	FZP	MXP	MYP	MZP
-70	.99	.50	1.76	.35	.05	-.03
-75	.99	.35	1.79	.49	.07	-.03
-80	.99	.23	1.54	.34	-.03	-.06
-85	.99	.17	1.26	.27	-.05	-.03
-90	.99	.10	.98	.29	.07	-.11
-105	.99	.25	-.16	-.01	-.22	.02

DATA FOR THE SANDIA PARABOLIC COLLECTOR — FORCE AND MOMENT COEFFICIENTS — FILE-NAME: MDPIM3

CONFIGURATION 3 — C = 2.94 — L = 10.80 INCHES

PITCH	HCL/C	FXP	FZP	MXP	MYP	MZP
0	.98	1.53	.03	.03	-.24	-.15
-15	.98	1.46	.51	.13	-.22	-.17
-30	.98	1.18	.85	.26	-.18	-.05
-45	.98	.94	1.20	.29	-.07	-.06
-60	.98	.75	1.61	.35	-.08	-.11

DETERMINATION OF THETA MAX,COLL#3

PITCH	HCL/C	FXP	FZP	MXP	MYP	MZP
-65	.98	.61	1.82	.39	-.02	-.10
-70	.98	.51	1.88	.44	-.14	-.13
-75	.98	.35	1.81	.23	-.04	-.02
-80	.98	.29	1.67	.42	-.07	-.09
-90	.98	.17	1.25	.26	-.14	-.03
-105	.98	.27	.14	.08	-.27	-.07

DATA FOR THE SANDIA PARABOLIC COLLECTOR — FORCE AND MOMENT COEFFICIENTS — FILE-NAME: MDPIM4

CONFIGURATION 4 — C = 3.00 — L = 10.80 INCHES

PITCH	HCL/C	FXP	FZP	MXP	MYP	MZP
0	.96	1.61	-.10	.04	-.35	.03
-15	.96	1.43	.30	.10	-.29	-.07
-30	.96	1.25	.77	.20	-.21	-.02
-45	.96	.81	1.19	.25	.08	-.01
-50	.96	.76	1.10	.24	.14	-.06

DETERMINATION OF THETA MAX,COLL#4

PITCH	HCL/C	FXP	FZP	MXP	MYP	MZP
-55	.96	.72	1.17	.28	-.11	-.02
-60	.96	.66	1.13	.29	-.17	-.08
-70	.96	.55	.96	.26	-.17	.07
-75	.96	.55	.85	.22	-.25	-.02
-90	.96	.54	.62	.05	-.39	-.03
-105	.96	.54	.43	.10	-.39	-.03

Table 4. EFFECT OF HEIGHT HCL ON SINGLE COLLECTOR LOADS AT $\theta = 0$, $\psi = 0$ FOR CONFIGURATIONS 1-4

DATA FOR THE SANDIA PARABOLIC COLLECTOR — FORCE AND MOMENT COEFFICIENTS — FILE-NAME: MDCDM1

CONFIGURATION 1 — C = 2.80 — L = 10.80 INCHES — HEIGHT EFFECT AT THETA=0 COLL#1

PITCH	HCL/C	FXP	FZP	MXP	MYP	MZP
0	.67	1.48	.10	.09	-.55	.05
0	.71	1.40	.02	.04	-.25	.01
0	.80	1.53	.10	-.04	-.34	-.13
0	.89	1.48	.10	.09	-.14	-.13

PITCH	HCL/C	FXP	FZP	MXP	MYP	MZP
0	1.03	1.52	.10	-.03	-.21	-.08
0	1.25	1.48	.03	.03	-.07	-.01
0	1.61	1.50	.03	.13	-.20	-.02
0	1.96	1.54	.03	.13	-.49	-.11

DATA FOR THE SANDIA PARABOLIC COLLECTOR — FORCE AND MOMENT COEFFICIENTS — FILE-NAME: MDCDM2

CONFIGURATION 2 — C = 2.92 — L = 10.80 INCHES — HEIGHT EFFECT AT THETA=0 COLL#2

PITCH	HCL/C	FXP	FZP	MXP	MYP	MZP
0	.64	1.37	.10	.10	-.18	-.12
0	.69	1.40	.02	-.19	-.05	-.15
0	.77	1.46	.02	.03	-.20	-.01
0	.86	1.45	.02	.03	-.15	-.05

PITCH	HCL/C	FXP	FZP	MXP	MYP	MZP
0	.99	1.56	.03	.03	-.24	-.15
0	1.20	1.45	.03	.03	-.13	-.05
0	1.56	1.46	.03	.07	-.14	-.07
0	1.88	1.48	.03	.12	-.45	-.10

DATA FOR THE SANDIA PARABOLIC COLLECTOR — FORCE AND MOMENT COEFFICIENTS — FILE-NAME: MDCDM3

CONFIGURATION 3 — C = 2.94 — L = 10.80 INCHES — HEIGHT EFFECT AT THETA=0 COLL#3

PITCH	HCL/C	FXP	FZP	MXP	MYP	MZP
0	.64	1.31	.18	.15	-.17	-.08
0	.68	1.45	.02	.04	-.26	-.20
0	.77	1.45	.02	.03	-.10	-.01
0	.85	1.51	.03	.03	-.18	-.09

PITCH	HCL/C	FXP	FZP	MXP	MYP	MZP
0	.98	1.50	.03	.13	-.29	-.02
0	1.19	1.56	.16	.11	-.29	-.11
0	1.53	1.43	.03	.13	-.18	-.10
0	1.87	1.46	.03	.12	-.29	-.10

DATA FOR THE SANDIA PARABOLIC COLLECTOR — FORCE AND MOMENT COEFFICIENTS — FILE-NAME: MDCDM4

CONFIGURATION 4 — C = 3.00 — L = 10.80 INCHES — HEIGHT EFFECT AT THETA=0 COLL#4

PITCH	HCL/C	FXP	FZP	MXP	MYP	MZP
0	.63	1.34	.10	-.03	-.18	-.00
0	.67	1.37	.10	.08	-.24	-.04
0	.75	1.52	-.11	.05	-.43	-.05
0	.83	1.57	-.19	.10	-.35	-.06

PITCH	HCL/C	FXP	FZP	MXP	MYP	MZP
0	.96	1.61	.16	.04	-.35	-.03
0	1.17	1.53	.03	.11	-.25	.01
0	1.56	1.62	.03	.19	-.27	.00
0	1.83	1.56	.09	.22	-.32	-.02

Table 5. EFFECT OF HEIGHT HCL ON SINGLE COLLECTOR LOADS AT θ_{max}, $\psi = 0$ FOR CONFIGURATIONS 1-4

DATA FOR THE SANDIA PARABOLIC COLLECTOR — FORCE AND MOMENT COEFFICIENTS — FILE-NAME: MDCLM1

CONFIGURATION 1 C = 2.80 L = 10.90 INCHES — HEIGHT EFFECT AT THETA MAX, COLL#1

PITCH	HCL/C	FXP	FZP	MXP	MYP	MZP
-65.	.67	.46	1.75	.34	.02	-.04
-65.	.71	.45	1.64	.29	.12	-.08
-65.	.80	.50	1.82	.56	.03	-.00
-65.	.89	.47	1.79	.48	.07	-.11

PITCH	HCL/C	FXP	FZP	MXP	MYP	MZP
-65	1.03	.53	1.90	.43	.05	-.03
-65	1.25	.52	1.95	.48	.13	-.14
-65	1.61	.52	1.92	.44	.11	-.04
-65	1.96	.57	2.00	.48	.00	-.10

DATA FOR THE SANDIA PARABOLIC COLLECTOR — FORCE AND MOMENT COEFFICIENTS — FILE-NAME: MDCLM2

CONFIGURATION 2 C = 2.92 L = 10.90 INCHES — HEIGHT AT THETA MAX, COLL#2

PITCH	HCL/C	FXP	FZP	MXP	MYP	MZP
-75.	.64	.33	1.76	.37	.14	.12
-75.	.68	.32	1.73	.37	.13	.00
-75.	.77	.31	1.74	.42	.19	-.10
-75.	.86	.36	1.68	.39	.04	.07

PITCH	HCL/C	FXP	FZP	MXP	MYP	MZP
-75	.99	.34	1.68	.31	.07	-.03
-75	1.03	.39	1.73	.36	.01	-.16
-75	1.20	.32	1.65	.35	.16	-.12
-75	1.54	.40	1.65	.40	-.07	-.17
-75	1.88	.33	1.67	.36	.15	-.04

DATA FOR THE SANDIA PARABOLIC COLLECTOR — FORCE AND MOMENT COEFFICIENTS — FILE-NAME: MDCLM3

CONFIGURATION 3 C = 2.94 L = 10.80 INCHES — HEIGHT EFFECT AT THETA MAX, COLL#3

PITCH	HCL/C	FXP	FZP	MXP	MYP	MZP
-70.	.64	.66	1.43	.27	-.13	-.02
-70.	.68	.71	1.49	.32	-.07	-.17
-70.	.77	.69	1.58	.40	-.05	-.05
-70.	.85	.78	1.54	.38	-.15	-.12

PITCH	HCL/C	FXP	FZP	MXP	MYP	MZP
-70	.98	.75	1.61	.46	-.08	-.11
-70	1.19	.76	1.65	.41	-.11	-.04
-70	1.53	.80	1.77	.54	-.16	-.09
-70	1.87	.83	1.61	.38	-.16	-.06

DATA FOR THE SANDIA PARABOLIC COLLECTOR — FORCE AND MOMENT COEFFICIENTS — FILE-NAME: MDCLM4

CONFIGURATION 4 C = 3.00 L = 10.80 INCHES — HEIGHT EFFECT AT THETA MAX, COLL#4

PITCH	HCL/C	FXP	FZP	MXP	MYP	MZP
-55.	.83	.62	.79	.24	-.10	.03
-55.	.96	.66	1.17	.28	.00	.01

PITCH	HCL/C	FXP	FZP	MXP	MYP	MZP
-55	1.17	.74	1.49	.31	-.02	.05
-55	1.50	.96	1.62	.52	-.16	.02
-55	1.83	.85	1.58	.45	-.07	-.01

Table 6a. MATRIX OF SINGLE COLLECTOR LOADS AT HCL/C = K_I (CONFIGURATION 1)

DATA FOR THE SANDIA PARABOLIC COLLECTOR — FORCE AND MOMENT COEFFICIENTS — FILE-NAME: MDCOL1

CONFIGURATION 1 — C = 2.80 — L = 10.80 INCHES — ONE SINGLE COLLECTOR, RIM ANGLE=90

WIND AZIM.	PITCH ANGLE	FXP	FZP	MXP	MYP	MZP
0.	0.00	1.42	.39	.22	-.14	-.05
0.	-15.00	1.35	.86	.29	-.20	-.10
0.	15.00	1.45	-.05	.23	-.18	-.02
0.	-30.00	1.11	1.04	.34	-.12	.05
0.	30.00	1.42	-.44	.23	-.22	-.05
0.	-45.00	.92	1.46	.51	-.11	-.03
0.	45.00	1.26	-.86	.26	-.30	-.05
0.	-60.00	.58	1.97	.46	-.12	.01
0.	60.00	.85	-1.08	.30	-.19	-.04
0.	-65.00	.50	1.92	.46	-.09	-.05
0.	65.00	.77	-.93	.33	-.12	-.10
0.	-75.00	.38	1.57	.28	-.06	-.07
0.	75.00	.51	-.41	.36	.09	-.04
0.	-90.00	.35	.85	.23	-.30	-.07
0.	90.00	.34	.49	.09	.14	-.11
0.	-135.0	.54	.30	.01	-.31	-.09
0.	135.00	.81	.62	.24	.15	-.03
0.	180.00	1.06	.33	.18	-.14	.07
-15.	0.00	1.41	.39	.18	-.16	.10
-15.	-65.00	.48	1.84	.37	-.03	.07
-15.	65.00	.79	-.93	.11	-.26	.17
-15.	180.00	1.00	.32	.19	-.07	.09
15.	0.00	1.45	.35	.34	-.17	-.17
15.	-65.00	.51	1.96	.61	.05	-.15
15.	65.00	.75	-.96	.10	-.08	-.22
15.	180.00	1.10	.29	.16	-.19	-.22
30.	0.00	1.42	.35	.12	-.21	-.40
30.	-15.00	1.34	.76	.46	-.12	-.31
30.	15.00	1.41	-.11	.04	-.20	-.42
30.	-30.00	1.18	1.08	.49	-.07	-.35
30.	30.00	1.33	-.36	.16	-.23	-.40
30.	-45.00	.95	1.48	.68	-.03	-.23
30.	45.00	1.20	-.84	.01	-.32	-.44

WIND AZIM.	PITCH ANGLE	FXP	FZP	MXP	MYP	MZP
30.	-60.00	.55	1.82	.70	.19	-.19
30.	60.00	.73	-.95	.19	-.12	-.27
30.	-65.00	.52	1.80	.71	-.01	-.21
30.	65.00	.73	-.88	.07	-.19	-.30
30.	-75.00	.37	1.52	.58	-.09	-.19
30.	75.00	.50	-.55	-.13	.05	-.15
30.	-90.00	.25	1.09	.47	-.13	-.10
30.	90.00	.30	.17	.13	.20	-.18
30.	-135.0	.54	.24	-.05	-.24	-.20
30.	135.00	.87	.73	.44	.08	-.32
30.	180.00	1.06	.29	.14	-.22	-.30
45.	0.00	1.23	.30	.29	-.05	-.44
45.	-65.00	.51	1.71	.57	-.47	.02
45.	65.00	.55	-.65	.11	.05	-.22
45.	180.00	1.11	.27	.16	-.28	-.64
60.	0.00	.98	.27	.26	-.16	-.53
60.	-15.00	.98	.64	.52	-.09	-.48
60.	15.00	1.13	-.05	.02	-.52	-.44
60.	-30.00	.73	.91	.53	-.06	-.35
60.	30.00	.91	-.30	.06	-.27	-.48
60.	-45.00	.49	1.07	.56	.05	-.23
60.	45.00	.63	-.35	.01	-.22	-.31
60.	-60.00	.31	1.12	.34	.01	-.19
60.	60.00	.40	-.36	.08	-.10	-.23
60.	-65.00	.24	1.11	.49	.04	-.20
60.	65.00	.32	-.26	-.05	-.04	-.14
60.	-75.00	.18	.95	.35	-.03	-.21
60.	75.00	.25	-.18	-.02	-.01	-.10
60.	-90.00	.17	.78	.43	-.20	-.07
60.	90.00	.20	.21	.24	.04	-.09
60.	-135.0	.34	.17	.09	-.12	-.24
60.	135.00	.61	.70	.43	.12	-.35
60.	180.00	.82	.28	.13	-.12	-.60

Table 6b. MATRIX OF SINGLE COLLECTOR LOADS AT HCL/C = K_1 (CONFIGURATION 2)

DATA FOR THE SANDIA PARABOLIC COLLECTOR FORCE AND MOMENT COEFFICIENTS FILE-NAME: MDCOL2

CONFIGURATION 2 C = 2 92 L = 19 80 INCHES ONE SINGLE COLLECTOR,RIM ANGLE=40

WIND AZIM	PITCH ANGLE	FXP	FZP	MXP	MYP	MZP
0	0 00	1 43	32	11	- 26	- 10
0	-15 00	1 29	62	23	- 13	- 02
0	15 00	1 35	- 06	13	- 12	06
0	-30 00	1 05	97	26	- 06	- 03
0	30 00	1 30	- 37	08	- 24	- 07
0	-45 00	84	1 26	33	08	- 03
0	45 00	1 11	- 65	19	- 21	- 06
0	-60 00	63	1 61	41	08	01
0	60 00	75	- 80	16	- 17	- 07
0	-75 00	27	1 89	43	16	- 06
0	75 00	29	- 62	14	- 11	- 01
0	-90 00	06	1 02	28	01	02
0	90 00	11	10	07	15	- 02
0	-135 0	79	- 38	05	- 11	01
0	135 00	90	1 17	35	03	- 07
0	180 00	1 26	13	08	- 16	- 03
-15	0 00	1 30	33	16	- 02	16
-15	-75 00	29	1 72	24	10	04
-15	75 00	34	- 61	16	- 23	- 05
-15	180 00	1 28	13	19	- 24	05
15	0 00	1 45	34	28	- 22	- 14
15	-75 00	26	1 77	48	14	- 02
15	75 00	34	- 61	12	- 22	- 01
15	180 00	1 19	17	09	- 10	- 17
30	0 00	1 31	36	24	- 04	- 20
30	-15 00	1 29	66	35	- 05	- 24
30	15 00	1 35	- 03	- 00	- 20	- 30
30	-30 00	1 07	1 01	42	- 04	- 30
30	30 00	1 22	- 32	11	- 17	- 35
30	-45 00	89	1 38	56	05	- 23
30	45 00	1 01	- 56	- 01	- 16	- 52
30	-60 00	63	1 73	72	07	- 16
30	60 00	68	- 72	- 09	- 23	- 16
30	-75 00	22	1 62	54	20	- 07
30	75 00	25	- 46	03	- 10	- 08
30	-90 00	- 00	1 01	33	13	- 16
30	90 00	09	32	23	15	- 10
30	-135 0	77	- 26	- 08	- 15	- 20
30	135 00	92	1 29	57	01	- 27
30	180 00	1 16	19	12	- 09	- 23
45	0 00	1 32	35	18	- 24	- 47
45	-75 00	22	1 32	49	01	- 11
45	75 00	22	- 25	04	- 15	- 16
45	180 00	1 17	29	34	- 27	- 54
60	0 00	96	30	23	- 18	- 52
60	-15 00	94	56	37	- 13	- 49
60	15 00	97	- 01	09	- 23	- 47
60	-30 00	89	90	52	- 11	- 44
60	30 00	83	- 14	02	- 23	- 41
60	-45 00	65	1 15	59	03	- 23
60	45 00	54	- 27	07	- 14	- 30
60	-60 00	33	1 16	49	08	- 10
60	60 00	30	- 18	- 03	- 16	- 20
60	-75 00	14	92	40	- 00	- 06
60	75 00	11	- 05	06	- 03	- 13
60	-90 00	01	55	26	00	- 00
60	90 00	06	31	19	02	00
60	-135 0	47	- 05	01	- 15	- 25
60	135 00	70	1 06	53	01	- 30
60	180 00	96	22	22	- 14	- 52

Table 6c. MATRIX OF SINGLE COLLECTOR LOADS AT HCL/C = K_I (CONFIGURATION 3)

DATA FOR THE SANDIA PARABOLIC COLLECTOR — FORCE AND MOMENT COEFFICIENTS — FILE-NAME: MDCOL3

CONFIGURATION 3 — C = 2.94 — L = 10.80 INCHES — ONE SINGLE COLLECTOR,RIM ANGLE=65

WIND AZIM.	PITCH ANGLE	FXP	FZP	MXP	MYP	MZP
0.	0.00	1.44	.40	.18	-.19	-.06
0.	-15.00	1.31	.69	.23	-.16	-.04
0.	15.00	1.40	-.05	.14	-.16	-.02
0.	-30.00	1.11	.96	.45	-.07	-.04
0.	30.00	1.38	-.36	.22	-.21	-.12
0.	-45.00	.82	1.34	.42	.01	-.01
0.	45.00	1.19	-.66	.21	-.22	-.00
0.	-60.00	.67	1.78	.36	.03	-.01
0.	60.00	.83	-1.05	.34	-.17	.01
0.	-70.00	.39	1.96	.49	.13	-.09
0.	70.00	.59	-1.04	.29	-.25	-.05
0.	-75.00	.22	1.83	.46	.20	-.02
0.	75.00	.44	-.94	.42	.06	.08
0.	-90.00	.17	1.33	.31	-.13	-.06
0.	90.00	.17	-.07	.09	.18	.01
0.	-135.0	.68	-.11	.14	-.19	-.09
0.	135.00	.83	.96	.34	.10	-.04
0.	180.00	1.17	.22	.24	-.12	-.01
-15.	0.00	1.40	.39	.06	-.22	.06
-15.	-70.00	.41	1.88	.23	.08	.09
-15.	70.00	.57	-.95	.40	-.28	.07
-15.	180.00	1.24	.25	.22	-.13	.12
15.	0.00	1.46	.38	.21	-.20	-.18
15.	-70.00	.47	1.96	.55	.02	-.04
15.	70.00	.62	-1.00	.15	-.37	-.19
15.	180.00	1.25	.20	.23	-.32	-.28
30.	0.00	1.39	.45	.29	-.12	-.38
30.	-15.00	1.37	.71	.34	-.23	-.26
30.	15.00	1.37	-.06	.10	-.17	-.35
30.	-30.00	1.20	1.00	.52	-.12	-.31
30.	30.00	1.27	-.31	.14	-.16	-.26
30.	-45.00	.92	1.36	.45	-.07	-.23
30.	45.00	1.08	-.66	-.03	-.17	-.29

WIND AZIM	PITCH ANGLE	FXP	FZP	MXP	MYP	MZP
30	-60.00	.65	1.78	.60	-.06	-.22
30	60.00	.78	-.94	.06	-.29	-.24
30	-70.00	.39	1.76	.61	-.03	-.18
30	70.00	.48	-.81	.17	-.21	-.16
30	-75.00	.27	1.70	.60	-.03	-.15
30	75.00	.39	-.74	.11	-.13	-.13
30	-90.00	.08	1.15	.51	.00	-.10
30	90.00	.18	-.02	.07	.14	-.05
30	-135.0	.73	-.11	.03	-.33	-.21
30	135.00	.92	1.06	.48	-.05	-.32
30	180.00	1.14	.22	.14	-.22	-.29
45	0.00	1.31	.33	.18	-.16	-.44
45	-70.00	.32	1.46	.56	-.02	-.12
45	70.00	.35	-.56	.08	-.11	-.03
45	180.00	1.00	.17	.08	-.11	-.38
60	0.00	1.08	.41	.32	-.28	-.59
60	-15.00	.93	.59	.35	-.08	-.43
60	15.00	1.01	-.03	.07	-.19	-.56
60	-30.00	.80	.92	.43	-.07	-.35
60	30.00	.88	-.23	.01	-.20	-.44
60	-45.00	.63	1.17	.51	-.04	-.23
60	45.00	.65	-.37	.04	-.22	-.33
60	-60.00	.33	1.15	.52	-.05	-.15
60	60.00	.34	-.29	.07	-.14	-.20
60	-70.00	.18	1.01	.47	-.06	-.12
60	70.00	.25	-.19	.09	-.15	-.08
60	-75.00	.13	.94	.42	-.04	-.06
60	75.00	.16	-.10	.01	-.05	-.10
60	-90.00	.05	.65	.23	-.04	-.03
60	90.00	.14	.20	.23	-.00	-.12
60	-135.0	.41	-.04	-.02	-.18	-.25
60	135.00	.72	.87	.46	-.02	-.34
60	180.00	.94	.26	.13	-.18	-.54

Table 6d. MATRIX OF SINGLE COLLECTOR LOADS AT HCL/C = K_I (CONFIGURATION 4)

DATA FOR THE SANDIA PARABOLIC COLLECTOR — FORCE AND MOMENT COEFFICIENTS — FILE-NAME: MDCOL4

CONFIGURATION 4 — C = 3.00 — L = 10.80 INCHES — ONE SINGLE COLLECTOR, RIM ANGLE=120

WIND AZIM	PITCH ANGLE	FXP	FZP	MXP	MYP	MZP
0	0.00	1.55	.18	.14	-.36	-.09
0	-15.00	1.32	.63	.25	-.26	-.09
0	15.00	1.60	-.23	.14	-.26	-.11
0	-30.00	1.13	1.10	.28	-.19	-.07
0	30.00	1.53	-.71	.21	-.36	-.04
0	-45.00	.80	1.25	.21	-.12	-.01
0	45.00	1.35	-.98	.30	-.34	-.06
0	-55.00	.65	1.23	.30	-.06	.03
0	55.00	1.22	-.83	.28	-.13	-.04
0	-60.00	.67	1.26	.37	-.23	-.04
0	60.00	1.04	-.61	.27	.08	-.05
0	-75.00	.58	.93	.24	-.34	-.17
0	75.00	.67	-.07	.09	.15	-.04
0	-90.00	.56	.61	.19	-.46	.00
0	90.00	.55	.87	.30	.24	-.05
0	-135.0	.49	.89	.24	-.43	-.01
0	135.00	.89	-.27	.17	.36	-.00
0	180.00	.89	.33	.18	-.17	-.07
-15	0.00	1.54	.24	.16	-.36	.05
-15	-55.00	.68	1.34	.21	-.08	.12
-15	55.00	1.16	-.78	.36	-.10	.09
-15	180.00	.85	.29	.07	-.10	.14
15	0.00	1.51	.33	.29	-.22	-.18
15	-55.00	.66	1.33	.38	-.08	.16
15	55.00	1.16	-.77	.18	-.16	-.22
15	180.00	.92	.33	.19	-.21	-.11
30	0.00	1.53	.23	.28	-.36	-.44
30	-15.00	1.40	.75	.36	-.29	-.32
30	15.00	1.51	-.22	-.00	-.26	-.35
30	-30.00	1.17	1.15	.45	-.19	-.31
30	30.00	1.50	-.65	.14	-.50	-.44
30	-45.00	.74	1.26	.51	.05	-.26
30	45.00	1.21	-.84	.14	-.35	-.40
30	-55.00	.65	1.26	.43	-.06	-.22
30	55.00	1.07	-.69	.13	-.12	-.37
30	-60.00	.67	1.37	.51	-.14	-.22
30	60.00	.99	-.57	.01	-.02	-.32
30	-75.00	.60	1.09	.40	-.33	-.22
30	75.00	.78	-.23	.01	.12	-.46
30	-90.00	.55	.91	.46	-.45	-.31
30	90.00	.64	.28	.00	.28	-.38
30	-135.0	.50	.79	.12	-.44	-.18
30	135.00	.88	-.07	.32	.28	-.32
30	180.00	.91	.32	.24	-.09	-.19
45	0.00	1.33	.22	.22	-.26	-.57
45	-55.00	.64	1.21	.47	-.15	-.27
45	55.00	1.05	-.75	.06	-.09	-.37
45	180.00	1.01	.30	.22	-.24	-.59
60	0.00	1.29	.22	.31	-.21	-.52
60	-15.00	1.18	.86	.41	-.11	-.46
60	15.00	1.36	-.24	.10	-.34	-.50
60	-30.00	.82	1.11	.46	-.07	-.30
60	30.00	1.29	-.58	.14	-.34	-.47
60	-45.00	.65	1.08	.41	-.05	-.23
60	45.00	1.11	-.73	.10	-.23	-.46
60	-55.00	.63	1.14	.45	-.15	-.24
60	55.00	1.06	-.73	.09	-.15	-.37
60	-60.00	.58	1.27	.58	-.12	-.21
60	60.00	.99	-.73	.04	-.03	-.28
60	-75.00	.57	1.09	.51	-.34	-.20
60	75.00	.77	-.46	-.01	.14	-.32
60	-90.00	.45	.96	.42	-.35	-.23
60	90.00	.58	.00	.01	.22	-.36
60	-135.0	.51	.53	.13	-.44	-.23
60	135.00	.92	.29	.56	.13	-.54
60	180.00	1.01	.33	.19	-.25	-.60

Table 7. LOADS FOR VARIOUS GAP SPACINGS FOR CONFIGURATION 5

DATA FOR THE SANDIA PARABOLIC COLLECTOR — FORCE AND MOMENT COEFFICIENTS — FILE-NAME: MD1800

CONFIGURATION 5 — C = 2.80 — L = 10.80 INCHES — GAP STUDY, ONE COLLECTOR ROW

PITCH	G/C	FXP	FZP	MXP	MYP	MZP	PITCH	G/C	FXP	FZP	MXP	MYP	MZP
0.	.57	1.57	.52	.36	-.30	-.10	-.65	.57	.53	2.10	.51	.04	-.01
0.	.71	1.60	.43	.28	-.33	-.03	-.65	.71	.54	2.06	.46	.02	-.14
0.	.89	1.56	.37	.22	-.24	-.12	-.65	.89	.53	2.01	.52	.02	-.07
0.	1.07	1.60	.42	.27	-.36	-.19	-.65	1.07	.50	1.98	.47	.04	.02
0.	1.25	1.60	.42	.28	-.29	-.01	-.65	1.25	.56	1.97	.42	-.06	-.06
0.	1.43	1.56	.41	.28	-.22	-.13	-.65	1.43	.48	1.93	.46	.12	-.06
0.	1.61	1.51	.44	.31	-.19	.06	-.65	1.61	.51	1.94	.52	.06	-.07
0.	1.79	1.50	.41	.35	-.10	-.01	-.65	1.79	.51	2.00	.56	.06	-.00
0.	2.14	1.58	.44	.24	-.34	-.06	-.65	2.14	.46	2.01	.54	.15	.05
0.	2.50	1.50	.49	.30	-.15	.04	-.65	2.50	.47	1.98	.46	.09	.04
0.	2.86	1.50	.47	.35	-.20	-.07	-.65	2.86	.48	1.98	.48	.11	-.07
0.	3.21	1.49	.45	.29	-.19	-.09	-.65	3.21	.45	1.94	.43	.12	.01
0.	3.57	1.49	.45	.32	-.18	-.06	-.65	3.57	.46	1.95	.50	.11	.03

DATA FOR THE SANDIA PARABOLIC COLLECTOR — FORCE AND MOMENT COEFFICIENTS — FILE-NAME: MDGAP2

CONFIGURATION 5 — C = 2.80 — L = 10.80 INCHES — GAP STUDY, ONE COLLECTOR ROW, ALTERNATE LEGS

PITCH	G/C	FXP	FZP	MXP	MYP	MZP	PITCH	G/C	FXP	FZP	MXP	MYP	MZP
0.	.06	1.50	.23	.20	-.35	-.14	-.65	.06	.61	1.68	.38	-.00	-.07
0.	.11	1.43	.11	.08	-.13	-.01	-.65	.11	.54	1.81	.44	.22	-.06
0.	.18	1.45	.05	.14	-.17	-.10	-.65	.18	.54	1.76	.41	.03	-.07
0.	.27	1.46	.11	.26	-.15	-.06	-.65	.27	.51	1.82	.48	.09	-.10
0.	.36	1.49	.10	-.11	-.22	-.09	-.65	.36	.48	1.80	.39	.11	-.04
0.	.54	1.41	.14	.14	-.08	-.03	-.65	.54	.46	1.80	.36	.20	-.02
0.	.71	1.51	.15	.18	-.32	-.15	-.65	.71	.34	1.76	.34	.42	.08
0.	.89	1.43	.20	.20	-.14	-.08	-.65	.89	.49	1.72	.31	.07	-.07
0.	1.07	1.41	.21	.17	-.12	-.04	-.65	1.07	.48	1.74	.39	.07	-.06
0.	1.25	1.46	.18	.25	-.23	-.05	-.65	1.25	.47	1.74	.40	.15	-.03

Table 8. DATA FOR ESTABLISHMENT OF ROW SPACING R (CONFIGURATION 9)

DATA FOR THE SANDIA PARABOLIC COLLECTOR — FORCE AND MOMENT COEFFICIENTS — FILE-NAME: MDR2.0

CONFIGURATION 9 C = 2.80 L = 10.80 INCHES — ROW STUDY, ROW SPACING=2.0*C

WIND AZIM.	PITCH ANGLE	FXP	FZP	MXP	MYP	MZP
0.	0.00	.04	-.11	-.19	-.05	-.06
0.	0.00	.05	-.11	-.15	-.06	-.07
0.	-60.00	.29	.36	-.06	.04	-.11
0.	-65.00	.25	.43	-.04	.03	-.07

WIND AZIM	PITCH ANGLE	FXP	FZP	MXP	MYP	MZP
15.	-60.00	.28	.30	.00	-.09	-.08
15.	-65.00	.25	.30	-.07	-.03	-.05
30.	-60.00	.29	.32	.03	-.09	-.16
30.	-65.00	.29	.37	.12	-.15	-.18

DATA FOR THE SANDIA PARABOLIC COLLECTOR — FORCE AND MOMENT COEFFICIENTS — FILE-NAME: MDR2.5

CONFIGURATION 9 C = 2.80 L = 10.80 INCHES — ROW STUDY, ROW SPACING=2.5*C

WIND AZIM.	PITCH ANGLE	FXP	FZP	MXP	MYP	MZP
0.	0.00	.15	-.08	-.08	-.19	-.19
0.	-60.00	.41	.40	-.23	-.18	-.16

WIND AZIM.	PITCH ANGLE	FXP	FZP	MXP	MYP	MZP
15.	-60.00	.35	.37	.13	-.19	-.27
30.	-60.00	.40	.42	.25	-.20	-.17

DATA FOR THE SANDIA PARABOLIC COLLECTOR — FORCE AND MOMENT COEFFICIENTS — FILE-NAME: MDR3.0

CONFIGURATION 9 C = 2.80 L = 10.80 INCHES — ROW STUDY, ROW SPACING=3.0*C

WIND AZIM.	PITCH ANGLE	FXP	FZP	MXP	MYP	MZP
0.	0.00	.17	-.09	.01	-.15	-.16
0.	-60.00	.48	.57	-.01	-.20	-.12

WIND AZIM.	PITCH ANGLE	FXP	FZP	MXP	MYP	MZP
15.	-60.00	.35	.53	.13	-.04	-.18
30.	-60.00	.44	.49	.17	-.23	-.18

Table 9a. LOADS ON ARRAY FIELDS (CONFIGURATIONS 5-9)

DATA FOR THE SANDIA PARABOLIC COLLECTOR — FORCE AND MOMENT COEFFICIENTS — FILE-NAME: MD8ROW

CONFIGURATION 8 — C = 2.80 — L = 10.80 INCHES — FOUR COLLECTOR ROWS, R/C=2.25

WIND AZIM	PITCH ANGLE	FXP	FZP	MXP	MYP	MZP
0	0.00	.10	.29	.03	-.23	-.10
0	-30.00	.06	.26	.14	-.23	-.22
0	30.00	.37	.10	.23	-.23	-.20
0	-45.00	.21	.41	.10	-.25	-.17
0	45.00	.48	-.13	.12	-.33	-.14
0	-60.00	.36	.86	.26	-.12	-.12
0	60.00	.46	-.31	.25	-.06	-.01
0	-75.00	.32	.99	.16	-.18	-.11
0	75.00	.47	-.21	.07	-.25	-.08
0	-90.00	.15	.68	.08	-.13	-.01
0	90.00	.29	.14	.13	-.10	-.06
0	-120.0	.14	.38	.24	-.26	-.10
0	120.00	.51	.37	.21	-.11	-.08
0	-135.0	.08	.28	.02	-.10	.00
0	135.00	.55	.58	.30	-.34	-.08
0	180.00	.20	.26	.17	-.09	-.04
15	0.00	.00	.27	.20	-.01	-.06
15	-60.00	.39	.71	.04	-.22	-.08
15	60.00	.46	.28	.11	-.14	-.07
15	180.00	.19	.23	.03	-.08	-.09
30	0.00	.10	.32	.20	-.14	-.04
30	-60.00	.29	.69	.26	-.08	-.13
30	60.00	.37	-.19	.02	-.16	-.23
30	180.00	.20	.33	.24	-.15	-.06

DATA FOR THE SANDIA PARABOLIC COLLECTOR — FORCE AND MOMENT COEFFICIENTS — FILE-NAME: MD9ROW

CONFIGURATION 9 — C = 2.80 — L = 10.80 INCHES — SIX COLLECTOR ROWS, R/C=2.25

WIND AZIM	PITCH ANGLE	FXP	FZP	MXP	MYP	MZP
0	0.00	.20	.26	.17	-.35	-.17
0	-30.00	.11	.22	.10	.07	-.01
0	30.00	.16	.28	.11	-.23	-.20
0	-45.00	.21	.33	.12	-.02	-.11
0	45.00	.32	.12	.08	-.41	-.26
0	-60.00	.27	.73	.08	.08	.01
0	60.00	.29	-.03	.19	-.20	-.16
0	-75.00	.23	.72	.05	-.02	-.01
0	75.00	.30	-.03	.22	-.11	-.08
0	-90.00	.24	.46	-.03	-.34	-.14
0	90.00	.22	.16	.25	-.00	-.07
0	-120.0	.10	.35	.19	-.25	-.10
0	120.00	.33	.36	.11	.09	-.05
0	-135.0	.11	.25	.08	-.18	-.13
0	135.00	.51	.38	.09	-.40	-.20
0	180.00	.17	.22	.20	-.15	-.13
15	0.00	.20	.29	.21	-.38	-.27
15	-60.00	.18	.58	.19	.12	-.01
15	60.00	.34	-.02	.06	-.29	-.20
15	180.00	.20	.31	.29	-.20	-.14
30	0.00	.31	.35	.24	-.23	-.23
30	-60.00	.24	.64	.30	.05	-.06
30	60.00	.32	.06	.05	-.29	-.17
30	180.00	.30	.27	.16	-.10	-.18

Table 9b. LOADS ON ARRAY FIELDS (CONFIGURATIONS 5-9)

DATA FOR THE SANDIA PARABOLIC COLLECTOR — FORCE AND MOMENT COEFFICIENTS — FILE-NAME: M06ROW

CONFIGURATION 6 — C = 2.80 — L = 10.80 INCHES — TWO COLLECTOR ROWS, R/C=2.25

WIND AZIM.	PITCH ANGLE	FXP	FZP	MXP	MYP	MZP
0	0.00	1.78	.31	.29	.10	.15
0	-30.00	1.53	1.14	.23	-.07	.08
0	30.00	1.79	-.70	.42	-.13	.06
0	-45.00	1.12	1.48	.39	.05	.01
0	45.00	1.38	-1.18	.24	.04	.13
0	-60.00	.72	1.60	.03	-.06	-.01
0	-60.00	.62	1.62	.11	.16	-.02
0	60.00	1.02	-1.79	.27	-.28	-.00
0	-75.00	.38	1.44	.41	.02	-.04
0	75.00	.65	-.66	.25	.06	-.00
0	-90.00	.31	.69	.19	-.18	-.01
0	90.00	.44	.63	.17	.03	-.08
0	-120.0	.42	.56	.34	-.38	-.01
0	120.00	.62	.24	.18	.37	.06
0	-135.0	.69	.41	.33	-.40	.00
0	135.00	.98	.50	.27	.21	-.02
0	180.00	1.44	.37	.28	-.18	.05
15	0.00	1.84	.35	.30	-.07	-.02
15	-60.00	.57	1.65	.34	.19	-.02
15	-60.00	.57	1.66	.38	.20	-.10
15	60.00	.98	-1.79	.11	-.22	-.15
15	180.00	1.41	.34	.15	-.24	-.27
30	0.00	1.64	.36	.37	-.09	-.27
30	-60.00	.58	1.58	.50	-.01	-.10
30	60.00	.93	-1.64	.13	-.22	-.25
30	180.00	1.23	.52	.44	.02	-.40

DATA FOR THE SANDIA PARABOLIC COLLECTOR — FORCE AND MOMENT COEFFICIENTS — FILE-NAME: M07ROW

CONFIGURATION 7 — C = 2.80 — L = 10.80 INCHES — THREE COLLECTOR ROWS, R/C=2.25

WIND AZIM.	PITCH ANGLE	FXP	FZP	MXP	MYP	MZP
0	0.00	.17	.27	.09	-.23	-.04
0	-30.00	.15	.34	.18	-.20	-.07
0	30.00	.19	.36	.13	-.26	-.06
0	-45.00	.17	.42	.16	.00	-.05
0	45.00	.33	.13	.23	-.20	-.06
0	-60.00	.51	.99	.27	-.34	-.14
0	60.00	.38	.01	.08	-.00	.06
0	-75.00	.39	1.04	.11	-.27	-.16
0	75.00	.46	-.12	.14	-.12	-.09
0	-90.00	.19	.78	.19	-.17	-.05
0	90.00	.29	.18	.17	.08	-.02
0	-120.0	.19	.40	.17	-.28	-.02
0	120.00	.59	.43	.12	.00	-.02
0	-135.0	.12	.32	.20	-.26	-.00
0	135.00	.48	.62	.19	-.24	-.10
0	180.00	.15	.39	.17	-.16	-.11
15	0.00	.23	.30	.13	-.26	-.27
15	-60.00	.44	.93	.22	-.23	-.16
15	60.00	.45	-.20	.13	-.15	-.11
15	180.00	.22	.42	.01	-.11	-.26
30	0.00	.26	.36	.25	-.08	-.18
30	-60.00	.43	.83	.34	-.30	-.11
30	60.00	.44	-.18	-.00	-.14	-.14
30	180.00	.35	.31	.11	-.17	-.18

Table 9c. LOADS ON ARRAY FIELDS (CONFIGURATIONS 5-9)

DATA FOR THE SANDIA PARABOLIC COLLECTOR — FORCE AND MOMENT COEFFICIENTS — FILE-NAME: MDEDIT

CONFIGURATION 5 — C = 2.80 — L = 10.80 INCHES — ONE ROW OF THREE COLLECTORS, G/C= .536

WIND AZIM.	PITCH ANGLE	FXP	FZP	MXP	MYP	MZP
0	0.00	1.59	.12	.21	-.15	-.03
0	-30.00	1.35	.93	.27	-.26	-.06
0	30.00	1.64	-.65	.30	-.33	-.16
0	-45.00	1.07	1.45	.36	-.03	-.04
0	45.00	1.42	-1.04	.41	-.35	-.13
0	-60.00	.62	1.85	.42	.29	-.00
0	60.00	.97	-1.38	.24	-.36	-.12
0	-75.00	.44	1.62	.30	-.06	-.08
0	75.00	.61	-.78	.21	-.03	-.07
0	-90.00	.29	.58	.14	-.14	-.03
0	90.00	.32	.37	.14	.25	-.02
0	-120.0	.45	.09	.14	-.31	-.10
0	120.00	.69	.07	.12	.18	-.09
0	-135.0	.75	-.07	.04	-.51	-.13
0	135.00	.98	.39	.14	.09	-.10
0	180.00	1.23	.09	.24	-.22	-.05
-15	0.00	1.61	.14	.11	-.18	.06
-15	-60.00	.69	1.78	.13	.07	.06
-15	60.00	.94	-1.36	.50	-.35	.01
-15	180.00	1.16	.06	.06	-.14	.08
15	0.00	1.63	.12	.15	-.16	-.14
15	-60.00	.64	1.86	.53	.18	-.06
15	60.00	.91	-1.37	.28	-.27	-.16
15	180.00	1.21	.07	.10	-.21	-.17
30	0.00	1.56	.17	.28	-.25	-.31
30	-30.00	1.20	.02	.41	-.05	-.23
30	30.00	1.53	-.69	.16	-.27	-.36
30	-45.00	.96	1.40	.65	-.01	-.15
30	45.00	1.30	-1.09	.11	-.26	-.34
30	-60.00	.61	1.65	.58	.03	-.16
30	60.00	.73	-1.21	.22	-.08	-.18
30	-75.00	.37	1.41	.39	-.06	-.12
30	75.00	.57	-.84	.05	-.04	-.18
30	-90.00	.25	.71	.34	-.15	-.09
30	90.00	.30	.09	.13	.18	-.15
30	-120.0	.39	.08	.12	-.26	-.16
30	120.00	.77	.46	.51	.07	-.33
30	-135.0	.66	-.04	.12	-.38	-.20
30	135.00	.98	.54	.48	.09	-.41
30	180.00	1.29	.11	.24	-.29	-.43
45	0.00	1.38	.10	.36	-.42	-.49
45	-60.00	.38	1.16	.52	.11	-.07
45	60.00	.67	-.92	.13	-.30	-.28
45	180.00	1.00	.02	.07	-.16	-.45
60	0.00	.71	.04	.14	-.07	-.27
60	-30.00	.60	.47	.32	-.10	-.17
60	30.00	.71	-.31	.14	-.28	-.25
60	-45.00	.42	.61	.28	-.10	-.11
60	45.00	.52	-.45	.07	-.19	-.16
60	-60.00	.19	.61	.21	.07	-.06
60	60.00	.32	-.41	.12	-.11	-.14
60	-75.00	.18	.54	.16	-.13	-.09
60	75.00	.22	-.26	.19	-.06	-.09
60	-90.00	.10	.32	.04	-.10	-.03
60	90.00	.15	.07	.23	.03	-.04
60	-120.0	.18	.00	.05	-.16	-.07
60	120.00	.30	.26	.18	.03	-.13
60	-135.0	.25	.01	.08	-.15	-.11
60	135.00	.39	.29	.35	.09	-.13
60	180.00	.61	.09	.01	-.17	-.20

Table 10a. FENCE STUDY

File: MDFNCE

RUN #	FENCE HEIGHT FH/C	SPACE BETWEEN THE FENCE AND FIRST COLL. ROW FS/C	PITCH ANGLE	CONFIGURATION WITH OR WITHOUT TORQUE TUBE
270	1.43	2	180	V without
271	1.43	2	120	V without
272	1.43	2	0	V without
273	1.43	2	-60	V without
274	0.71	3	0	V without
275	0.71	3	-60	V without
276	0.71	3	0	VI without
277	0.71	3	-60	VI without
278	0.71 alt fence	3	0	VI without
279	0.71 alt fence	3	-60	VI without
280	1.07	3	0	VI without
281	1.07	3	-60	VI without
282	1.43	3	0	VI without
283	1.43	3	-60	VI without
284	0.36	3	0	VI with
285	0.36	3	-60	VI with
286	0.36	3	-60	VI without
287	0.36	3	0	VI without
288	0.71 alt fence	3	-60	VI with
289	0.71 alt fence	3	0	VI with
290	1.07	3	120	VI with

Table 10b. FENCE STUDY (CONTINUED)

File: MDFNC1

RUN #	FENCE HEIGHT FH/C	SPACE BETWEEN THE FENCE AND FIRST COLL. ROW FS/C	PITCH ANGLE	CONFIGURATION WITH OR WITHOUT TORQUE TUBE
291	1.07	3	180	VI with
292	1.07	3	180	VI without
293	1.07	3	120	VI without
294	1.07	5	0	VI without
295	1.07	5	-60	VI without
296	1.07	3	0	VII without
297	1.07	3	-60	VII without
298	1.07	3	-60	IX without
299	1.07	3	0	IX without
300	1.07	3	0	IX without (ψ=30°)

Table 10c. EFFECT OF FENCES ON ARRAY FIELD LOADS

DATA FOR THE SANDIA PARABOLIC COLLECTOR — FORCE AND MOMENT COEFFICIENTS — FILE-NAME: MDFNCE

C = 2.80 L = 10.80 INCHES FENCE STUDY

RUN #	FXP	FZP	MXP	MYP	MZP	RUN #	FXP	FZP	MXP	MYP	MZP
270	.20	.25	.24	-.32	-.12	281	-.04	.28	.17	.14	-.02
271	.18	.22	.13	-.31	-.13	282	.10	.24	.19	-.05	-.04
272	.27	.20	.14	-.23	-.05	283	.07	.22	.11	-.12	-.12
273	.08	.33	.12	-.01	-.04	284	1.10	.41	.38	-.19	-.07
274	.36	.27	.17	-.03	-.08	285	.23	.29	.17	-.02	-.03
275	.06	.28	.28	-.12	-.11	286	.07	.50	.25	.06	-.07
276	.26	.32	.32	.16	-.01	287	1.03	.27	.00	-.05	.03
277	.14	.16	.14	-.30	-.29	288	.09	.20	.18	-.21	-.14
278	.33	.29	.23	-.09	-.11	289	.37	.25	.08	-.15	-.14
279	.01	.23	.15	-.04	-.05	290	.09	.35	.51	-.04	-.12
280	.11	.18	.15	-.03	-.05	291	.06	.20	.22	-.02	-.09

DATA FOR THE SANDIA PARABOLIC COLLECTOR — FORCE AND MOMENT COEFFICIENTS — FILE-NAME: MDFNC1

C = 2.80 L = 10.80 INCHES FENCE STUDY

RUN #	FXP	FZP	MXP	MYP	MZP	RUN #	FXP	FZP	MXP	MYP	MZP
292	.19	.34	.22	-.29	-.10	296	.14	.29	.26	-.35	-.11
293	.26	.35	.19	-.46	-.20	297	.05	.29	.20	-.15	-.05
294	.17	.34	.30	-.30	-.11	298	.17	.41	.26	-.25	-.16
295	.05	.24	.14	-.13	-.15	299	.13	.28	.13	-.09	-.07
						300	.23	.40	.33	-.13	-.14

Table 11a. BERM STUDY

File: MDBERM

RUN #	BERM HEIGHT FH/C	SPACE BETWEEN THE BERM AND FIRST COLL. ROW FS/C	PITCH ANGLE	CONFIGURATION
301	1.07	3	0	IX
302	1.07	3	0	IX (ψ=30°)
303	1.07	3	0	VI
304	1.07	3	-60	VI
305	0.71	3	-60	VI
306	0.71	3	0	VI
307	0.36	3	0	VI
308	0.36	3	-60	VI
309	0.36	2	-60	VI

Table 11b. EFFECT OF BERMS ON ARRAY FIELD LOADS

DATA FOR THE SANDIA PARABOLIC COLLECTOR FORCE AND MOMENT COEFFICIENTS FILE-NAME: MOBERM

C = 2.80 L = 10.80 INCHES BERM STUDY

RUN #	FXP	FZP	MXP	MYP	MZP
301	.23	.49	.26	-.17	-.14
302	.14	.40	.16	.07	-.10
303	-.05	.50	.09	-.17	-.10
304	.16	.57	.20	-.36	-.16
305	.01	.36	.21	-.15	-.06
306	.24	.51	.12	-.06	-.07
307	1.13	.47	.07	-.32	-.18
308	.27	.71	.26	-.22	-.10
309	.32	.77	.18	-.34	-.17

Table 12. LOADS WITH A TORQUE TUBE ON COLLECTOR 1

DATA FOR THE SANDIA PARABOLIC COLLECTOR
C = 2.80 L = 10.80 INCHES

FORCE AND MOMENT COEFFICIENTS
TORQUE TUBE EFFECTS.COLL#1 ALONE

FILE-NAME: MDTOR1

WIND	PITCH	FXP	FZP	MXP	MYP	MZP
0	0	1.39	.41	.30	-.02	-.06
0	-30	.92	1.10	.16	.08	-.08
0	30	1.50	-.59	.26	-.25	-.09
0	-60	.55	1.36	.11	-.00	-.03
0	60	.78	-.18	-.01	.06	-.11
0	-90	.53	.21	.01	-.27	.00
0	90	.59	1.15	.18	.15	-.06
0	-120	.74	.46	-.02	-.41	-.06

Table 13. EFFECT OF θ ON PITCHING MOMENT COEFFICIENTS (CONFIGURATIONS 1-4)

CONFIGURATION 1 FILE NAME:MDPIM1

C = 2.80 L = 10.80

DETERMINATION OF THETA MAX, COLL#1

PITCH ANGLE	HCL/C	MYP	MYB	MYF	MYG
0	1.03	-.31	1.30	-.32	-.31
-15	1.03	-.41	1.12	-.43	-.42
-30	1.03	-.34	.99	-.39	-.36
-45	1.03	-.13	.95	-.18	-.14
-50	1.03	-.20	.82	-.24	-.21
-55	1.03	.02	.84	-.05	.00
-60	1.03	-.07	.69	-.14	-.10
-65	1.03	-.09	.51	-.16	-.12
-70	1.03	-.12	.41	-.15	-.13
-75	1.03	-.05	.37	-.05	-.05
-90	1.03	-.32	.05	-.23	-.29
-105	1.03	-.26	.14	-.16	-.22
-120	1.03	-.32	.18	-.21	-.28

CONFIGURATION 2 FILE NAME:MDPIM2

C = 2.92 L = 10.80

DETERMINATION OF THETA MAX, COLL#2

PITCH ANGLE	HCL/C	MYP	MYB	MYF	MYG
0	.99	-.24	1.30	-.26	-.24
-15	.99	-.21	1.20	-.30	-.21
-30	.99	.03	1.15	-.09	.03
-45	.99	.06	.93	-.10	.05
-60	.99	-.07	.67	-.16	-.08
-65	.99	-.11	.53	-.18	-.12
-70	.99	.05	.55	-.03	.05
-75	.99	.07	.41	-.02	.06
-80	.99	-.03	.20	-.05	-.03
-85	.99	-.05	.12	-.01	-.05
-90	.99	-.07	.03	-.00	-.07
-105	.99	-.22	.03	-.08	-.21

CONFIGURATION 3 FILE NAME:MDPIM3

C = 2.94 L = 10.80

DETERMINATION OF THETA MAX, COLL#3

PITCH ANGLE	HCL/C	MYP	MYB	MYF	MYG
0	.98	-.24	1.28	-.25	-.24
-15	.98	-.32	1.10	-.37	-.33
-30	.98	-.18	.97	-.24	-.19
-45	.98	-.07	.85	-.14	-.08
-60	.98	-.08	.65	-.15	-.09
-65	.98	-.02	.58	-.10	-.03
-70	.98	-.14	.36	-.21	-.15
-75	.98	-.04	.30	-.10	-.05
-80	.98	-.07	.21	-.07	-.07
-90	.98	-.14	.02	-.07	-.13
-105	.98	-.27	-.00	-.15	-.25

CONFIGURATION 4 FILE NAME:MDPIM4

C = 3.00 L = 10.80

DETERMINATION OF THETA MAX, COLL#4

PITCH ANGLE	HCL/C	MYP	MYB	MYF	MYG
0	.96	-.35	1.13	-.34	-.33
-15	.96	-.20	1.17	-.19	-.19
-30	.96	-.31	.89	-.32	-.32
-45	.96	-.08	.70	-.11	-.12
-50	.96	-.14	.59	-.16	-.16
-55	.96	-.11	.57	-.13	-.13
-60	.96	-.17	.47	-.17	-.17
-70	.96	-.17	.36	-.14	-.14
-75	.96	-.25	.28	-.20	-.20
-90	.96	-.39	.13	-.32	-.30
-105	.96	-.39	.13	-.29	-.27

Table 14. EFFECT OF HEIGHT HCL ON SINGLE COLLECTOR PITCHING MOMENT COEFFICIENTS AT $\theta = 0, \psi = 0$ (CONFIGURATIONS 1-4)

CONFIGURATION 1 FILE NAME:MDCDM1

C = 2.80 L = 10.80

HEIGHT EFFECT AT THETA=0,COLL#1

PITCH ANGLE	HCL/C	MYP	MYB	MYF	MYG
0.	.67	-.55	.44	-.58	-.56
0.	.71	-.25	.75	-.25	-.25
0.	.80	-.34	.89	-.37	-.35
0.	.89	-.14	1.18	-.17	-.15
0.	1.03	-.21	1.36	-.23	-.22
0.	1.25	-.07	1.77	-.08	-.07
0.	1.61	-.20	2.21	-.20	-.20
0.	1.96	-.49	2.54	-.49	-.49

CONFIGURATION 2 FILE NAME:MDCDM2

C = 2.92 L = 10.80

HEIGHT EFFECT AT THETA=0,COLL#2

PITCH ANGLE	HCL/C	MYP	MYB	MYF	MYG
0.	.64	-.18	.70	-.25	-.18
0.	.68	-.05	.91	-.07	-.05
0.	.77	-.20	.92	-.22	-.20
0.	.86	-.15	1.10	-.17	-.15
0.	.99	-.24	1.30	-.26	-.24
0.	1.20	-.19	1.55	-.21	-.19
0.	1.54	-.14	2.01	-.20	-.14
0.	1.88	-.45	2.33	-.47	-.45

CONFIGURATION 3 FILE NAME:MDCDM3

C = 2.94 L = 10.80

HEIGHT EFFECT AT THETA=0,COLL#3

PITCH ANGLE	HCL/C	MYP	MYB	MYF	MYG
0.	.64	-.17	.67	-.24	-.18
0.	.68	-.26	.73	-.27	-.26
0.	.77	-.10	1.01	-.11	-.10
0.	.85	-.18	1.11	-.19	-.18
0.	.98	-.29	1.17	-.30	-.29
0.	1.19	-.29	1.57	-.35	-.29
0.	1.53	-.18	2.01	-.19	-.18
0.	1.87	-.29	2.45	-.30	-.29

CONFIGURATION 4 FILE NAME:MDCDM4

C = 3.00 L = 10.80

HEIGHT EFFECT AT THETA=0,COLL#4

PITCH ANGLE	HCL/C	MYP	MYB	MYF	MYG
0.	.63	-.18	.66	-.19	-.20
0.	.67	-.24	.67	-.25	-.26
0.	.75	-.49	.66	-.47	-.47
0.	.83	-.35	.95	-.33	-.32
0.	.96	-.35	1.19	-.34	-.33
0.	1.17	-.25	1.63	-.26	-.26
0.	1.50	-.27	2.16	-.28	-.28
0.	1.83	-.32	2.54	-.34	-.34

Table 15. EFFECT OF HEIGHT HCL ON SINGLE COLLECTION PITCHING MOMENT COEFFICIENTS AT $\theta = \theta_{max}$, $\psi = 0$ (CONFIGURATIONS 1-4)

CONFIGUSATION 1 FILE NAME:MDCLM1

C = 2.80 L = 10.80

HEIGHT EFFECT AT THETA MAX, COLL#1

PITCH ANGLE	HCL/C	MYP	MYB	MYF	MYG
-65	.67	.02	.33	-.07	-.01
-65	.71	.12	.44	.05	.09
-65	.86	.03	.43	-.05	.00
-65	.89	.07	.49	-.01	.04
-65	1.03	.05	.59	-.03	.02
-65	1.25	.13	.78	.04	.09
-65	1.61	.11	.94	.03	.08
-65	1.96	.00	1.12	-.08	-.03

CONFIGURATION 2 FILE NAME:MDCLM2

C = 2.92 L = 10.80

HEIGHT EFFECT AT THETA MAX, COLL#2

PITCH ANGLE	HCL/C	MYP	MYB	MYF	MYG
-75	.64	.14	.35	.05	.14
-75	.68	.13	.35	.03	.13
-75	.77	.19	.43	.09	.19
-75	.86	.04	.34	-.03	.03
-75	.99	.07	.41	-.00	.07
-75	1.03	.01	.42	-.03	.01
-75	1.20	.16	.55	.09	.16
-75	1.54	-.07	.54	-.10	-.07
-75	1.88	.15	.77	.07	.14

CONFIGURATION 3 FILE NAME:MDCLM3

C = 2.94 L = 10.80

HEIGHT EFFECT AT THETA MAX, COLL#3

PITCH ANGLE	HCL/C	MYP	MYB	MYF	MYG
-70	.64	-.13	.30	-.07	-.12
-70	.68	-.07	.41	-.01	-.06
-70	.77	-.05	.48	-.00	-.04
-70	.85	-.15	.51	-.07	-.14
-70	.98	-.08	.66	-.02	-.07
-70	1.19	-.11	.79	-.06	-.11
-70	1.53	-.16	1.06	-.11	-.15
-70	1.87	-.16	1.39	-.07	-.15

CONFIGURATION 4 FILE NAME:MDCLM4

C = 3.00 L = 10.80

HIEGHT EFFECT AT THETA MAX, COLL#4

PITCH ANGLE	HCL/C	MYP	MYB	MYF	MYG
-55	.83	-.10	.42	-.09	-.09
-55	.96	.00	.64	-.02	-.02
-55	1.17	-.02	.85	-.05	-.06
-55	1.50	-.16	1.13	-.19	-.20
-55	1.83	-.07	1.50	-.10	-.10

Table 16a. MATRIX OF SINGLE COLLECTOR PITCHING MOMENT COEFFICIENTS AT HCL/C = K_I (CONFIGURATION 1)

CONFIGURATION 1 FILE NAME:MDCOL1

C = 2.80 L = 10.80

ONE SINGLE COLLECTOR,RIM ANGLE=90

WIND AZIM	PITCH ANGLE	MYP	MYB	MYF	MYG
0	0.00	-.14	.93	-.24	-.17
0	-15.00	-.20	.81	-.30	-.24
0	15.00	-.18	.91	-.26	-.21
0	-30.00	-.12	.71	-.21	-.16
0	30.00	-.22	.84	-.30	-.25
0	-45.00	-.11	.58	-.21	-.15
0	45.00	-.30	.65	-.37	-.32
0	-60.00	.12	.56	.00	.09
0	60.00	-.19	.44	-.24	-.21
0	-65.00	.09	.47	.00	.06
0	65.00	-.12	.46	-.20	-.15
0	-75.00	-.06	.22	-.07	-.07
0	75.00	.09	.48	-.01	.06
0	-90.00	-.30	-.04	-.21	-.27
0	90.00	.14	.39	.05	.11
0	-135.00	-.31	.03	-.16	-.26
0	135.00	.15	.76	.12	.14
0	180.00	-.14	.66	-.06	-.11
-15	0.00	-.16	.99	-.25	-.19
-15	-65.00	.03	.39	-.06	-.00
-15	65.00	-.26	.33	-.34	-.29
-15	180.00	-.07	.68	.02	-.04
15	0.00	-.17	.92	-.25	-.20
15	-65.00	.05	.44	-.04	.02
15	65.00	-.08	.48	-.15	-.10
15	180.00	-.19	.63	-.12	-.17
30	0.00	-.21	.86	-.29	-.24
30	-15.00	-.12	.88	-.22	-.16
30	15.00	-.20	.86	-.27	-.23
30	-30.00	-.07	.82	-.15	-.10
30	30.00	-.23	.77	-.31	-.26
30	-45.00	-.03	.68	-.13	-.07
30	45.00	-.32	.57	-.39	-.35
30	-60.00	.19	.61	.08	.15
30	60.00	-.12	.43	-.16	-.14
30	-65.00	-.01	.38	-.08	-.03
30	65.00	-.19	.35	-.27	-.22
30	-75.00	-.09	.19	-.09	-.09
30	75.00	.05	.43	-.04	.02
30	-90.00	-.13	.06	-.07	-.11
30	90.00	.20	.43	.12	.17
30	-135.00	-.24	.16	-.10	-.19
30	135.00	.08	.73	.05	.07
30	180.00	-.22	.58	-.15	-.19
45	0.00	-.05	.87	-.12	-.08
45	-65.00	-.47	-.09	-.54	-.50
45	65.00	-.05	.36	-.10	-.07
45	180.00	-.28	.55	-.22	-.26
60	0.00	-.16	.58	-.22	-.19
60	-15.00	-.09	.58	-.18	-.12
60	15.00	-.52	.32	-.58	-.54
60	-30.00	-.06	.49	-.17	-.10
60	30.00	-.27	.41	-.32	-.29
60	-45.00	.05	.41	-.06	.01
60	45.00	-.22	.25	-.27	-.24
60	-60.00	.01	.25	-.06	-.01
60	60.00	-.10	.29	-.15	-.12
60	-65.00	.04	.23	-.02	.02
60	65.00	-.04	.29	-.09	-.06
60	-75.00	-.03	.11	-.05	-.04
60	75.00	-.01	.18	-.03	-.02
60	-90.00	-.20	-.07	-.15	-.18
60	90.00	.04	.19	-.01	.02
60	-135.00	-.12	.13	-.03	-.09
60	135.00	.12	.58	.13	.12
60	180.00	-.12	.50	-.05	-.09

Table 16b. MATRIX OF SINGLE COLLECTOR PITCHING MOMENT COEFFICIENTS AT HCL/C = K_I (CONFIGURATION 2)

CONFIGURATION 2. FILE NAME:MDCOL2

C = 2.22 L = 10.80

ONE SINGLE COLLECTOR,RIM ANGLE=40

WIND AZIM	PITCH ANGLE	MYP	MYB	MYF	MYG
0	0.00	-.26	.72	-.48	-.27
0	-15.00	-.13	.75	-.31	-.14
0	15.00	-.12	.80	-.33	-.13
0	-30.00	-.06	.66	-.27	-.07
0	30.00	-.24	.65	-.47	-.25
0	-45.00	.08	.65	-.14	.07
0	45.00	-.21	.55	-.43	-.22
0	-60.00	.08	.51	-.10	.07
0	60.00	-.17	.34	-.34	-.18
0	-75.00	.16	.35	.02	.16
0	75.00	-.11	.09	-.19	-.12
0	-90.00	.01	.05	.05	.01
0	90.00	.15	.23	.08	.15
0	135.00	-.11	.43	.11	-.10
0	135.00	.03	.64	.16	.04
0	180.00	-.16	.70	-.07	-.16
15	0.00	-.02	.87	-.25	-.03
15	15.00	.10	.30	-.01	.09
15	75.00	-.23	.00	-.35	-.24
15	135.00	-.24	.63	-.15	-.24
15	180.00	-.22	.77	-.45	-.23
15	-75.00	.14	.31	-.01	.13
15	75.00	-.22	.01	-.34	-.22
15	180.00	-.10	.71	.02	-.10
30	0.00	.04	.85	-.28	-.05
30	15.00	-.05	.83	-.26	-.06
30	30.00	-.20	.72	-.42	-.21
30	60.00	-.04	.69	-.27	-.05
30	90.00	.17	.66	-.40	-.18
30	135.00	.05	.65	-.19	.03
30	180.00	-.16	.53	-.37	-.17
30	-60.00	.07	.50	-.15	.06
30	60.00	-.23	.24	-.38	-.23
30	-75.00	.20	.35	.06	.19
30	75.00	-.10	.07	-.18	-.10
30	-90.00	.13	.13	.13	.13
30	90.00	.15	.21	.09	.15
30	135.00	-.15	.38	.10	-.14
30	135.00	.01	.63	.19	.01
30	180.00	-.09	.70	.04	-.09
45	0.00	.24	.66	-.48	-.25
45	-15.00	.01	.16	-.07	.01
45	15.00	-.15	.00	-.25	-.16
45	180.00	-.27	.53	-.07	-.26
60	0.00	-.18	.48	-.38	-.19
60	-15.00	-.13	.52	-.33	-.13
60	15.00	-.23	.44	-.39	-.23
60	-30.00	-.11	.49	-.34	-.12
60	30.00	-.23	.34	-.43	-.23
60	-45.00	.03	.47	-.21	.02
60	45.00	-.14	.23	-.28	-.15
60	-60.00	.08	.31	-.12	.07
60	60.00	-.16	.04	-.27	-.16
60	-75.00	-.00	.09	-.07	-.01
60	75.00	-.03	.04	-.10	-.04
60	-90.00	.00	.01	.01	.00
60	90.00	.02	.06	-.02	.02
60	-135.00	-.15	.16	.05	-.15
60	135.00	.01	.48	.18	.01
60	180.00	-.14	.52	.01	-.13

Table 16c. MATRIX OF SINGLE COLLECTOR PITCHING MOMENT COEFFICIENTS AT HCL/C = K_I (CONFIGURATION 3)

CONFIGURATION 3 FILE NAME:MDCOL3

C = 2.94 L = 10.80

ONE SINGLE COLLECTOR,RIM ANGLE=65

WIND AZIM	PITCH ANGLE	MYP	MYB	MYF	MYG
0.	0.00	-.19	.82	-.35	-.21
0.	-15.00	-.16	.76	-.29	-.18
0.	15.00	-.16	.82	-.28	-.18
0.	-30.00	-.07	.71	-.18	-.09
0.	30.00	-.21	.75	-.36	-.23
0.	-45.00	-.01	.58	-.14	-.01
0.	45.00	-.22	.62	-.37	-.24
0.	-60.00	.03	.49	-.10	.01
0.	60.00	-.17	.41	-.25	-.18
0.	-70.00	.13	.40	.01	.11
0.	70.00	-.25	.17	-.33	-.26
0.	-75.00	.20	.36	.10	.19
0.	75.00	-.08	.23	-.15	-.09
0.	-90.00	-.13	.02	-.07	-.12
0.	90.00	.18	.32	.12	.17
0.	-135.00	-.19	.29	-.03	-.16
0.	135.00	.10	.68	.13	.10
0.	180.00	-.12	.72	-.03	-.10
15.	0.00	-.22	.77	-.37	-.24
15.	-70.00	.08	.37	-.02	.07
15.	70.00	-.28	.12	-.37	-.29
15.	180.00	-.13	.73	-.04	-.12
15.	0.00	-.20	.82	-.35	-.22
15.	-70.00	.02	.35	-.07	.01
15.	70.00	-.37	.06	-.47	-.39
15.	180.00	-.32	.56	-.24	-.31
30.	0.00	-.12	.86	-.29	-.14
30.	-15.00	-.23	.73	-.36	-.25
30.	15.00	-.17	.89	-.28	-.18
30.	-30.00	-.12	.71	-.23	-.14
30.	30.00	-.16	.73	-.31	-.18
30.	-45.00	-.07	.58	-.19	-.09
30.	45.00	-.17	.58	-.29	-.19
30.	-60.00	.06	.51	-.07	.04
30.	60.00	-.29	.25	-.37	-.31
30.	-70.00	.03	.39	-.07	.01
30.	70.00	-.21	.13	-.28	-.22
30.	-75.00	.03	.22	-.04	.02
30.	75.00	-.13	.14	-.20	-.14
30.	-90.00	.00	.06	.03	.01
30.	90.00	.14	.27	.07	.13
30.	-135.00	-.33	.18	-.15	-.30
30.	135.00	-.05	.59	-.01	-.05
30.	180.00	-.22	.59	-.13	-.20
45.	0.00	-.16	.76	-.29	-.18
45.	-70.00	-.02	.20	-.10	-.03
45.	70.00	-.11	.14	-.16	-.11
45.	180.00	-.11	.59	-.04	-.10
60.	0.00	-.28	.48	-.44	-.30
60.	-15.00	-.08	.57	-.21	-.10
60.	15.00	-.19	.52	-.28	-.20
60.	-30.00	-.07	.49	-.23	-.10
60.	30.00	-.20	.42	-.29	-.21
60.	-45.00	-.04	.40	-.20	-.06
60.	45.00	-.22	.24	-.30	-.23
60.	-60.00	.05	.28	-.06	.04
60.	60.00	-.14	.10	-.20	-.15
60.	-70.00	.06	.18	-.01	.05
60.	70.00	-.15	.03	-.21	-.15
60.	-75.00	.04	.14	-.00	.04
60.	75.00	-.05	.06	-.10	-.05
60.	-90.00	-.04	-.00	-.02	-.04
60.	90.00	-.00	.09	-.06	-.01
60.	-135.00	-.18	.11	-.07	-.16
60.	135.00	-.02	.48	.02	-.02
60.	180.00	-.18	.48	-.08	-.16

Table 16d. MATRIX OF SINGLE COLLECTOR PITCHING MOMENT COEFFICIENTS AT HCL/C = K_I (CONFIGURATION 4)

CONFIGURATION 4 FILE NAME:MDCOL4

C = 3.00 L = 10.80

ONE SINGLE COLLECTOR,RIM ANGLE=120

WIND AZIM	PITCH ANGLE	MYP	MYB	MYF	MYG
0	0.00	-.36	.96	-.38	-.39
0	-15.00	-.26	.07	-.30	-.31
0	15.00	-.26	1.10	-.29	-.29
0	-30.00	-.19	.77	-.25	-.26
0	30.00	-.36	.95	-.38	-.38
0	-45.00	-.12	.56	-.17	-.18
0	45.00	-.34	.81	-.37	-.38
0	-55.00	-.06	.49	-.08	-.09
0	55.00	-.13	.99	-.21	-.23
0	-60.00	-.23	.35	-.23	-.23
0	60.00	.08	.96	-.01	-.02
0	-75.00	-.34	.16	-.29	-.28
0	75.00	.15	.72	.06	.04
0	-90.00	-.46	.02	-.38	-.36
0	90.00	.24	.71	.16	.14
0	-135.00	-.43	-.01	-.29	-.26
0	135.00	.36	1.11	.24	.22
0	180.00	-.17	.58	-.13	-.12
-15	0.00	-.36	.94	-.40	-.40
-15	-55.00	-.08	.59	-.11	-.12
-15	55.00	-.10	.89	-.17	-.18
-15	180.00	-.19	.63	-.06	-.05
15	0.00	-.22	1.07	-.26	-.27
15	-55.00	-.08	.48	-.11	-.12
15	55.00	-.16	.93	-.23	-.24
15	180.00	-.21	.57	-.16	-.15
30	0.00	-.36	.94	-.39	-.40
30	-15.00	-.29	.99	-.35	-.36
30	15.00	-.26	1.03	-.28	-.29
30	-30.00	-.19	.80	-.25	-.27
30	30.00	-.50	.77	-.53	-.54
30	-45.00	.05	.68	-.01	-.02
30	45.00	-.35	.69	-.38	-.39
30	-55.00	-.06	.50	-.09	-.09
30	55.00	-.12	.79	-.19	-.20
30	-60.00	-.14	.43	-.16	-.16
30	60.00	-.02	.82	-.10	-.12
30	-75.00	-.33	.18	-.28	-.27
30	75.00	.12	.78	.02	-.00
30	-90.00	-.45	.02	-.37	-.35
30	90.00	.28	.83	.19	.17
30	-135.00	-.44	-.02	-.31	-.28
30	135.00	.28	1.03	.18	.16
30	180.00	-.09	.68	-.04	-.03
45	0.00	-.26	.87	-.29	-.30
45	-55.00	-.15	.39	-.18	-.18
45	55.00	-.09	.81	-.15	-.16
45	180.00	-.24	.62	-.20	-.19
60	0.00	-.21	.89	-.24	-.24
60	15.00	-.11	.80	-.19	-.20
60	-15.00	-.34	.82	-.36	-.36
60	30.00	-.07	.63	-.15	-.17
60	-30.00	-.34	.75	-.36	-.36
60	45.00	-.05	.59	-.09	-.10
60	-45.00	-.23	.71	-.27	-.28
60	55.00	-.15	.39	-.17	-.17
60	-55.00	-.15	.75	-.22	-.23
60	60.00	-.12	.37	-.14	-.14
60	-60.00	-.03	.82	-.10	-.11
60	75.00	-.34	.14	-.30	-.30
60	-75.00	.14	.79	.05	.04
60	90.00	-.35	.04	-.28	-.27
60	-90.00	.22	.71	.13	.12
60	135.00	-.44	-.01	-.33	-.31
60	-135.00	.13	.92	.07	.05
60	180.00	-.25	.61	-.20	-.19

Table 17. PITCHING MOMENT COEFFICIENTS FOR VARIOUS GAP SPACINGS (CONFIGURATION 5)

CONFIGURATION 5 FILE NAME:MD1800

C = 2.80 L = 10.80

GAP STUDY,ONE COLLECTOR ROW

PITCH ANGLE	G/C	MYP	MYB	MYF	MYG
0	.57	-.30	.88	-.43	-.35
0	.71	-.33	.87	-.44	-.37
0	.89	-.24	.93	-.33	-.27
0	1.07	-.36	.84	-.46	-.40
0	1.25	-.29	.91	-.40	-.33
0	1.43	-.22	.95	-.32	-.26
0	1.61	-.19	.95	-.30	-.23
0	1.79	-.10	1.02	-.21	-.14
0	2.14	-.34	.85	-.45	-.38
0	2.50	-.15	.98	-.27	-.19
0	2.86	-.20	.93	-.32	-.24
0	3.21	-.19	.93	-.30	-.23
0	3.57	-.18	.94	-.29	-.22
-65	.57	.04	.44	-.06	.00
-65	.71	.02	.42	-.08	-.02
-65	.89	.02	.41	-.07	-.01
-65	1.07	.04	.41	-.06	.00
-65	1.25	-.06	.35	-.14	-.09
-65	1.43	.12	.48	.02	.08
-65	1.61	.06	.44	-.03	.02
-65	1.79	.06	.44	-.04	.02
-65	2.14	.15	.49	.04	.11
-65	2.50	.09	.44	-.01	.05
-65	2.86	.11	.47	.01	.07
-65	3.21	.12	.46	.02	.09
-65	3.57	.11	.46	.01	.07

CONFIGURATION 5 FILE NAME:MDGAP2

C = 2.80 L = 10.80

GAP STUDY,ALTERNATE LEGS

PITCH ANGLE	G/C	MYP	MYB	MYF	MYG
0	.06	-.35	.78	-.40	-.37
0	.11	-.13	.94	-.15	-.14
0	.18	-.17	.92	-.18	-.17
0	.27	-.15	.95	-.17	-.16
0	.36	-.22	.90	-.24	-.23
0	.54	-.08	.98	-.12	-.10
0	.71	-.32	.81	-.36	-.34
0	.89	-.14	.94	-.19	-.16
0	1.07	-.12	.94	-.17	-.14
0	1.25	-.23	.87	-.27	-.24
-65	.06	-.00	.45	-.04	-.02
-65	.11	.22	.62	.15	.19
-65	.18	.03	.43	-.03	.01
-65	.27	.09	.48	.01	.06
-65	.36	.11	.47	.03	.08
-65	.54	.20	.54	.11	.16
-65	.71	.42	.67	.31	.38
-65	.89	.07	.44	-.00	.04
-65	1.07	.07	.43	-.01	.04
-65	1.25	.15	.59	.07	.12

Table 18. PITCHING MOMENT COEFFICIENTS FOR ESTABLISHMENT OF ROW SPACING R (CONFIGURATION 9)

CONFIGURATION 9 FILE NAME:MDR2.0

C = 2.80 L = 10.80

ROW STUDY,ROW SPACING=2.0*C

WIND AZIM	PITCH ANGLE	MYP	MYB	MYF	MYG
0.	0.00	-.05	-.02	-.02	-.04
0	0.00	-.06	-.03	-.03	-.05
0.	-60.00	.04	.25	.06	.04
0	-65.00	.03	.22	.05	.04
15.	-60.00	-.09	.12	-.07	-.08
15.	-65.00	-.03	.16	-.00	-.02
30.	-60.00	-.09	.13	-.06	-.08
30.	-65.00	-.15	.06	-.12	-.14

CONFIGURATION 9 FILE NAME:MDR2.5

C = 2.80 L = 10.80

ROW STUDY,ROW SPACING=2.5*C

WIND AZIM	PITCH ANGLE	MYP	MYB	MYF	MYG
0.	0.00	-.19	-.08	-.17	-.18
0.	-60.00	-.18	.13	-.14	-.17
15.	-60.00	-.19	.07	-.16	-.18
30.	-60.00	-.20	.09	-.17	-.19

CONFIGURATION 9 FILE NAME:MDR3.0

C = 2.80 L = 10.80

ROW STUDY,ROW SPACING=3.0*C

WIND AZIM	PITCH ANGLE	MYP	MYB	MYF	MYG
0.	0.00	-.15	-.02	-.13	-.14
0.	-60.00	-.20	.16	-.16	-.19
15.	-60.00	-.04	.22	-.03	-.04
30.	-60.00	-.23	.19	-.20	-.22

Table 19a. PITCHING MOMENT COEFFICIENTS FOR ARRAY FIELDS (CONFIGURATION 5)

CONFIGURATION 5 FILE NAME:MDEDIT

C = 2.80 L = 10.80

ONE ROW OF THREE COLLECTORS, G/C=.536

WIND AZIM	PITCH ANGLE	MYP	MYB	MYF	MYG
0	0.00	-.15	1.05	-.18	-.16
0	-30.00	-.26	.75	-.30	-.27
0	30.00	-.33	.90	-.40	-.36
0	-45.00	-.03	.77	-.09	-.05
0	45.00	-.35	.71	-.42	-.38
0	-60.00	.29	.75	.19	.26
0	60.00	-.36	.36	-.40	-.38
0	-75.00	-.06	.27	-.05	-.06
0	75.00	-.03	.43	-.13	-.06
0	-90.00	-.14	.08	-.07	-.11
0	90.00	.25	.49	.17	.22
0	-120.00	-.31	.03	-.20	-.27
0	120.00	.18	.70	.05	.13
0	-135.00	-.51	.06	-.39	-.46
0	135.00	.09	.83	-.01	.05
0	180.00	-.22	.70	-.20	-.22
-15	0.00	-.18	1.03	-.21	-.19
-15	-60.00	.07	.58	-.01	.04
-15	60.00	-.35	.35	-.39	-.37
-15	180.00	-.14	.73	-.12	-.13
15	0.00	-.16	1.07	-.18	-.17
15	-60.00	.18	.66	.09	.15
15	60.00	-.27	.41	-.30	-.28
15	180.00	-.21	.69	-.19	-.21
30	0.00	-.25	.92	-.29	-.26
30	-30.00	-.05	.85	-.08	-.06
30	30.00	-.27	.87	-.31	-.29
30	-45.00	-.01	.71	-.09	-.04
30	45.00	-.26	.71	-.30	-.27
30	-60.00	.03	.49	-.05	.00
30	60.00	-.08	.47	-.08	-.08
30	-75.00	-.06	.22	-.06	-.06
30	75.00	-.04	.39	-.12	-.07
30	-90.00	-.15	.03	-.09	-.13
30	90.00	.18	.40	.10	.15
30	-120.00	-.26	.04	-.16	-.22
30	120.00	.07	.65	-.04	.03
30	-135.00	-.38	.12	-.27	-.34
30	135.00	.09	.83	.01	.06
30	180.00	-.29	.68	-.26	-.28
45	0.00	-.42	.61	-.45	-.43
45	-60.00	.11	.39	.04	.08
45	60.00	-.30	.20	-.33	-.31
45	180.00	-.16	.58	-.16	-.16
60	0.00	-.07	.46	-.08	-.07
60	-30.00	-.10	.35	-.13	-.11
60	30.00	-.28	.25	-.30	-.29
60	-45.00	-.10	.22	-.13	-.11
60	45.00	-.19	.19	-.20	-.20
60	-60.00	.07	.21	.04	.06
60	60.00	-.11	.13	-.13	-.11
60	-75.00	-.13	.01	-.12	-.12
60	75.00	-.06	.11	-.10	-.07
60	-90.00	-.10	-.02	-.07	-.09
60	90.00	.03	.14	-.00	.02
60	-120.00	-.16	-.02	-.12	-.15
60	120.00	.03	.25	-.00	.02
60	-135.00	-.15	.03	-.11	-.14
60	135.00	.09	.38	.07	.09
60	180.00	-.17	.29	-.15	-.16

Table 19b. PITCHING MOMENT COEFFICIENTS FOR ARRAY FIELDS (CONFIGURATIONS 6-7)

CONFIGURATION 6 FILE NAME:MD6ROW

C = 2.80 L = 10.80

TWO COLLECTOR ROWS,R/C=2.25

WIND AZIM	PITCH ANGLE	MYP	MYB	MYF	MYG
0	0.00	.10	1.43	.02	.07
0	-30.00	-.07	1.08	-.12	-.09
0	30.00	-.13	1.21	-.20	-.16
0	-45.00	.05	.89	-.01	.03
0	45.00	.04	1.07	.01	.03
0	-60.00	-.06	.48	-.10	-.07
0	-60.00	.16	.62	.09	.13
0	60.00	-.28	.48	-.28	-.28
0	-75.00	.02	.30	.02	.02
0	75.00	.06	.55	-.05	.02
0	-90.00	-.18	.05	-.10	-.15
0	90.00	.03	.36	-.08	-.01
0	-120.00	-.38	-.07	-.22	-.32
0	120.00	.37	.83	.26	.33
0	-135.00	-.40	.12	-.20	-.33
0	135.00	.21	.95	.13	.18
0	180.00	-.18	.90	-.09	-.15
15	0.00	-.07	1.30	-.16	-.11
15	-60.00	.19	.62	.11	.16
15	-60.00	.20	.63	.12	.17
15	60.00	-.22	.51	-.21	-.22
15	180.00	-.24	.02	-.15	-.21
30	0.00	-.09	1.14	-.18	-.12
30	-60.00	-.01	.42	-.08	-.04
30	60.00	-.22	.48	-.22	-.22
30	180.00	.02	.94	.15	.07

CONFIGURATION 7 FILE NAME:MD7ROW

C = 2.80 L = 10.80

THREE COLLECTOR ROWS,R/C=2.25

WIND AZIM	PITCH ANGLE	MYP	MYB	MYF	MYG
0	0.00	-.23	-.11	-.30	-.25
0	-30.00	-.20	-.09	-.25	-.22
0	30.00	-.26	-.11	-.36	-.29
0	-45.00	.00	.13	-.04	-.02
0	45.00	-.20	.05	-.28	-.23
0	-60.00	-.34	.04	-.35	-.35
0	60.00	-.00	.28	-.09	-.03
0	-75.00	-.27	.02	-.24	-.26
0	75.00	-.12	.23	-.22	-.16
0	-90.00	-.17	-.03	-.12	-.15
0	90.00	.08	.30	.01	.05
0	-120.00	-.28	-.13	-.18	-.24
0	120.00	.00	.44	-.07	-.02
0	-135.00	-.26	-.17	-.18	-.23
0	135.00	-.24	.12	-.22	-.23
0	180.00	-.16	-.05	-.06	-.13
15	0.00	-.26	-.09	-.34	-.29
15	-60.00	-.23	.10	-.25	-.23
15	60.00	-.15	.13	-.22	-.17
15	180.00	-.11	.05	-.01	-.07
30	0.00	-.08	.11	-.17	-.12
30	60.00	-.30	.03	-.31	-.30
30	60.00	-.14	.18	-.22	-.17
30	180.00	-.17	.09	-.09	-.14

Table 19c. PITCHING MOMENT COEFFICIENTS FOR ARRAY FIELDS (CONFIGURATIONS 8-9)

CONFIGURATION 8 FILE NAME:MD8ROW

C = 2.80 L = 10.80

FOUR COLLECTOR ROWS,R/C=2.25

WIND AZIM	PITCH ANGLE	MYP	MYB	MYF	MYG
0.	0.00	-.23	-.16	-.31	-.26
0.	-30.00	-.23	-.19	-.28	-.25
0.	30.00	-.23	.05	-.30	-.26
0.	-45.00	-.25	-.10	-.29	-.27
0.	45.00	-.33	.03	-.39	-.35
0.	-60.00	-.12	.15	-.15	-.13
0.	60.00	-.06	.28	-.12	-.08
0.	-75.00	-.18	.06	-.17	-.18
0.	75.00	-.25	.10	-.35	-.28
0.	-90.00	-.13	-.01	-.09	-.11
0.	90.00	-.10	.12	-.17	-.13
0.	-120.00	-.26	-.16	-.18	-.23
0.	120.00	-.11	.27	-.17	-.13
0.	-135.00	-.10	-.04	-.04	-.08
0.	135.00	-.34	.07	-.33	-.34
0	180.00	-.09	.06	-.02	-.07
15.	0.00	-.01	-.01	-.08	-.04
15.	-60.00	-.22	.08	-.22	-.22
15.	60.00	-.14	.20	-.21	-.17
15	180.00	-.08	.06	-.03	-.06
30.	0.00	-.14	-.07	-.22	-.17
30.	-60.00	-.08	.13	-.11	-.09
30.	60.00	-.16	.11	-.22	-.18
30.	180.00	-.15	-.00	-.07	-.12

CONFIGURATION 9 FILE NAME:MD9ROW

C = 2.80 L = 10.80

SIX COLLECTOR ROWS,R/C=2.25

WIND AZIM	PITCH ANGLE	MYP	MYB	MYF	MYG
0.	0.00	-.35	-.20	-.42	-.37
0.	-30.00	.07	.15	.03	.05
0.	30.00	-.23	-.11	-.31	-.26
0.	-45.00	-.02	.14	-.04	-.02
0.	45.00	-.41	-.17	-.49	-.44
0.	-60.00	.08	.29	.05	.07
0.	60.00	-.20	.02	-.26	-.22
0.	-75.00	-.02	.15	-.01	-.02
0.	75.00	-.11	.12	-.17	-.13
0.	-90.00	-.34	-.16	-.28	-.32
0.	90.00	-.00	.16	-.06	-.02
0.	-120.00	-.25	-.17	-.18	-.23
0.	120.00	.09	.33	.06	.08
0.	-135.00	-.18	-.10	-.12	-.16
0.	135.00	-.40	-.01	-.42	-.40
0.	180.00	-.15	-.03	-.10	-.13
15.	0.00	-.38	-.22	-.45	-.40
15.	-60.00	.12	.26	.09	.11
15.	60.00	-.29	-.04	-.37	-.32
15.	180.00	-.20	-.05	-.12	-.17
30.	0.00	-.23	.04	-.32	-.26
30.	-60.00	.05	.23	.02	.04
30.	60.00	-.29	-.05	-.36	-.31
30.	180.00	-.10	.13	-.04	-.08

Table 20. EFFECTS OF FENCES AND BERMS ON ARRAY FIELDS, PITCHING MOMENT COEFFICIENTS

FILE NAME:MDFNCE

C = 2.80 L = 10.80

FENCE STUDY

RUN#	MYP	MYB	MYF	MYC
270	-.32	-.17	-.25	-.29
271	-.31	-.17	-.32	-.31
272	-.23	-.03	-.28	-.25
273	-.01	.05	-.03	-.02
274	-.03	.24	-.10	-.06
275	-.12	-.08	-.15	-.13
276	.16	.35	.08	.13
277	-.30	-.20	-.29	-.30
278	-.09	.16	-.16	-.12
279	-.04	-.03	-.07	-.05
280	-.03	.06	-.07	-.04
281	.14	.11	.10	.13
282	-.05	.02	-.11	-.07
283	-.12	-.07	-.14	-.13
284	-.19	.63	-.29	-.23
285	-.02	.15	-.01	-.02
286	.06	.12	.02	.05
287	-.05	.73	-.11	-.07
288	-.21	-.14	-.21	-.21
289	-.15	.13	-.21	-.17
290	-.04	.02	-.02	-.04
291	-.02	.03	.03	.00

FILE NAME:MDFNC1

C = 2.80 L = 10.80

FENCE STUDY

RUN#	MYP	MYB	MYF	MYC
292	-.29	-.15	-.21	-.26
293	-.46	-.26	-.47	-.46
294	-.30	-.17	-.38	-.37
295	-.13	-.10	-.15	-.14
296	-.35	-.24	-.42	-.37
297	-.15	-.11	-.18	-.16
298	-.25	-.13	-.27	-.26
299	-.09	.01	-.16	-.12
300	-.13	.05	-.23	-.16

FILE NAME:MDBERM

C = 2.80 L = 10.80

BERM STUDY

RUN#	MYP	MYB	MYF	MYC
301	-.17	.00	-.29	-.21
302	.07	.17	-.04	.03
303	-.17	-.20	-.29	-.21
304	-.36	-.24	-.40	-.37
305	-.15	-.14	-.19	-.16
306	-.06	.12	-.19	-.11
307	-.32	.53	-.44	-.36
308	-.22	-.02	-.25	-.23
309	-.34	-.10	-.36	-.35

Table 21. PITCHING MOMENT COEFFICIENTS WITH A TORQUE TUBE (CONFIGURATION 1)

CONFIGURATION 1 FILE NAME:MOTOR1

C = 2.80 L = 10.80

TORQUE TUBE EFFECTS,COLL#1 ALONE

WIND AZIM	PITCH ANGLE	MYP	MYB	MYF	MYG
0.	0.00	-.02	1.02	-.12	-.06
0.	-30.00	.08	.77	-.05	.03
0.	30.00	-.25	.87	-.31	-.27
0.	-60.00	-.00	.41	-.05	-.02
0.	60.00	.06	.65	-.08	.01
0.	-90.00	-.27	.13	-.13	-.22
0.	90.00	.15	.60	.01	.10
0.	-120.00	-.41	.14	-.19	-.33
0.	120.00	-.01	.70	-.16	-.07

DISTRIBUTION:

TID-4500-R66, UC-62 (263)

Solar Total Energy Program
American Technological University
P. O. Box 1416
Killeen, TX 76541
Attn: B. L. Hale

Argonne National Laboratory (3)
9700 South Cass Avenue
Argonne, IL 60439
Attn: W. W. Schertz
R. Winston

Dr. A. Balakrishnan
Aerospace Systems Division
Acurex Corporation
485 Clyde Avenue
Mountain View, CA 94042

Herman Bank
Bldg. 506, Rm. 340
Jet Propulsion Laboratory
133 North Altadena Drive
Pasadena, CA 91103

Battelle Memorial Institute
Pacific Northwest Laboratory
P. O. Box 999
Richland, WA 99352
Attn: K. Drumheller

Joe Bogetich
Hyperion, Inc.
7214 Valtec Court
Boulder, CO 80301

Lynn Brock
Harrison Radiator Division
General Motors Corporation
Lockport, NY 14094

Brookhaven National Laboratory
Associated Universities, Inc.
Upton, LI, NY 11973

Greg Brucker
Suntec Systems
2101 Waddale Drive
St. Paul, MN 55119

Dr. Jack Cherne
Energy Systems Group
TRW, Inc.
One Space Park
Redondo Beach, CA 90278

J. Philip Dechov
Columbia Gas Service System
1600 Dublin Road
Columbus, OH 43215

Danny Deffenbaugh
Southwest Research Institute
6220 Culebra Road
San Antonio, TX 78284

Hans Dehne
Acurex Corporation
485 Clyde Avenue
Mountain View, CA 94042

Mark Dilello
General Electric Company (Rm. 20B56)
P. O. Box 8661
Philadelphia, PA 19101

Vince Dinc...
Bldg. 11
General Electric Company
P. O. Box 8666
Philadelphia, PA 19101

EPRI
3412 Hillview Avenue
Palo Alto, CA 94303
Attn: J. E. Bigger

Edison Electric Institute
90 Park Avenue
New York, NY 10016
Attn: L. O. Elsaesser,
Director of Research

Bernard Eldridge
Jacobs-Del Solar Systems, Inc.
251 South Lake Avenue
Pasadena, CA 91101

Energy Institute
1700 Las Lomas
Albuquerque, NM 87131
Attn: J. Dritt

Albert Fong
The BDM Corporation
2600 Yale Boulevard SE
Albuquerque, NM 87106

Mark Gelderloos
H. A. Williams and Associates
980 W. Henderson
Columbus, OH 43220

Georgia Institute of Technology
Atlanta, GA 30332
Attn: J. D. Walton

Georgia Power Company
270 Peachtree
P. O. Box 4545
Atlanta, GA 30302
Attn: W. Hensley
Vice President Economics
Services

George Goranson
Viking Solar Systems, Inc.
3467 Ocean View Blvd.
Glendale, CA 91208

Shelley Gordon
Chilton Engineering
1570 Linda Way
Sparks, NV 89512

Dr. Gopal Gupta
Foster Wheeler Development Corp.
12 Peach Tree Hill Road
Livingston, NJ 07039

Gil Herrera
Del Manufacturing Company
905 Monterey Pass Road
Monterey Park, CA 91754

Gus Hutchinson
Solar Kinetics, Inc.
8120 Chancellor Row
Dallas, TX 75247

Mr. Leonard Jaffe
Stop 507-228
Jet Propulsion Laboratory
4800 Oak Grove Drive
Pasadena, CA 91103

Jet Propulsion Laboratory
4800 Oak Grove Drive
Pasadena, CA 91103
Attn: V. C. Truscello

Lawrence Berkeley Laboratory
University of California
Berkeley, CA 94720
Attn: M. Wallig

Lawrence Livermore Laboratory
University of California
P. O. Box 808
Livermore, CA 94500
Attn: W. C. Dickinson

I. Earl Lewis
Western Development Laboratories
Division
Ford Aerospace & Communications
Corporation
3439 Fabian Way
Palo Alto, CA 94303

Los Alamos Scientific Laboratory (3)
Los Alamos, NM 87545
Attn: J. D. Balcomb
D. D. Bankston
D. P. Grimmer

James Maginnis
Team, Inc.
140 W. Broadway #41
Tucson, AZ 85701

NASA-Lewis Research Center
Cleveland, OH 44135
Attn: R. Hyland

New Mexico State University
Solar Energy Department
Las Cruces, NM 88001

Oak Ridge National Laboratory (4)
P. O. Box Y
Oak Ridge, TN 37830
Attn: J. R. Blevins
C. V. Chester
J. Johnson
S. I. Kaplan

Office of Technology Assessment
U. S. Congress
Washington, D. C. 20510
Attn: Dr. H. Kelly

PRC Energy Analysis Co.
7600 Old Spring House Rd.
McLean, VA 22102
Attn: K. T. Cherian

Solar Energy Research Institute (4)
1536 Cole Blvd.
Golden, CO 80401
Attn: C. J. Bishop
K. Brown
B. L. Butler
M. D. Cotton
J. Finegold
B. P. Gupta
D. Kearney
F. Kreith
A. Rabl
J. Thornton
L. Mrig
H. Luaffenburger
Library (2)

Howard Steele
Stop 507-239
Jet Propulsion Laboratory
4800 Oak Grove Drive
Pasadena, CA 91103

U. S. Department of Energy (6)
Albuquerque Operations Office
P. O. Box 5400
Albuquerque, NM 87185
Attn: D. L. Krenz
D. Graves
G. N. Pappas
C. B. Quinn
J. R. Roder
J. Weisiger

U. S. Department of Energy
Division of Energy Storage
Systems
Washington, D. C. 20545
Attn: J. Gahimer

U. S. Department of Energy (6)
Division of Solar Thermal
Energy Systems
Washington, D. C. 20545
Attn: R. H. Annan
G. W. Braun
M. U. Gutstein
J. E. Rannels
W. Aller
J. Dollard

U. S. Department of Energy
Los Angeles Operations Office
350 S. Figeuroa Street, Suite 285
Los Angeles, CA 90071
Attn: Fred Glaski

U. S. Department of Energy
San Francisco Operations Office
1333 Boradway, Wells Fargo Bldg.
Oakland, CA 94612
Attn: R. W. Hughey

University of Delaware
Institute of Energy Conversion
Newark, DE 19711
Attn: K. W. Boer

University of New Mexico (2)
Department of Mechanical Eng.
Albuquerque, NM 87113
Attn: W. A. Cross
M. W. Wilden

Robert W. Weaver
Jet Propulsion Laboratory
4800 Oak Grove Drive
Pasadena, CA 91103

Lee E. Wilson
Energetics Corporation
833 E. Arapaho Road
Suite 202
Richardson, TX 75081

Stan Youngblood
Acurex Corporation
485 Clyde Avenue
Mountain View, CA 94042

400 C. Winter
2323 C. M. Gabriel
2323 S. B. Martin
2324 R. S. Pinkham
2326 G. M. Heck
4000 A. Narath
4700 J. H. Scott
4710 G. E. Brandvold
4713 B. W. Marshall
4714 R. P. Stromberg
4715 R. H. Braasch
4719 D. G. Schueler
4719 H. N. Post
4720 V. L. Dugan
4721 J. V. Otts
4722 J. F. Banas
4722 R. L. Champion
4722 S. Thunborg
4723 W. P. Schimmel
4725 J. A. Leonard
4725 D. E. Randall (25)
4725 K. Wally
5000 J. K. Galt
5100 F. L. Vook
5500 O. E. Jones
5512 H. C. Hardee
5523 R. C. Reuter, Jr.
5600 D. B. Shuster
5610 A. A. Lieber
5620 M. M. Newsom
5630 R. C. Maydew
5631 H. R. Vaughn
5632 C. W. Peterson
5633 S. McAlees, Jr.
5634 D. D. McBride (10)
5634 R. E. Tate
5635 W. R. Barton
5636 J. K. Cole
5640 G. J. Simmons
5800 R. S. Claassen
5830 M. J. Davis
5840 H. J. Saxton
5844 F. P. Gerstle
8266 E. A. Aas
8453 W. G. Wilson
3141 T. L. Werner (4)
3151 W. L. Garner (3)
For DOE/TIC
(Unlimited Release)